ABSTRACT

ADAPTIVE DS-CDMA MULTIUSER DETECTION FOR TIME VARIANT FREQUENCY SELECTIVE RAYLEIGH FADING CHANNEL

by
Xin Tang

The current digital wireless mobile system such as IS-95, which is based on direct sequence Code Division Multiple Access (DS-CDMA) technology, will not be able to meet the growing demands for multimedia service due to low information exchanging rate. Its capacity is also limited by multiple accessed interference (MAI) signals.

This work focuses on the development of adaptive algorithms for multiuser detection (MUD) and interference suppression for wideband direct sequence code division multiple access (DS-CDMA) systems over time-variant frequency selective fading channels. In addition, channel acquisition and delay estimation techniques are developed to combat the uncertainty introduced by the wireless propagation channel. This work emphasizes fast and simple techniques that can meet practical needs for high data rate signal detection.

Most existing literature is not suitable for the large delay spread in wideband systems due to high computational/hardware complexity. A de-biasing decorrelator is developed whose computational complexity is greatly reduced without sacrificing performance. An adaptive bootstrap symbol-based signal separator is also proposed for a time-variant channel. These detectors achieve MUD for asynchronous, large delay spread, fading channels without training sequences.

To achieve high data rate communication, a finite impulse response (FIR) filter based detector is presented for M-ary QAM modulated signals in a multipath Rayleigh fading channel. It is shown that the proposed detector provides a stable performance for QAM signal detection with unknown fading and phase shift. It is

also shown that this detector can be easily extended to the reception of any M-ary quadrature modulated signal.

A minimum variance decorrelating (MVD) receiver with adaptive channel estimator is presented in this dissertation. It provides comparable performance to a linear MMSE receiver even in a deep fading environment and can be implemented blindly. Using the MVD receiver as a building-block, an adaptive multistage parallel interference cancellation (PIC) scheme and a successive interference cancellation (SIC) scheme were developed. The total number of stages is kept at a minimum as a result of the accurate estimating of the interfering users at the earliest stages, which reduces the implementation complexity, as well as the processing delay. Jointly with the MVD receiver, a new transmit diversity (TD) scheme, called TD-MVD, is proposed. This scheme improves the performance without increasing the bandwidth. Unlike other TD techniques, this TD-MVD scheme has the inherent advantage to overcome asynchronous multipath transmission. It brings flexibility in the design of TD antenna systems without restrict signal coordination among those multiple transmissions, and applicable for both existing and next generation of CDMA systems.

A maximum likelihood based delay and channel estimation algorithm with reduced computational complexity is proposed. This algorithm uses a diagonal simplicity technique as well as the asymptotically uncorrelated property of the received signal in the frequency domain. In combination with oversampling, this scheme does not suffer from a singularity problem and the performance quickly approaches the Cramer-Rao lower bound (CRLB) while maintaining a computational complexity that is as low as the order of the signal dimension.

ADAPTIVE DS-CDMA MULTIUSER DETECTION FOR TIME VARIANT FREQUENCY SELECTIVE RAYLEIGH FADING CHANNEL

by
Xin Tang

A Dissertation
Submitted to the Faculty of
New Jersey Institute of Technology
in Partial Fulfillment of the Requirements for the Degree of
Doctor of Philosophy in Electrical Engineering

Department of Electrical and Computer Engineering

August 2002

APPROVAL PAGE

Adaptive DS-CDMA Multiuser Detection for Time Variant Frequency Selective Rayleigh Fading Channel

Xin Tang

Dr. Yeheskel Bar-Ness, Dissertation Advisor — Date
Distinguished Professor of Electrical and Computer Engineering, NJIT

Dr. Alexander Haimovich, Committee Member — Date
Professor of Electrical and Computer Engineering, NJIT

Dr. Nirwan Ansari, Committee Member — Date
Professor of Electrical and Computer Engineering, NJIT

Dr. Zoi-Heleni Michalopoulou, Committee Member — Date
Associate Professor of Mathematics, NJIT

Dr. Narayan Mandayam, Committee Member — Date
Associate Professor of Electrical and Computer Engineering, Rutgers University

BIOGRAPHICAL SKETCH

Author: Xin Tang

Degree: Doctor of Philosophy

Date: August 2002

Undergraduate and Graduate Education:

- Doctor of Philosophy in Electrical Engineering, August 2002
  New Jersey Institute of Technology, Newark, NJ
- Master of Science in Electrical Engineering, February 1992
  Nanjing University of Aeronautics and Astronautics, Nanjing, China
- Bachelor of Science in Electrical Engineering, July 1989
  Nanjing University of Aeronautics and Astronautics, Nanjing, China

Major: Electrical Engineering

Publications:

X. Tang and Y. Bar-Ness, "Minimum Variance Decorrelating CDMA Receiver in Time Variant Frequency Selective Rayleigh Fading Channel", *for submitting*

X. Tang and Y. Bar-Ness, "Maximum Likelihood Channel Delay Estimation with Limited Number of Samples Using Diagonal Matrix Approximation", *submitted to Wireless Personal Communications, an international journal*

X. Tang and Y. Bar-Ness, "Minimum Variance Decorrelating Receiver for Downlink with Transmit Diversity", *VTC 2001 Fall, Atlantic City, NJ, vol.1, pp.72-76, Oct. 7-11, 2001*

X. Tang and Y. Bar-Ness, "Frequency Domain Channel Estimation for Asynchronous CDMA Signals", *ICC 2001, Helsinki, Finland, vol.8, pp.2515-2519, Jun. 30 - Jul. 3, 2001*

X. Tang and Y. Bar-Ness, "Minimum Variance Decorrelating Receiver in Time Variant Frequency Selective Rayleigh Fading CDMA Channel", *VTC Spring 2001, Rhodes, Greece, vol.3, pp.1760-1764, May 6-9, 2001*

X. Tang and Y. Bar-Ness, "Subspace Adaptive Detection for Asynchronous Multiuser CDMA with Frequency Domain Channel Response and Delay Estimation", *ICASSP 2001, Salt Lake City, vol.4, pp.2277-2280, May 7-11, 2001*

X. Tang and Y. Bar-Ness, "Effect of Synchronization Error on the Performance of Adaptive Bootstrap Multiuser Detection", *The 35th Annual Conference on Information Science and Systems, John Hopkins Univ., Baltimore, Mar. 21-23, 2001*

X. Tang and Y. Bar-Ness, "M-ary QAM Receiver in Time Variant Asynchronous Frequency Selective Rayleigh Fading CDMA Environment", *The 34th Annual Conference on Information Science and Systems, Princeton University, NJ, vol.1, pp. WA2 7-10, Mar. 15-17, 2000*

X. Tang and Y. Bar-Ness, "Adaptive Multishot Canceler for Wideband CDMA Systems", *VTC 1999 Fall, Amsterdam, The Netherlands, vol.1, pp.213-217, Sep. 19-22, 1999*

献 给 我 的 家 人

ACKNOWLEDGMENT

I would like to express my sincere gratitude to my advisor, Professor Bar-Ness. His constant support, detailed guidance, and encouragement cover every aspect during my student life from problem solving to technical writing. My study is always inspired by his enthusiasm and hard work for research in communications and signal processing area.

I would also like to express my appreciation to the distinguished members of the dissertation committee: Professor Alexander Haimovich, Professor Nirwan Ansari, Professor Zoi-Heleni Michalopoulou, and Professor Narayan Mandayam, for their active participation and remarkable comments.

Thanks are given to my present and former colleagues at the Center for Communications and Signal Processing Research at NJIT, for their help during my graduate life. Special appreciation is delivered to Dr. Matthijs A. Visser for his careful revising of my finial version of the dissertation and valuable recommendations.

My grateful gratitude goes to my parents and parents-in-law. With their support and efforts of taking care of my son during the passed years, I am able to concentrate on my Ph.D. program.

Finally, I am and will always be grateful to my wife for her endless support and encouragement in my life.

TABLE OF CONTENTS

Chapter **Page**

TABLE OF CONTENTS
(Continued)

Chapter **Page**

TABLE OF CONTENTS

(Continued)

Chapter **Page**

LIST OF FIGURES

Figure **Page**

LIST OF FIGURES
(Continued)

Figure **Page**

LIST OF FIGURES

(Continued)

CHAPTER 1

INTRODUCTION

1.1 Wireless Propagation Channel

Unlike a wireline channel, which is stationary and predictable, a wireless radio channel has random characteristics. It varies with the transmitter and receiver's locations, their movements, and variations in the surrounding environment. Hence, its study is typically performed using statistical tools.

A typical phenomenon which has been widely used in wireless communication system design is called small-scale *fading*, or simply *fading*. It represents the rapid fluctuation of the amplitude of a radio signal over a short period of time or traveling distance. Fading is caused by the combination of several versions of the transmitted signal, called multipath, which arrive at the receiver at slightly different times. The random phase and amplitude of the different multipath components causes fluctuations in signal strength, signal distortion, or both. Multipath propagation extends the time required for the transmitted signals to reach the receiver and thus, introduces inter-symbol-interference (ISI). Multipath delay spread leads to time dispersion and frequency selective fading.

If the multipaths do not contain a dominant path, which is usually a line of sight signal component, the amplitude envelope of the received signal for each path can be statistically described as a Rayleigh distributed random variable. Otherwise, when a dominant path is present, as is typically the case in indoor applications, the envelope of the received signal is more suitably modeled as a Rician distributed random variable.

Due to the mobile nature of transmitters and receivers, each path experiences an apparent shift in frequency. The shift is called Doppler shift. A Doppler spread leads to frequency dispersion and time selective fading, which describes the time varying nature of the wireless channel.

The uncertainty in the signals received over a time-variant multipath fading channel increases the difficulty in the design of the receivers. In this work, the propagation channel is modeled as an asynchronous Rayleigh faded channel. That is, beside being a Rayleigh faded multipath channel, signals from different users are non-synchronous in time. The principal objective is to propose adaptive signal detection and estimation algorithms which can be applied to this wireless channel with lower computational complexity.

1.1.1 Model for Time-varying Rayleigh Fading Channel

In order to evaluate the performance of the proposed schemes, a correlated time varying Rayleigh fading channel should be generated. For this, a model defined as Witter's method [1] is employed. This model is depicted in Figure 1.1.

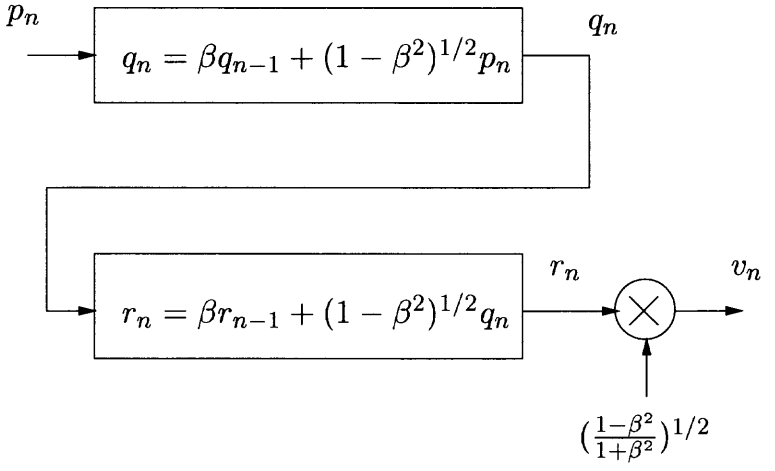

Figure 1.1 Generating correlated Gaussian process with Witter's method

Here, the input p_n are samples of a complex white Gaussian noise process with $E[p_n^* p_{n+l}] = \delta(l)$. In Figure 1.1, $\beta = exp(-\alpha/T)$ and $\alpha = 2.146/\tau_0$, where T is the time interval between samples, and τ_0 is the coherence time, defined as the value of time τ after which the correlation function has decreased to $1/e$. The fading rate is defined as $1/\tau_0$. The output v_n is then a correlated complex Gaussian sample

sequence, with a correlation function approximatly given (for $\tau_0/T \geq 10$) by,

$$R_v(l) = E[v_n^* v_{n+l}] = (1 + \alpha l T)e^{-\alpha l T} \tag{1.1}$$

where l is the sampling distance between the two samples. The norm $\gamma_n = \|v_n\|$ of the complex Gaussian samples v_n is a Rayleigh distributed random variable. In a multipath time-variant fading channel, the fading on different paths is in general statistically uncorrelated. Thus, a generator as in Figure 1.1 is used for each path, such that the fading on each individual path is temporally correlated while uncorrelated with other paths.

The correlation function with $\tau_0 = 1000$ and $T = 1$ is given in Figure 1.2. The solid line is obtained using the approximation of equation (1.1), and dashed line using simulation with the model in Figure 1.1.

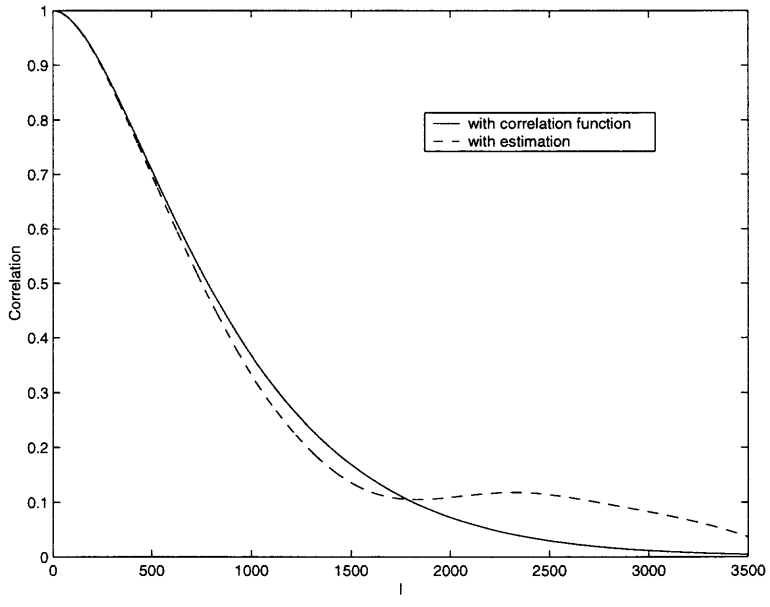

Figure 1.2 Correlation function vs correlation time l (samples)

In this work, the attention is focused on adaptive algorithms for wideband CDMA systems with a high transmitted data. Without further notice, the channel is generated with a carrier frequency of 1.9 GHz, a data rate of 1 Mbits/s, and

receiver velocity of 30 meters/s. In Figure 1.3, a sample of such a channel with two multipaths is depicted,

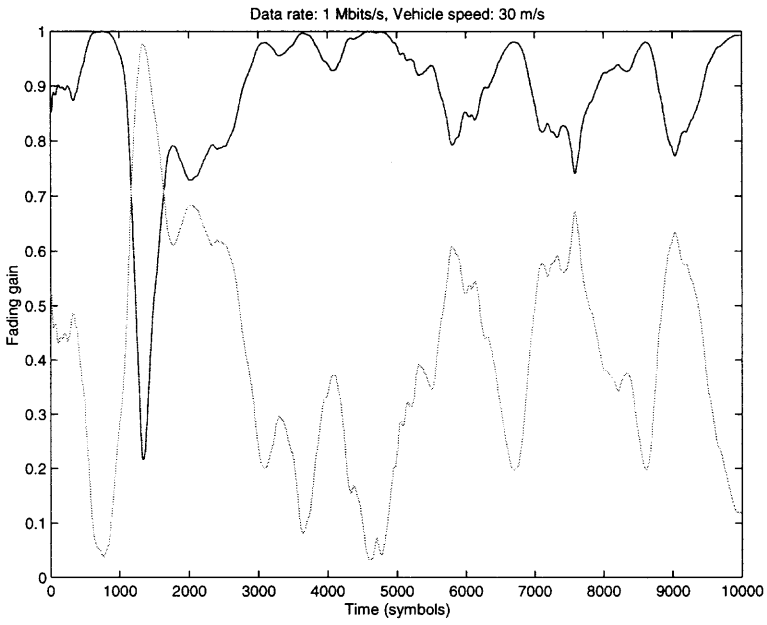

Figure 1.3 Time-variant channel in high data rate systems

The figure shows that the signal changes quite slowly over a small number of symbols, so that, if the processing window size is short, the channel may be approximated as quasi-static. However, for a larger window of time, adaptive tracking of the channel variation is needed.

1.2 Multiple Access Systems

Wireless communication technology has advanced rapidly during the past decade. Analog systems have migrated into digital systems, and quickly evolve into high capacity wideband systems, so as to provide multimedia services to meet market demands.

The limited resources, particularly the scarce channel bandwidth, make it desirable that multiple users can communicate simultaneously over the same channel. As a result, multiple access techniques have been developed. Among these, the

CDMA technique exhibits unique advantages as a multiplexing method, and has been widely accepted as a major technology for digital wireless systems.

In CDMA systems, all users utilize the same carrier frequency and may transmit and receive messages simultaneously. The narrowband messages of all users are spread by pseudo-random code sequences. The code sequences assigned to users are distinct and in cases orthogonal to each others. At the receiver, the corresponding spreading code sequence is employed to decorrelate the desired message from others. If the orthogonality is maintained among these codewords, there would be no interference from undesired signals. Users can then share the same channel without interference.

As mentioned before, the CDMA signals when travelling across the wireless channel, may experience small-scale fading. If the channel frequency response is non-flat, then multiple signals will reach the receiver as a result of multipath. In an uplink channel, the distance between each mobile and base station is different, and varies in time due to the movement of the mobiles. As a result, it is almost impossible to have signals from different users arrive at the base station synchronously. Hence, the orthogonality of the CDMA spreading codes is eliminated due to these inherent asynchronous and frequency selective fading characteristics of the wireless channel. In other words, the multiple access signals at the receiver's front end will no longer be orthogonal to each other, even if originally orthogonal codes were used and were synchronized at the transmitters. The detector's output may then contains ISI, and multiple access interference (MAI) from other users, which degrades the desired output's signal-to-noise ratio (SNR), and hence, reduces the system capacity. The amount of MAI in the output depends on the cross correlation, and relative delay between the desired and interfering codewords, as well as on the interference strength.

To overcome performance loss due to MAI, many different directions have been pursued. Power control has been used in IS-95 CDMA implementations, and

even more stringent power control schemes have been proposed for 3G systems. As presented in the next section, MUD techniques have been studied over the past decade, and proposed in 3G systems as an option for performance improvement.

1.2.1 Multiple User Detection

In a CDMA system, the capacity is mainly limited by MAI due to the co-existence of multiple access users with non-orthogonal signature codes. The well known near-far problem is one of the principle obstacles, for which various MUD techniques have been proposed.

The optimum MUD technique, initiated by Verdu [2], considers MAI not as additive Gaussian noise, as in previous analysis, but rather as a realistic optimization problem. For optimal MUD, a maximum likelihood sequence detector was used. This detector calculates the Euclidean distances between the received matched filter output sequence and each of the possible transmitted sequences, and chooses the sequence with the minimum distance. This optimal MUD has extremely high computational complexity which is exponential in the number of users. Therefore, later research targeted suboptimum algorithms of practical complexity.

The decorrelator proposed by Lupas and Verdu [3, 4] belongs to a set of suboptimal linear (linearity in the sense of computational complexity as well) multiuser detectors. It applies an inverse of the correlation matrix to separate the multiuser signals, and the detector doesn't require knowledge of the users' energy information. This makes the bit error rate (BER) performance of this decorrelator independent of the interfering users' energies. An attractive aspect of such a detector is that it is inherently immune to the near-far problem. In fact, the near-far resistance property of the decorrelating detector is optimum [4]. However, one of its major drawback is that it enhances the noise at its outputs, which causes a reduction in SNR and loss of performance. Although increasing the desired user's

transmitting energy would compensate for a decreasing SNR, and theoretically not result in enhanced MAI to other users, it consumes important system resources in terms of battery life, particularly on the mobile side.

The decorrelating multiuser detector requires knowledge of the signature waveforms and timing information of the desired and interfering users, which usually requires some complexity in the detector. As a result, attention has been focused on adaptive multiuser detection [5] where only the desired user's information is required. The minimization of the mean-square-error (MMSE) based adaptive detector exhibits comparable near-far resistance performance as the decorrelating detector. However, to achieve multiuser detection, MMSE replaces the complexity for acquiring information of interfering users with additional training sequences for every active user.

The challenge then becomes to eliminate the need for training sequences while maintaining comparable performance to that of the MMSE detector. This can be accomplished by using a minimum variance technique employed previously in adaptive array processing [6], and which resulted in the blind adaptive detectors [7, 8]. The minimum variance detector (MVD) is basically the constrained minimum output energy (MOE) linear detector. It minimizes the output energy in canonical form, which means using a linear transformation that consists of the desired user's signature waveform and its orthogonal component. Implementing MOE blindly means that there is no need for a training sequence. However, in a time-variant fading channel the performance of such a scheme deteriorates significantly as a result of very low received energy of the desired user when in a deep fade. In this dissertation solutions have been developed to overcome this effect of the time varying fading.

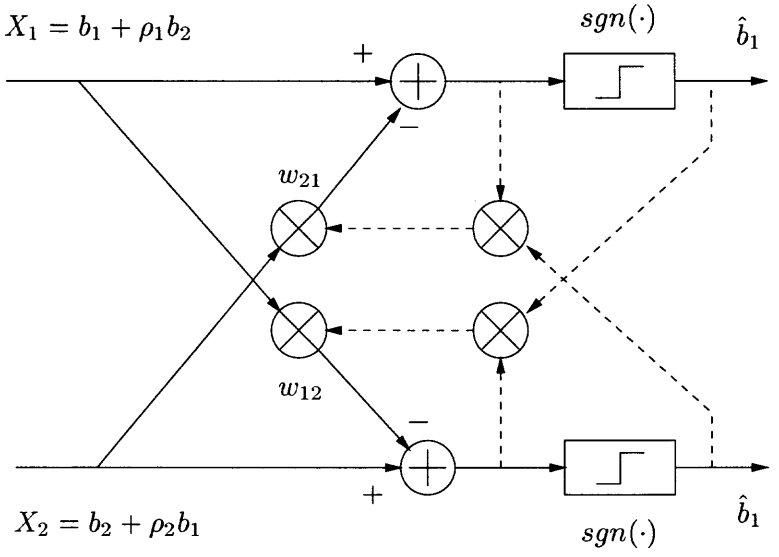

Figure 1.4 FF structure of bootstrap decorrelator with two inputs

1.2.2 Bootstrap Detector

One of the adaptive decorrelating detectors is called bootstrap decorrelator. It is based on the bootstrap algorithm which was initially proposed for interference cancellation in [9]. It was then applied to cross-polarization for satellite communication in [10].

The bootstrap is often referred to as a signal separator rather than an interference canceler because it removes the cross correlation components between output ports, and results in "cleaned" outputs for all users' signals, a desired property for multiuser detection applications. There are basically three different structures of the bootstrap decorrelator: the backward-backward (BB) structure which uses a minimum power criterion, the forward-forward (FF) structure which utilizes a correlation criterion, and the forward-backward (FB) structure which employs a combination of the first two structures. Among these three structures, the FF bootstrap detector has been widely studied and applied to multiuser detection [11, 12, 13]. A two input-two output FF structure is given in Figure 1.4.

The comparative study in [14] shows that even though the linear minimum mean squared error (LMMSE) based multiuser detector and bootstrap multiuser detector are derived from different criteria, they exhibit approximately equal performance in CDMA multiuser applications. They differ in that the adaptive bootstrap detector has no requirement for a training sequence. In this sense, it can be implemented blindly. On the other hand, the bootstrap detector should have knowledge of signature codes and delays for all active users.

1.2.3 Interference Cancellation (IC)

Two categories of IC techniques have been studied intensively: parallel interference cancellation (PIC) and successive interference cancellation (SIC). PIC [15, 16] suggests to estimate and simultaneously remove all interferences from the received signals so as to increased the signal-to-interference-plus-noise ratio (SINR) and hence, improve detection performance. On the other hand, with SIC [17, 18] the interfering signals are canceled sequentially, i.e. one after the other. SIC first ranks the interfering signals in terms of their energies or amplitudes, then it estimates and cancels these interferers starting with the strongest and ending with the weakest. By removing the stronger interferer, weaker signals are detected more accurately. It was shown in [19], by simulation, that linear SIC outperforms one and two stage linear PIC in a flat fading channel. The SIC scheme is not only robust in performing cancellation but also relatively simple. For both schemes, stronger interference result in improved detection and more accurate regeneration of these signals, and therefore, provides better cancellation. Thus, PIC and SIC schemes have superior near-far resistance when interference-to-signal ratios (ISR) are high. In a low ISR environment, a poor estimate of the interference may degrade the detection performance due to the introduction of a large cancellation noise.

To obtain a clean decision output, PIC and SIC are usually implemented in multistage structures. An example was described in [20] where a multistage SIC was arranged in a matrix structure. It was shown in [21] that a linear (linear in the sense that the signal cancellation is performed with a linear transformation, while non-linear means interference is re-generated using a non-linear transformation, for example using hard decision outputs) multistage SIC's performance becomes asymptotically close to that of the decorrelator when the number of stages increases. The non-linear multistage SIC outperforms the linear multistage SIC, especially in a frequency selective fading channel. In a multistage PIC scheme each stage uses the tentative decisions of all users from the previous stage to produce more accurate decision outputs. However, as shown by Divsalar [22], this is not necessarily a good approach, particularly when the interference estimation is poor at the early stages. Total cancellation of the estimated interference may introduce a significant cancellation error. Instead, cancellation of a portion of the estimated interference at thoses stages would lead to a more reliable performance.

1.2.4 Transmit Diversity (TD)

Transmit diversity, with multiple transmission antennas was initially introduced in [23]. TD is attractive for the downlink in current cellular systems as well as in the forthcoming 3rd generation wideband systems, due to the increase in channel capacity without sacrificing bandwidth, although at the expense of computational complexity. Moreover, it can be implemented in the existing system infrastructure without significant modification.

A number of different TD techniques have been proposed. With delay transmit diversity (DTD) [23], the same information is transmitted over all the antennas with different transmission delays. This approach artificially creates a dispersive channel such that the receiver can take advantage of diversity gain. This method, which is

particularly suitable for a small time dispersion channel, such as with indoor wireless applications, is attractive due to its simplicity. For real performance advantage, the relative delays between different transmission, need to be chosen carefully [24]. Also, as shown in [25], DTD has limited performance gain due to loss of orthogonality among transmissions.

Orthogonal transmit diversity (OTD) [26] simulcasts the information over different antennas to obtain code diversity. In order to maintain orthogonality among the transmitted information, a unique orthogonal code (e.g. Walsh codes) is assigned to each different transmit antenna. The code length is usually doubled (for a two-antenna case) to maintain the same effective number of codes as for a single transmit antenna scheme [27]. A doubled chip rate is then required to transmit the information data at the same rate which results in a loss of bandwidth efficiency. Also, to preserve orthogonality between different transmissions, the OTD scheme requires signals from different antennas to be synchronous.

In [28] Alamouti proposed a simple space-time transmit diversity (STD) scheme which exploits both spatial and temporal diversity for a synchronous situation. This scheme is also of the OTD kind because two consecutive symbols are coded on a two-dimension orthogonal basis. Unlike other OTD techniques in CDMA that use two codes per user for two transmit antennas, this scheme requires only one spreading code per user. As was shown in [29], the Alamouti scheme yields the same diversity order as one transmit antenna and two receive antennas with MRC combining when perfect channel estimation is assumed. However, it is significantly more sensitive to the accuracy of the channel estimation. If perfect channel estimation is not available, the two transmit/one receive antenna scheme provides inferior performance to that of a one transmit/two receive antenna scheme with MRC combining.

In [30], differential detection was implemented with the two transmit antennas. It requires neither knowledge of the channel nor the pilot signal, while its performance

suffers a 3dB loss compared to that in [28]; the channel was assumed synchronous flat fading.

An overview of these TD techniques shows that the multiple transmissions should be well coordinated, or synchronized. When signals travel through a frequency selective fading channel, and particularly when TD antennas are mounted at different site locations, it results in multipath and asynchronous reception. Consequently, this will violate the synchronization condition required by the aforementioned schemes, and hence deteriorate the receiver's performance. Therefore, in such an environment these TD techniques require channel equalizers at the receiver to overcome signal distortion, increasing the receiver complexity. How to combat the effect of multipaths with reduced computational complexity is an important topic to be discussed in this work.

1.2.5 Channel Parameter Estimation in Time-variant Fading Channel

To obtain sufficient performance gain, accurate knowledge of the channel and user parameters is necessary for most proposed MUD schemes. This includes parameters such as propagation delay, user's spreading codes, complex channel response, etc [7].

Even though knowledge of the transmitted signal's energy is not required for many detectors, it becomes necessary when M-ary quadrature amplitude modulated (M-QAM) signals [12, 31] are used. Then, a sorter, which can detect levels in M-ary signal constellation, is used for decision making instead of the hard limiter for BPSK modulation. When M-QAM signals go through the propagation channel, their constellation may be distorted by channel fading. At the receiver, the detector requires sufficiently accurate information of the channel response to correctly recover the original signal constellation. In a multipath channel, the response corresponding to each path can be exploited to maximize the receiver performance by using MRC

combining. Therefore, channel gain estimation in a time-variant channel environment is a major subject of wireless signal detection.

M-ary quadrature signals may suffer phase distortion (a form of phase rotation) in the propagation channel. In addition, the local coherent detector at the receiver can also add a phase error to the outputs. Phase shift estimation and correction is crucial for M-ary quadrature signal detection. Furthermore, due to the time-variant nature of the channel, these phase errors change in time. Thus, an adaptive phase correction process before the decision-making will significantly improve the performance of M-ary modulated signal detection.

Knowledge of path delays is another important condition for high performance MUD. Almost all multiuser detectors assume knowledge of the propagation delays for all users or at least the desired user. Detection performance is, in general, sensitive to a propagation delay estimation error [32], especially in a near-far situation. Thus, propagation delays should be estimated with as accurately as possible. A robust receiving technique which can tolerate a large delay error is preferable.

In [33, 34], path delays were estimated using MUSIC algorithms, assuming the number of users and the noise covariance matrix are known. The total number of users should be limited to maintain a large enough noise subspace dimension. Special codes were designed by Missiroli [35] to estimate both delay and channel phase shift at the expense of implementation complexity. Another popular estimator based on the Maximum-Likelihood (ML) algorithm was shown in [36], which made use of a whitening process such that the interference becomes approximately white and Gaussian.

These estimation schemes require knowledge of the covariance or autocorrelation matrix, which is in general unknown and should be estimated from observation samples. For an accurate estimate, a large number of samples is required. However, in a time-variant channel the number of samples used for estimation should be kept

small to avoid significant channel change during the estimation. On the other hand, an insufficient number of samples will result in an erroneous estimate of the covariance or autocorrelation matrix, and introduce a timing error.

Considering the importance of the channel response and propagation delay in MUD, their estimation in a time-variant channel is an important part of this work. The parameter estimation is based on the received observation samples, either with or without pilot reference signals. This work focuses on estimation schemes that use a limited number of samples, making them suitable for practical systems with a requirement for low computational complexity and fast estimation.

1.3 Low-pass Signal Model over Time-variant Frequency Selective Rayleigh Fading Channel

Assuming the information symbols, from user k, are spread by the signature code c_k. Then, the n-th transmitted symbol of user k is given by

$$s_{k,n}(t) = \sqrt{a_k} b_k(n) c_k(t - nT) \qquad 0 < t \leq T, \tag{1.2}$$

where a_k is the signal transmitted energy of user k, and T is the symbol interval. Spreading codes c_k, $k = 1, \cdots, K$, are given by

$$c_k(t) = \sum_{j=0}^{N-1} g_k(j) p(t - jT_c), \tag{1.3}$$

where the chip interval $T_c = T/N$, N is the processing gain, $g_k(j)$ is the j-th chip of the codeword for user k, and $p(t - jT_c)$ is the chip pulse-shaping filter, which is assumed rectangular. Transmitted signals experience independent asynchronous selective fading channels. Let L_k be the number of resolvable discrete multipath components associated with the transmission, then, the multipath channel impulse response is,

$$h_{k,n}(t) = \sum_{l=1}^{L_k} \gamma_{kl}(n) \delta(t - \tau_{kl}), \tag{1.4}$$

where τ_{kl} is the delay of the l-th path of user k. In a time-variant channel, τ_{kl} varies in time. However, its variation is usually slow, such that, for simplicity, it is assumed fixed. Without loss of generality, it is assumed that $0 \leq \tau_{k1} < \tau_{k2} < \cdots < \tau_{kL_k}$, and $min\{\tau_{k1}\} = 0$. Also, $\gamma_{kl}(n)$ is the independent channel fading experienced by user k on the l-th path at the n-th symbol. The received signal may be represented as

$$\begin{aligned} r_{k,n}(t) &= s_{k,n}(t) * h_{k,n}(t) \\ &= \sqrt{a_k} b_k(n) \sum_{l=1}^{L_k} \gamma_{kl}(n) c_k(t - nT - \tau_{kl}). \end{aligned} \tag{1.5}$$

Consider all active users and multipath transmissions. Then, the equivalent low-pass received data sequence at the input of the receiver's front end is the superposition of all transmissions, which is given by

$$\begin{aligned} r(t) &= \sum_{n} \sum_{k=1}^{K} r_{k,n}(t) + v(t) \\ &= \sum_{n} \sum_{k=1}^{K} b_k(n) \sqrt{a_k} \sum_{l=1}^{L_k} \gamma_{kl}(n) c_k(t - nT - \tau_{kl}) + v(t) \end{aligned} \tag{1.6}$$

where K is the number of total active users. $v(t)$ is a zero-mean Gaussian noise with variance σ^2. Without further mention, this work assumes that the n-th symbol of the 1st user is the desired symbol of the desired user.

Expression (1.6) represents the equivalent baseband asynchronous received signal in a time-variant frequency selective fading channel. This model should be modified in accordance with the specific environment. For example, in a downlink channel, the signals for different users may suffer the same channel fading and propagation delay as they travel through a common path. As such, the fading $\gamma_{kl}(n)$, number of multipath L_k, and delay τ_{kl} will be the same for all users, such that the subscript k can be dropped.

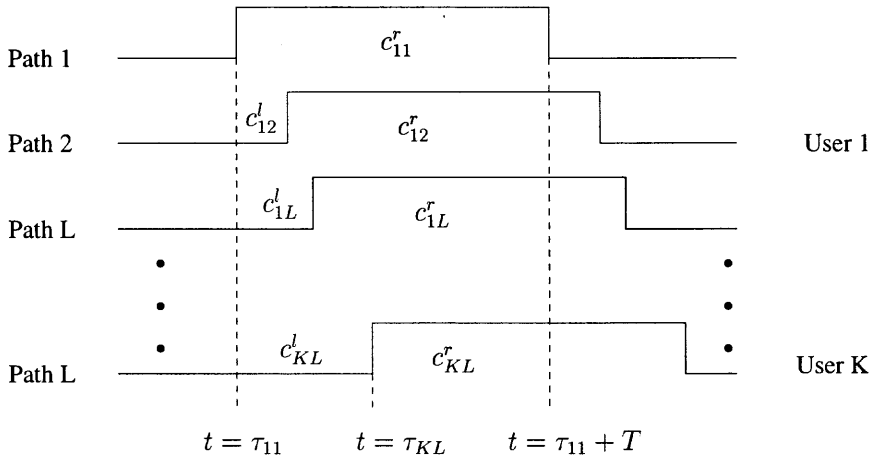

Figure 1.5 One-shot matched-filter receiver

1.3.1 One-shot and Multi-shot Matched Filter for Asynchronous Channel

At the matched-filter (MF) bank of the receiver front end there are basically two methods for signal processing, termed "One-shot" [37, 38] and "Multi-shot" [39], respectively.

Figure 1.5 is the "One-shot" processing structure, where the MF bank is synchronized to the first path of user 1, and all path delays are assumed within one symbol interval T. This structure requires $c_{kl}^l(t)$ and $c_{kl}^r(t)$, where

$$c_{kl}^l(t) = \begin{cases} c_k(t + T - \tau_{kl}) & 0 \le t \le \tau_{kl} \\ 0 & \tau_{kl} < t \le T \end{cases} \tag{1.7}$$

and

$$c_{kl}^r(t) = \begin{cases} 0 & 0 \le t \le \tau_{kl} \\ c_k(t - \tau_{kl}) & \tau_{kl} < t \le T \end{cases} \tag{1.8}$$

for $l = 1, \cdots, L$ and $k = 1, \cdots, K$, which are used to correlate the received signal for the l-th path of user k during $[0, T]$. Since the outputs for all multipaths, except the first, contain only part of the desired signal, the output corresponding to $c_{kl}^r(t)$ can be combined with the next symbol's output corresponding to $c_{kl}^l(t)$ to obtain better performance. Another potential problem for the "One-shot" approach is the fact that for some spreading codes and delay patterns, the "partial correlation matrix"

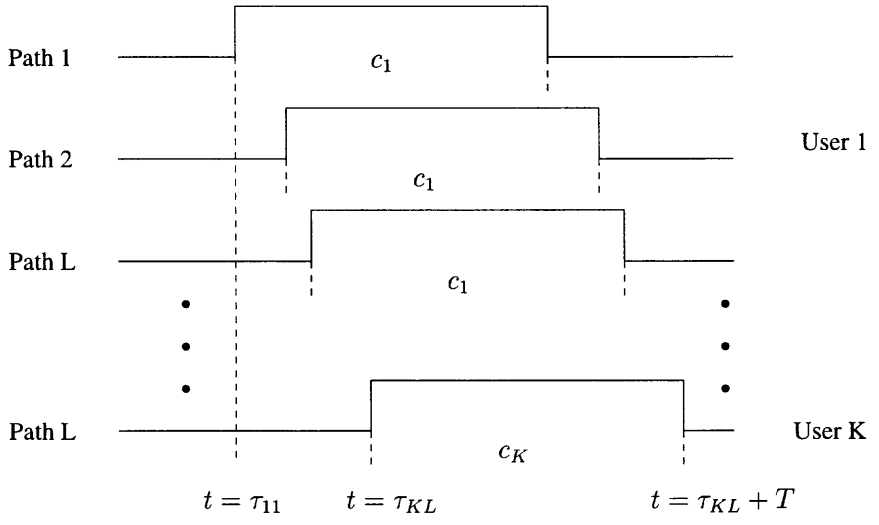

Figure 1.6 Multi-shot matched-filter receiver

between these partial codes may be singular. This condition can give difficulties to MUD detection.

Instead of a single correlation window as in one-shot MF, a "Multi-shot" MF uses multiple correlation windows, as shown in Figure 1.6. In the "Multi-shot" MF, each delayed version of the different codes is synchronized to each path of every user. For the l-th path of user k, the MF correlates the received signal with signature $c_k(t)$ synchronized to $[nT+\tau_{kl}, (n+1)T+\tau_{kl}]$. This approach doesn't require an additional delay-and-combining process. To explore all information, a few information bits of all paths of all users must be stacked together. The extended correlation matrix, which corresponds to the stacked data, is non-singular and in general diagonal dominant. In this work, "Multi-shot" MF is used to handle the received signal.

1.4 Overview of the Dissertation

The application of high data rates to wideband CDMA brings new challenges in terms of MAI and ISI suppression due to the fact that, in comparison to "regular" CDMA, the delay spread is no longer a few chips but could be significantly more.

Most current literature on multiuser detection is focused on algorithms that are not suitable for channels with large delay spread without high computational/hardware complexity.

In Chapter 2, a de-biasing based MUD detector is derived. By exploiting the structure of the extended correlation matrix, a simplified algorithm is proposed, which effectively removes redundancy in the signal processing without loss in performance. An adaptive symbol-based signal separator, based on multi-shot MF, which is suitable for the asynchronous large delay spread fading channels, is presented.

M-ary quadrature modulation is an efficient approach to increase the transmitted data rate while preserving the radio spectrum resource. However, the transmission of M-ary modulated signals is more sensitive to channel variations. The received signal constellation may be distorted and rotated due to the channel fading and phase shift, which dramatically degrades the receiver's performance.

In Chapter 3, an FIR decorrelating receiver is proposed that has low implementation complexity. Together with an adaptive channel gain estimator and a bootstrap based adaptive phase corrector, a blind detector is obtained. This blind detector is shown to provide promising performance in a time-variant fading channel if the phase error is limited within a certain range. It is worth emphasizing that the proposed structure is suitable for to both PSK and M-ary QAM modulated signals.

In Chapter 4, the MVD based receiver is presented. To overcome the performance loss due to the time-variant fading channel, a decision aided adaptive channel estimator is derived, which is shown to be insensitive to MAI and ISI if low BER condition is satisfied. With the proposed channel estimator, the MVD receiver has a performance comparable to that of a linear MMSE receiver in a time-variant Rayleigh fading channel. Since the MVD receiver is basically a single user detector, and its performance approaches that of linear MMSE, adaptive MVD

based multistage PIC and SIC schemes are proposed, in which the MVD receiver is used as the building-block. The proposed schemes provide sufficiently accurate estimation at the first stage, such that the following stage is able to remove a significant amount of interference. As a result, the required number of stages will be small.

If power control is used the received signal energy, and thus the SINR, of all users is maintained at an equal level. As a result, their BER performance is at the same level. Consequently, an SIC scheme whose operation is based on signals' level ordering, may not provide performance improvement for detection of the remaining signals after interference is canceled, since it could enhance the interference with a probability comparable to the BER before cancellation. However, a sufficient condition is derived that ensures the SIC scheme work in a strict power control situation. It is shown that when the BER is very small and this sufficient condition is satisfied, the SIC scheme, which cancels interference in arbitrary order, is able to improve detection performance for users in a successive order.

With the MVD receiver, a new transmit diversity scheme, called TD-MVD, is proposed. Most transmit diversity schemes assume the channel is flat fading, or require a channel equalizer when the channel is selective fading. However, the proposed TD-MVD is inherently suitable for an asynchronous multipath environment. This provides a significant design convenience for practical implementation of transmit diversity. Signals can be transmitted from diversity antennas located at the same base station or at separate base stations without sophisticated coordination for synchronization.

As was emphasized earlier, this dissertation focuses on the development of algorithms for a time-variant fading channel. This means signal acquisition should be performed within a small processing window, otherwise the channel may have changed significantly, resulting in erroneous outputs. This is particularly important

in time-variant channel acquisition for real time processing. The effect of a delay error on the adaptive bootstrap receiver's performance is analyzed in Chapter 5. And in Chapter 6, a simplified maximum likelihood (ML) channel response and delay estimation scheme is developed. The simplification is a result of the reduced correlation between different elements of the signal samples when transforming the received temporal data into frequency domain data. It is shown that, when using an oversampling technique on the temporal data, the proposed estimator exhibits a performance close to the CRLB besides its reduced computational complexity. Furthermore, with this scheme the processing window size can be made smaller than the dimension of the sample vector. In comparison, a traditional ML estimator can't function correctly in such a situation, because the correlation matrix becomes singular due to insufficient data samples. Therefore, the proposed estimator is very suitable for a time-variant channel where fast acquisition is required. Chapter 7 presents conclusions based on the work in the previous chapters.

CHAPTER 2

MULTI-SHOT CANCELER FOR WIDEBAND CDMA SYSTEMS

Due to its potential for increased system capacity, CDMA has become a major technology for wireless communication in the past decade. However, the performance and capacity of CDMA systems significantly deteriorate when MAI is present. Verdú, in [2], proposed a way to combat MAI that employs the knowledge of the correlation between code words. A number of single-stage suboptimum receivers using decorrelating detectors and linear transformations of the matched filter outputs have been discussed in [3] while a multi-stage detector was discussed in [40].

Due to the increasing demand for multimedia services, CDMA technology is applied to higher data-rate applications. As a consequence, the delay spread in multipath propagation channels, in terms of symbol intervals, becomes larger. In most of the literature, the maximum assumed delay spread is limited to within one symbol interval. However, in wideband CDMA (WCDMA) delay spread can be larger than one symbol interval, resulting in significantly increased ISI and MAI, and hence, deteriorated system performance. Combating these effects is an important aspect of WCDMA receiver design.

The "Bootstrap" algorithm, presented in [41], provides an efficient approach to adaptive separation of multi-user signals without the use of training sequences. As described in [11], this algorithm features low-complexity and quite satisfactory performance for CDMA applications. The linear transformation controlled by the algorithm is obtained by minimizing the correlation between the transformed outputs and the estimated data.

Multi-shot approaches to CDMA signal separation, shown in [42], use a debiasing method based on diagonal dominance properties of the extended cross-correlation matrix. These multi-shot detectors have been shown to improve

performance. In previous work, however, maximum path delay was taken to be less than one bit time.

In this chapter, the effect on the performance of increased path delay, to more than one symbol, is examed. Simplified decorrelating structures are derived, which reduce the computational burden without loss of detection performance by eliminating redundant operation. The adaptive Bootstrap receiver is also proposed. To combat channel fading, an adaptive channel gain estimator, similar to the one introduced in [43] is used.

2.1 Multi-shot Matched Filter Receiver

Assuming perfect phase tracking at the input of the multi-shot matched filter bank, and number of multipath is same for all users, i.e. $L_k = L$ for all k, we define the combined multipath signature c_{ck} for user k as

$$c_{ck}(t) = \sum_{l=1}^{L} \gamma_{kl}(t) c_k(t - \tau_{kl}). \tag{2.1}$$

This combination of multipath signals associated with user k is also depicted in Figure 2.1.

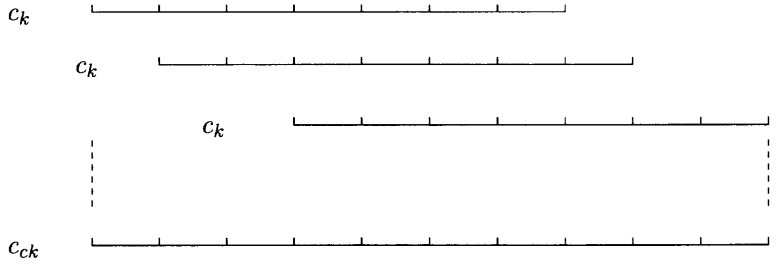

Figure 2.1 Combined multipath signature for user k

Let $\mathbf{c}_c(t) = [c_{c1}(t), c_{c2}(t), ..., c_{cK}(t)]^T$, and $\mathbf{y}(n) = A\mathbf{b}(n)$, where, $\mathbf{y}(n) = [y_1(n), y_2(n), \cdots, y_K(n)]^T$, $A = diag[\sqrt{a_1}, \sqrt{a_2}, \cdots, \sqrt{a_K}]$, $\mathbf{b}(n) = [b_1(n), b_2(n), \cdots, b_K(n)]^T$. Then, the receiver input signal can be written as

$$r(t) = \sum_{n} \sum_{k=1}^{K} c_{ck}(t - nT) y_k(n) + n(t) = \sum_{n} \mathbf{c}_c^T(t - nT)\mathbf{y}(n) + v(t). \tag{2.2}$$

Assume the maximum path delay is less than mT, m integer. Then, apply a matched filter to correlate the received signal from τ_{min} to $T+\tau_{max}$, where τ_{min} and τ_{max} are the minimum and maximum delays respectively among all delays τ_{kl}. The output of the matched-filter sampled at the n-th symbol is

$$\begin{aligned}\mathbf{x}(n) &= \int_{\tau_{min}}^{T+\tau_{max}} r(t)\mathbf{c}_c(t)dt \\ &= \sum_{i=1}^{m}[P_i^u\mathbf{y}(n-i)+P_i^l\mathbf{y}(n+i)]+P\mathbf{y}(n)+\mathbf{v}(n), \end{aligned} \tag{2.3}$$

where, $\mathbf{x}(n)=[x_1(n),x_2(n),\cdots,x_K(n)]^T$, and

$$\begin{aligned} P &= \int_{\tau_{min}}^{T+\tau_{max}} \mathbf{c}_c(t)\mathbf{c}_c(t)^T dt; \\ P_i^u &= \int_{iT+\tau_{min}}^{\tau_{max}+T} \mathbf{c}_c(t-iT)\mathbf{c}_c(t)^T dt = \int_{\tau_{min}}^{\tau_{max}-(i-1)T} \mathbf{c}_c(t)\mathbf{c}_c(t+iT)^T dt; \\ P_i^l &= \int_{\tau_{min}}^{\tau_{max}-(i-1)T} \mathbf{c}_c(t+iT)\mathbf{c}_c(t)^T dt = (P_i^u)^T; \\ \mathbf{v}(n) &= \int_{\tau_{min}}^{T+\tau_{max}} v(t)\mathbf{c}_c(t)dt. \end{aligned} \tag{2.4}$$

Stacking M symbols together (M is odd, $M>m$), the vector of matched filter outputs is obtained as

$$\begin{bmatrix} \mathbf{x}(n-\frac{M-1}{2}) \\ \vdots \\ \mathbf{x}(n) \\ \vdots \\ \mathbf{x}(n+\frac{M-1}{2}) \end{bmatrix} = \begin{bmatrix} P_m^u & \cdots & P & \cdots & P_m^l & & 0 \\ & \ddots & \ddots & \ddots & \ddots & & \\ & P_m^u & \cdots & P & \cdots & P_m^l & \\ & & \ddots & \ddots & \ddots & \ddots & \\ 0 & & P_m^u & \cdots & P & \cdots & P_m^l \end{bmatrix} \cdot \begin{bmatrix} \mathbf{y}(n-\frac{M+2m-1}{2}) \\ \vdots \\ \mathbf{y}(n) \\ \vdots \\ \mathbf{y}(n+\frac{M+2m-1}{2}) \end{bmatrix} + \begin{bmatrix} \mathbf{v}(n-\frac{M-1}{2}) \\ \vdots \\ \mathbf{v}(n) \\ \vdots \\ \mathbf{v}(n+\frac{M-1}{2}) \end{bmatrix}. \tag{2.5}$$

The matrix above can be written as

$$\underbrace{\begin{bmatrix} \mathbf{x}(n-\frac{M-1}{2}) \\ \vdots \\ \mathbf{x}(n) \\ \vdots \\ \mathbf{x}(n+\frac{M-1}{2}) \end{bmatrix}}_{\mathbf{x}(:,n)} = \underbrace{\begin{bmatrix} P & \cdots & \cdots & P_m^l & & 0 \\ \ddots & \ddots & \ddots & \ddots & \ddots & \\ & P_m^u & \cdots & P & \cdots & P_m^l \\ & & \ddots & \ddots & \ddots & \ddots \\ 0 & & P_m^u & \cdots & \cdots & P \end{bmatrix}}_{\mathcal{P}} \cdot \underbrace{\begin{bmatrix} \mathbf{y}(n-\frac{M-1}{2}) \\ \vdots \\ \mathbf{y}(n) \\ \vdots \\ \mathbf{y}(n+\frac{M-1}{2}) \end{bmatrix}}_{\mathbf{y}(:,n)}$$

$$+\underbrace{\begin{bmatrix} \sum_{i=1}^{m} P_i^u \mathbf{y}(n - \frac{M+2i-1}{2}) \\ \sum_{i=2}^{m} P_i^u \mathbf{y}(n - \frac{M+2i-1}{2}) \\ \vdots \\ 0 \\ \vdots \\ \sum_{i=2}^{m} P_i^l \mathbf{y}(n + \frac{M+2i-1}{2}) \\ \sum_{i=1}^{m} P_i^l \mathbf{y}(n + \frac{M+2i-1}{2}) \end{bmatrix}}_{Bias} + \underbrace{\begin{bmatrix} \mathbf{v}(n - \frac{M-1}{2}) \\ \mathbf{v}(n - \frac{M-3}{2}) \\ \vdots \\ \mathbf{v}(n) \\ \vdots \\ \mathbf{v}(n + \frac{M-3}{2}) \\ \mathbf{v}(n + \frac{M-1}{2}) \end{bmatrix}}_{\mathbf{v}(:,n)}, \tag{2.6}$$

where, the correlation matrix $\mathcal{P}$ of dimension $MK \times MK$ is diagonal dominant due to the correlation property of the signature codes. A three-users example of $\mathcal{P}$, with $M = 5$, $m = 2$ and $L = 3$ is given in Figure 2.2, which depicts diagonal dominance.

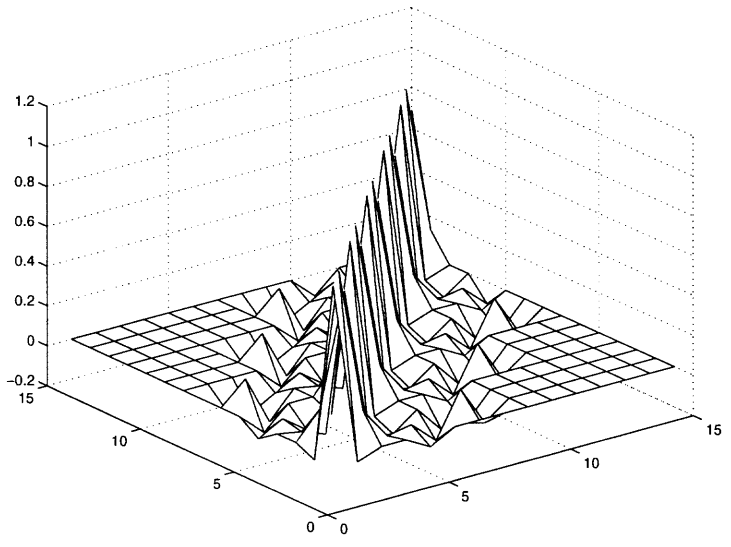

Figure 2.2 An example of the extended correlation matrix, showing diagonal dominance

Equation (2.6) indicates that if the sequence length M is large enough, the midterm of $\mathbf{x}(:, n)$, i.e. $\mathbf{x}(n)$, has zero bias. It is obvious that the signal data can be recovered by taking the inverse of matrix $\mathcal{P}$ and applying it to $\mathbf{x}(:, n)$:

$$\mathbf{y}(:, n) = \mathcal{P}^{-1}\mathbf{x}(:, n) - \mathcal{P}^{-1}Bias - \mathcal{P}^{-1}\mathbf{v}(:, n) \tag{2.7}$$

Due to the diagonal dominant property of matrix $\mathcal{P}^{-1}$, bias has the smallest effect on the midterm of $\mathbf{y}(:,n)$, $\mathbf{y}(n)$. We call performing $\mathcal{P}^{-1}\mathbf{x}(:,n)$ and choosing its midterm a de-biasing detection.

To achieve de-biasing detection, the symbol stack M must increase when the delay m increases. As a result, the calculation of the inverse of $\mathcal{P}$ becomes more challenging. When m is not very large, it is proposed to use a block matrix approach to simplify this calculation as described in section 2.2.

2.2 Simplified De-biasing Method for Small Maximum Path Delay m

Here, two cases of m are discussed.

2.2.1 $m = 2$

Using equation (2.6) and for a delay $\tau_{max} < 2T$ $(m = 2)$, it can be shown that, to minimize the bias effect to $\mathbf{y}(n)$, the minimum number of stacked symbols M is 5. In this case, only the mid-term of the bias is zero, and is given as,

$$\mathbf{x}(:,n) = \begin{bmatrix} P & P_1^l & P_2^l & 0 & 0 \\ P_1^u & P & P_1^l & P_2^l & 0 \\ P_2^u & P_1^u & P & P_1^l & P_2^l \\ 0 & P_2^u & P_1^u & P & P_1^l \\ 0 & 0 & P_2^u & P_1^u & P \end{bmatrix} \mathbf{y}(:,n) + Bias + \mathbf{v}(:,n). \tag{2.8}$$

To simplify the inverse matrix calculation, $\mathcal{P}$ is grouped to form a new block matrix

$$\mathcal{P} = \begin{bmatrix} P & P_1^l & P_2^l & 0 & 0 \\ P_1^u & P & P_1^l & P_2^l & 0 \\ P_2^u & P_1^u & P & P_1^l & P_2^l \\ 0 & P_2^u & P_1^u & P & P_1^l \\ 0 & 0 & P_2^u & P_1^u & P \end{bmatrix} = \begin{bmatrix} P & A & 0 \\ A^T & \hat{P} & B^T \\ 0 & B & P \end{bmatrix} \tag{2.9}$$

, where,

$$\hat{P} = \begin{bmatrix} P & P_1^l & P_2^l \\ P_1^u & P & P_1^l \\ P_2^u & P_1^u & P \end{bmatrix}; A^T = \begin{bmatrix} P_1^u \\ P_2^u \\ 0 \end{bmatrix}; B^T = \begin{bmatrix} 0 \\ P_2^l \\ P_1^l \end{bmatrix}.$$

Then,

$$\begin{aligned}\mathbf{x}(:,n) &= [\mathbf{x}^T(n-2),\mathbf{x}^T(n-1),\mathbf{x}^T(n),\mathbf{x}^T(n+1),\mathbf{x}^T(n+2)]^T \\ &\triangleq \begin{bmatrix}\mathbf{x}(n-2)\\ \hat{\mathbf{x}}(n)\\ \mathbf{x}(n+2)\end{bmatrix} = \begin{bmatrix}P & A & 0\\ A^T & \hat{P} & B^T\\ 0 & B & P\end{bmatrix}\begin{bmatrix}\mathbf{y}(n-2)\\ \hat{\mathbf{y}}(n)\\ \mathbf{y}(n+2)\end{bmatrix} + Bias + \mathbf{v}(:,n).\end{aligned} \tag{2.10}$$

Using the partial matrix inverse lemma, a simplified expression can be derived,

$$\hat{\mathbf{y}}(n) = [\hat{P} - A^T P^{-1} A - B^T P^{-1} B]^{-1}[-A^T P^{-1} : I : -B^T P^{-1}]\mathbf{x}(:,n) \tag{2.11}$$

where, $\hat{\mathbf{y}}(n)$ is the de-biasing detection of $[\mathbf{y}^T(n-1),\mathbf{y}^T(n),\mathbf{y}^T(n+1)]^T$. The mid-term vector of $\hat{\mathbf{y}}(n)$, of dimension K, i.e. $\mathbf{y}(n)$, is the de-biasing detection output. It can be sent to a hard limiter for the final symbol decision when BPSK modulation is employed.

The output $\hat{\mathbf{y}}(n)$ contains redundant information about the desired data. In fact, the data stream might be arranged into a matrix form:

$$\begin{bmatrix}\mathbf{y}(n-1) & \mathbf{y}(n) & \mathbf{y}(n+1) & \mathbf{y}(n+2) & \cdots\\ \mathbf{y}(n) & \mathbf{y}(n+1) & \mathbf{y}(n+2) & \mathbf{y}(n+3) & \cdots\\ \mathbf{y}(n+1) & \mathbf{y}(n+2) & \mathbf{y}(n+3) & \mathbf{y}(n+4) & \cdots\end{bmatrix}.$$

Back diagonal averaging for de-biasing output $\hat{\mathbf{y}}(n)$ will make use of the desired information contained in the different positions, and may provide improved detection performance.

2.2.2 $m = 3$

Extending the same approach to a maximum path delay less than 3T ($m = 3$) is straight forward. Here, the structure of the block matrix is presented.

From equation (2.6), it can be shown that the minimum number M is 7 to minimize the bias effect to $\mathbf{y}(n)$. To simplify the calculation of the inverse matrix $\mathcal{P}^{-1}$, the block matrix inverse lemma is used. The matrix $\mathcal{P}$ is grouped as follows,

$$\mathcal{P} = \begin{bmatrix}\tilde{P} & A & 0\\ A^T & \hat{P} & B^T\\ 0 & B & \tilde{P}\end{bmatrix}, \tag{2.12}$$

where the elements of the block matrix $\mathcal{P}$ are:

$$\tilde{P} = \begin{bmatrix} P & P_1^l \\ P_1^u & P \end{bmatrix}; A = \begin{bmatrix} P_2^l & P_3^l & 0 \\ P_1^l & P_2^l & P_3^l \end{bmatrix}; B = \begin{bmatrix} P_3^u & P_2^u & P_1^u \\ 0 & P_3^u & P_2^u \end{bmatrix}, \tag{2.13}$$

and $\hat{P}$ is given as before. Then, the detector's output becomes:

$$\hat{\mathbf{y}}(n) = [\hat{P} - A^T\tilde{P}^{-1}A - B^T\tilde{P}^{-1}B]^{-1}[-A^T\tilde{P}^{-1} : I : -B^T\tilde{P}^{-1}]\mathbf{x}(:,n). \tag{2.14}$$

The final decisions are therefore based on the detector's outputs.

2.3 Iterative Solution

Consider again the linear relation in equation (2.6):

$$\mathbf{x}(:,n) = \mathcal{P}\mathbf{y}(:,n) + Bias + \mathbf{v}(:,n). \tag{2.15}$$

a few iterative methods can be applied for solving the linear equations. Unlike the decorrelating detector, which requires cumbersome inverse matrix computation of the correlation matrix $\mathcal{P}$, iterative algorithms provide computational simplicity with promising detection performance provided that the algorithms converge fast enough to the steady-state solution.

2.3.1 Richardson's Method

One iterative method to solve the linear equations is by Richardson [44] in which the $(p+1)$-th iterative output for the n-th symbol is given as:

$$\begin{aligned} \mathbf{y}_{p+1}(:,n) &= \mathbf{y}_p(:,n) + \mu[\mathbf{x}(:,n) - \mathcal{P}\mathbf{y}_p(:,n)] \\ &= (I - \mu\mathcal{P})\mathbf{y}_p(:,n) + \mu\mathbf{x}(:,n), \end{aligned} \tag{2.16}$$

where, μ is a step size, that controls the convergence rate. When equation (2.16) reaches the steady state, the detection output is the hard decision of $\mathbf{y}_{p+1}(:,n)$.

The iterative Richardson's algorithm can also use the Gauss-Seidel method to improve the convergence rate. Instead of using the p-th iterative output $\mathbf{y}_p(:,n)$ in

equation (2.16), the Gauss-Seidel method suggests using the most recent estimates of $\mathbf{y}_{p+1}(:,n)$ to replace previous estimates during the $(p+1)$-th iteration:

$$\begin{aligned} y_{p+1}(l,n) &= y_p(l,n) + \mu\{x(l,n) - \sum_{m<l} \mathcal{P}(l,m) y_{p+1}(m,n) \\ &\quad - \sum_{m \geq l} \mathcal{P}(l,m) y_p(m,n)\} \end{aligned} \tag{2.17}$$

for $l = 0, 1, ..., MK-1$. The $x(l,n)$ and $y_p(l,n)$ refer to the l-th element of vector $\mathbf{x}(:,n)$ and $\mathbf{y}_p(:,n)$, respectively. The convergence rate comparison of the two algorithms is shown in Figure 2.3, where 3 users, each with 3 paths are used. It is clear that the Richardson + Gauss-Seidel method converges faster than Richardson's method because it exploits more available information.

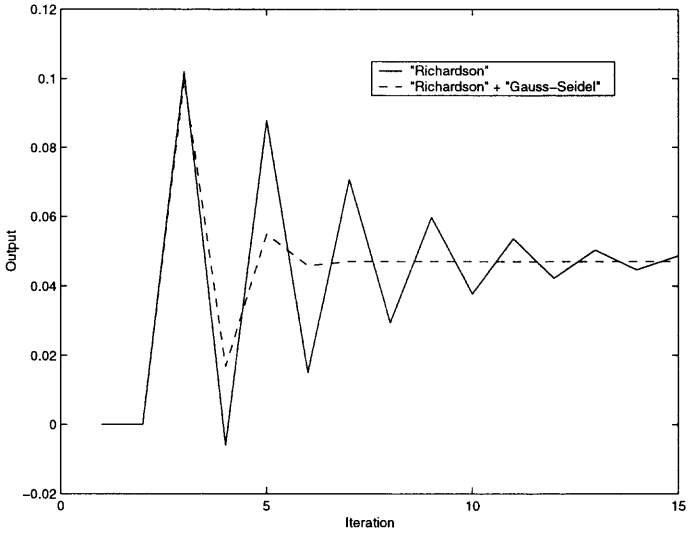

Figure 2.3 Convergence rate comparison with two algorithms

2.3.2 Convergence Analysis

Since matrix $\mathcal{P}$ is invertable, we can define $\mathbf{y}^*(:,n)$ by

$$\mathbf{y}^*(:,n) = \mathcal{P}^{-1}\mathbf{x}(:,n) \tag{2.18}$$

At each stage of iteration, the estimation error $\mathbf{e}_p$ is equal to $\mathbf{e}_p = \mathbf{y}_p(:,n) - \mathbf{y}^*(:,n)$. Using equation (2.16), it is easy to obtain that

$$\mathbf{e}_{p+1} = (I - \mu\mathcal{P})\mathbf{e}_p = (I - \mu\mathcal{P})^p\mathbf{e}_1 \tag{2.19}$$

The matrix $\mathcal{P}$ is Hermitian, i.e. $\mathcal{P} = \mathcal{P}^H$. By applying eigenvalue decomposition (EVD), the matrix $\mathcal{P}$ can be written as

$$\mathcal{P} = Q_{\mathcal{P}}\Lambda_{\mathcal{P}}Q_{\mathcal{P}}^H \tag{2.20}$$

where the diagonal matrix $\Lambda_{\mathcal{P}} = diag([\lambda_0, \lambda_1, ..., \lambda_{MK-1}])$ with λ_i the eigenvalues of $\mathcal{P}$, and the column vectors of the matrix $Q_{\mathcal{P}}$ are the corresponding eigenvectors, which satisfies $Q_{\mathcal{P}}^H Q_{\mathcal{P}} = I$. Therefore, equation (2.19) becomes

$$\mathbf{e}_{p+1} = Q_{\mathcal{P}}(I - \mu\Lambda_{\mathcal{P}})^p Q_{\mathcal{P}}^H\mathbf{e}_1 \tag{2.21}$$

For convergence, equation (2.21) should approach zero when p increases. This results in the following condition

$$|1 - \mu\lambda_l| < 1 \qquad => \qquad 0 < \mu < \frac{2}{\lambda_l} \tag{2.22}$$

for all eigenvalues $\lambda_l, l = 0, ..., MK - 1$. Therefore, μ must satisfy,

$$0 < \mu < \frac{2}{\max\{\lambda_l\}} \tag{2.23}$$

2.4 Bootstrap Adaptive Detection and Gain Estimation for Wideband Rayleigh Fading Channel

From the above derivation, it is clear that due to the inversion of the extended correlation matrix $\mathcal{P}$ the calculation complexity of the debiasing decorrelator grows rapidly with increasing M. Also, due to the fading channel characteristics, it is very difficult to track changes of the channel for updating the matrix $\mathcal{P}$. It is suggested to use the adaptive bootstrap decorrelator instead of the fixed decorrelator for a wideband fading channel.

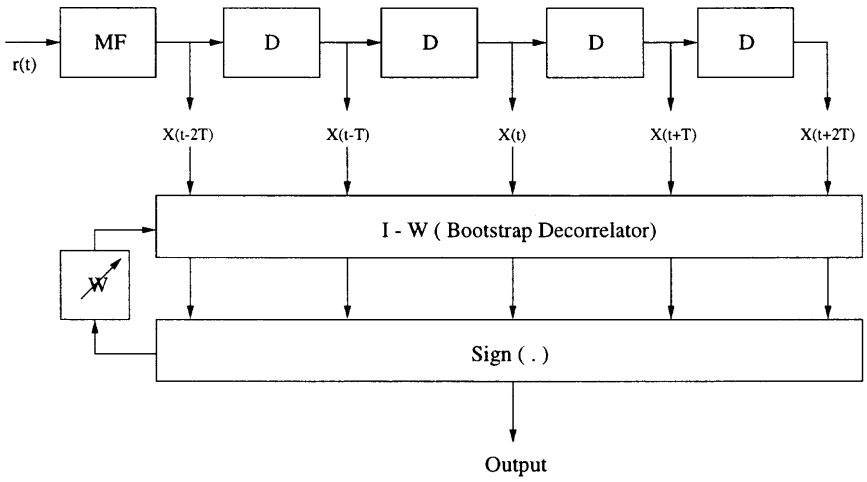

Figure 2.4 Bootstrap structure for maximum delay less than 2T and M=5

The bootstrap structure has been shown to be a robust decorrelator in low signal to interference and noise ratio environments [41]. It is an adaptive algorithm that requires no training sequence. For a multiuser system with a multipath channel, it is represented in matrix form as,

$$\hat{\mathbf{y}}(:,n) = (I - W)\mathbf{x}(:,n) \tag{2.24}$$

where, $\hat{\mathbf{y}}(:,n)$ is the decorrelator output and $\mathbf{x}(:,n)$ is the output of multi-shot matched filters with M symbols stacked. I is the $MK \times MK$ identity matrix. W is an $MK \times MK$ matrix with diagonal elements equal to zero. The recursive algorithm for the other elements in W is,

$$w_{a,b}(n+1) = w_{a,b}(n) + \mu y(a,n) sign(y(b,n)) \tag{2.25}$$

In [43], a simplified channel gain estimation scheme was proposed, which uses the correlation of each path's matched filter output x_{kl} with bit decision $\hat{b}_k$ to estimate each path's channel fading γ_{kl}. The block diagram for such an estimation is given in Figure 2.5.

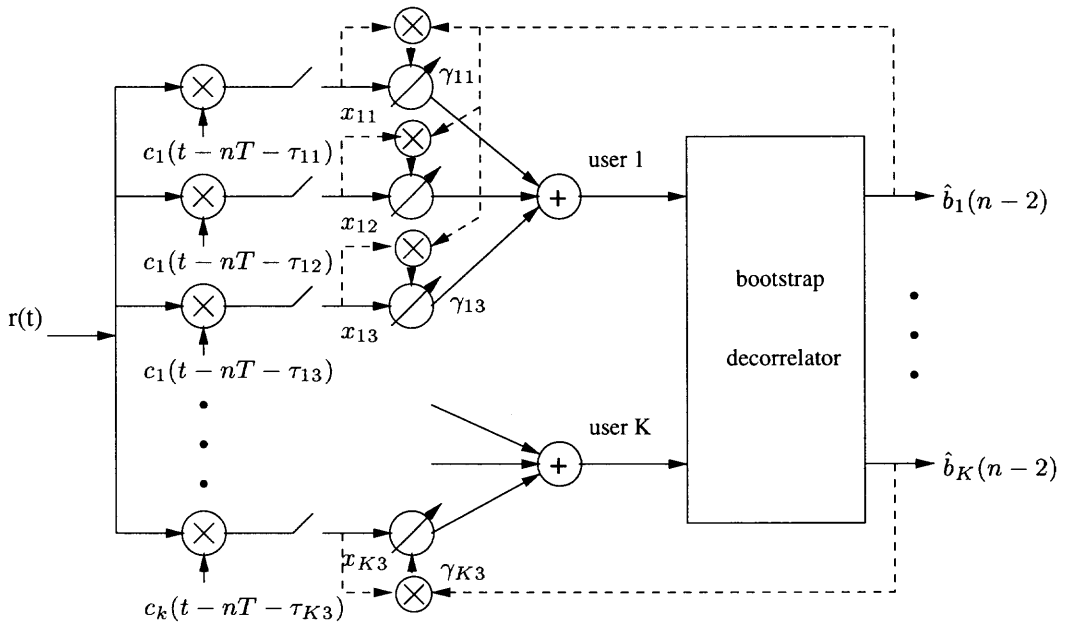

Figure 2.5 Receiver structure with channel gain estimation algorithm. 3 multipaths are assumed, and M=5.

In Figure 2.5,

$$\begin{aligned} E[x_{kl}(n)\hat{b}_k(n)] &= E[\{\int_{nT+\tau_{min}}^{(n+1)T+\tau_{max}} r(t)c_k(t-nT-\tau_{kl})dt\}\hat{b}_k(n)] \\ &\approx \sqrt{a_k}(\gamma_{kl}(n)+\sum_{i=1,i\neq l}^{L}\rho_{li}\gamma_{ki}(n))E[b_k(n)\hat{b}_k(n)], \end{aligned} \tag{2.26}$$

where, it is assumed that the probability of error of user k, i.e. P_{ek}, is sufficiently small such that $b_k(n) \approx \hat{b}_k(n)$ and MAI is suppressed due to its approximate uncorrelation with $\hat{b}_k(n)$. The correlation ρ_{li} is,

$$\rho_{li} = \int_{nT+\tau_{min}}^{(n+1)T+\tau_{max}} c_k(t-nT-\tau_{kl})c_k(t-nT-\tau_{ki})dt. \tag{2.27}$$

It is easy to show that

$$E[b_k(n)\hat{b}_k(n)] = 1-2P_{ek}, \tag{2.28}$$

Then, (2.26) becomes:

$$E[x_{kl}(n)\hat{b}_k(n)] \approx \sqrt{a_k}(1-2P_{ek})(\gamma_{kl}(n)+\sum_{i=1,i\neq l}^{L}\rho_{li}\gamma_{ki}(n)). \tag{2.29}$$

Since $\sqrt{a_k}(1-2P_{ek})$ is the same for all paths of user k, $E[x_{kl}(n)\hat{b}_k(n)]$ is used as the estimation of the channel gain for each path. The estimation accuracy depends on the partial correlation between different paths, and P_{ek}. They need to be small to ensure an acceptable estimate. To adaptively track the time variant fading channel, the following recursive equation is proposed:

$$\hat{\gamma}_{kl}(n) = \lambda\hat{\gamma}_{kl}(n-1) + x_{kl}(n-2)\hat{b}_k(n-2). \tag{2.30}$$

In the steady state, the mean $E[\hat{\gamma}_{kl}(n)] = E[x_{kl}(n-2)\hat{b}_k(n-2)]/(1-\lambda) = E[x_{kl}(n)\hat{b}_k(n)]/(1-\lambda)$. When channel fading varies according to section 1.1.1, the recursive algorithm in equation (2.30) provides the estimation of channel gain $\gamma_{kl}(n)$. The coefficient $(1-\lambda)$ is the same for different paths of user k, and can be removed with normalization before $\hat{\gamma}_{kl}(n)$ is used for MRC combining.

2.5 Simulation Results and Conclusion

In simulations, three users with three paths for each user were used. Gold codes with length $N = 15$ were chosen as signature waveforms. The bit signal-to-noise ratio of the desired user, defined as

$$SNR = 10log_{10}\frac{a_1}{2\sigma^2} \tag{2.31}$$

was set to 8 dB. Considering the spreading gain with a code length of 15, the chip SNR is about 11.8 dB lower. For simplicity, the channel was assumed invariant for the de-biasing detector such that the delays remained constant and the extended correlation matrix $\mathcal{P}$ remained unchanged.

Different detection methods were compared. De-biasing (mid) detection made decisions based on the mid-bit of de-biasing output vector $\hat{\mathbf{y}}(:,n)$. De-biasing (ave) detection used a diagonal averaging process. As a comparison, the bootstrap detector was also applied to the same channel. A random delay distribution was used in the simulations and all the results were based on averaging over the different delays.

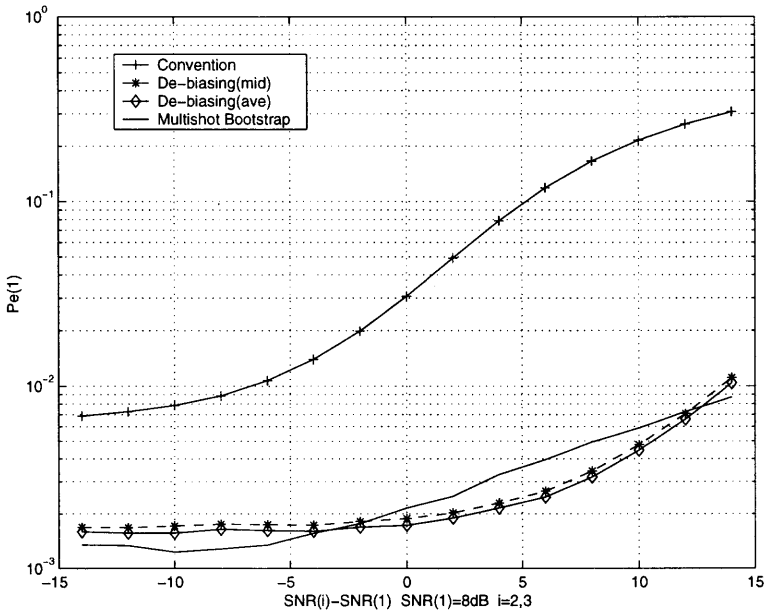

Figure 2.6 De-biasing and bootstrap approach with maximum delay$< 2T$. SNR(1) is desired user's signal-to-noise ratio and SNR(2) and SNR(3) is of interference

Simulations for the bit error rate were run for $M = 5$ and $M = 7$ symbol stacks for a maximum delay of 2T or 3T respectively. Figure 2.6 and 2.7 show that de-biasing detection and bootstrap detection have better performance than the conventional matched filter over a large range of interference strength. Note that, even when the interference energy is very small, the proposed detection algorithms have a significantly lower BER than the conventional detector. The reason is that when the delay spread is assumed to be more than one symbol interval, there is the possibility that the delay difference between different paths of the desired user is an integer multiple of the symbol interval, i.e. $|\tau_{kl_1} - \tau_{kl_2}| = jT, l_1 \neq l_2$ and j is integer. In such a situation, the matched filter detector suffers a dramatical performance loss due to severe ISI, while the proposed de-biasing detectors or bootstrap detector, which exploits the correlation between different paths and users, can effectively remove the ISI. As a result, the proposed detectors significantly outperform the matched filter detector.

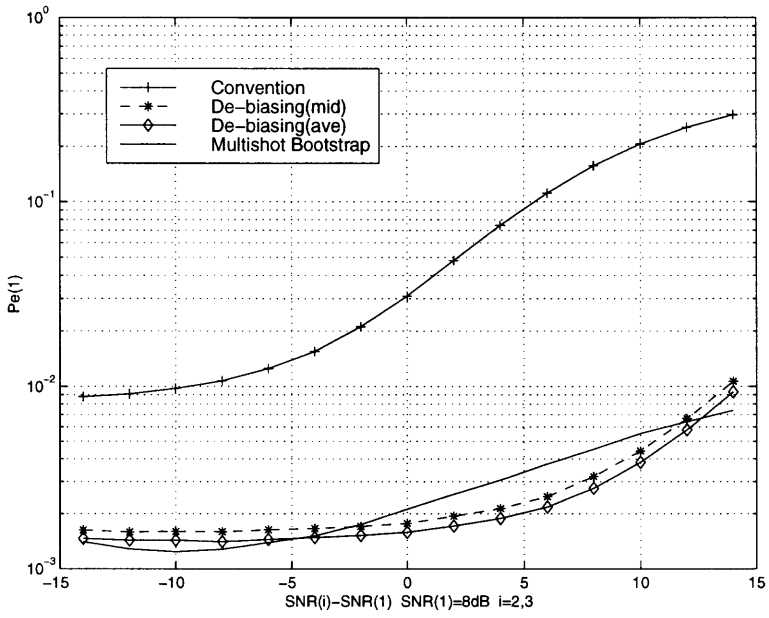

Figure 2.7 De-biasing and bootstrap approach with maximum delay$< 3T$

This explanation is emphasized in Figure 2.8. Here, the maximum path delay spread was limited to within one symbol interval while for the de-biasing detector it employed the scheme assuming maximum delay$\leq 2T$. Since the delay difference $|\tau_{kl_1} - \tau_{kl_2}| < T$, the most detrimental delay pattern, i.e. integer multiples of the symbol interval, does not occur. Therefore, the conventional detector and de-biasing detector both approach the same BER when the interference energy decreases. However, the latter still exhibits significantly greater near-far resistance. In conclusion, the de-biasing detector provides improved performance in large delay spread environments at the expense of complexity. Figure 2.9 depicts detection performance with the Richardson + Gauss-Seidel method. It provides comparable performance with de-biasing and bootstrap algorithm as shown in Figure 2.6 and 2.7.

Clearly the performance of the de-biasing detector can be improved by reducing the effect of the bias, which is achieved with a large stacking size M. In Figure 2.10,

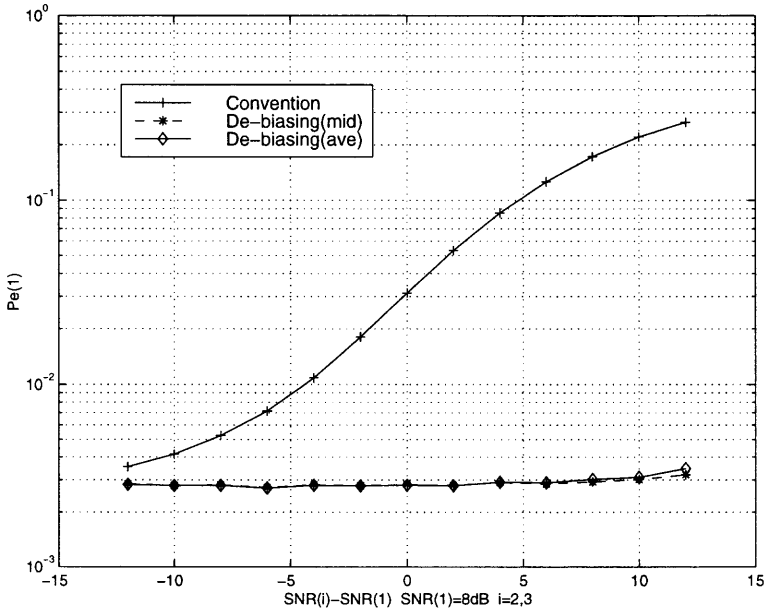

Figure 2.8 Apply maximum delay$< 2T$ de-biasing detector to maximum delay$< T$

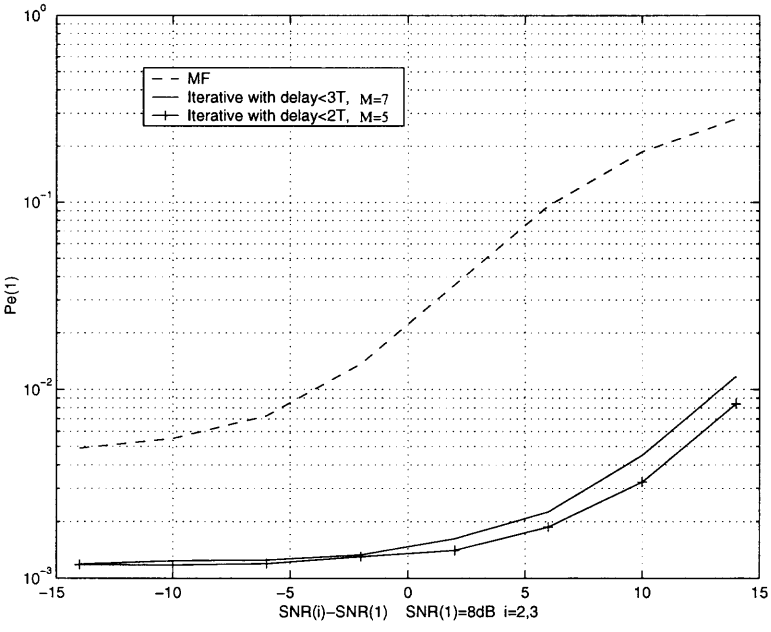

Figure 2.9 Detection performance with Richardson and Gauss-Seidel methods

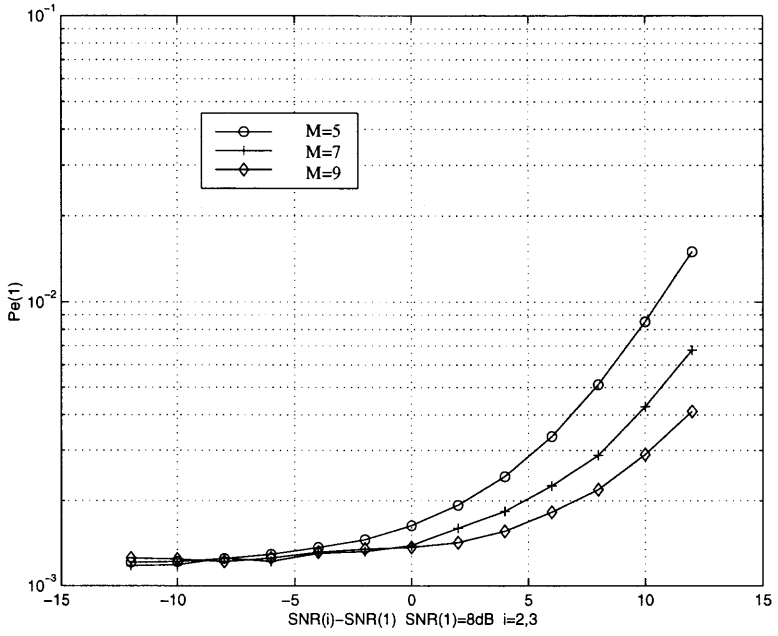

Figure 2.10 Comparison of maximum delay< $2T$ detector with different stacking length M

the performance of the de-biasing detector is shown for different M with a maximum delay< $2T$. The selection of M is a trade-off between detector performance and complexity.

If the maximum delay is over 3T, the calculation of the correlation matrix $\mathcal{P}$ and its inverse become prohibitively complicated. Fortunately, the signals with larger delay usually suffer significant propagation attenuation and can thus be ignored for most applications.

In Figure 2.11, the bootstrap detector with the channel estimator given in section 2.4 was also evaluated using a time-variant channel as described in previous chapter. The BER performance is compared using equal gain combining (EGC), maximal ratio combining (MRC) with the actual channel gains, and MRC with adaptive gain estimation. The bootstrap detector with actual channel gain used shows comparable performance as the detectors in Figure 2.6 for the time invariant channel. However, the bootstrap detector with MRC and adaptive channel

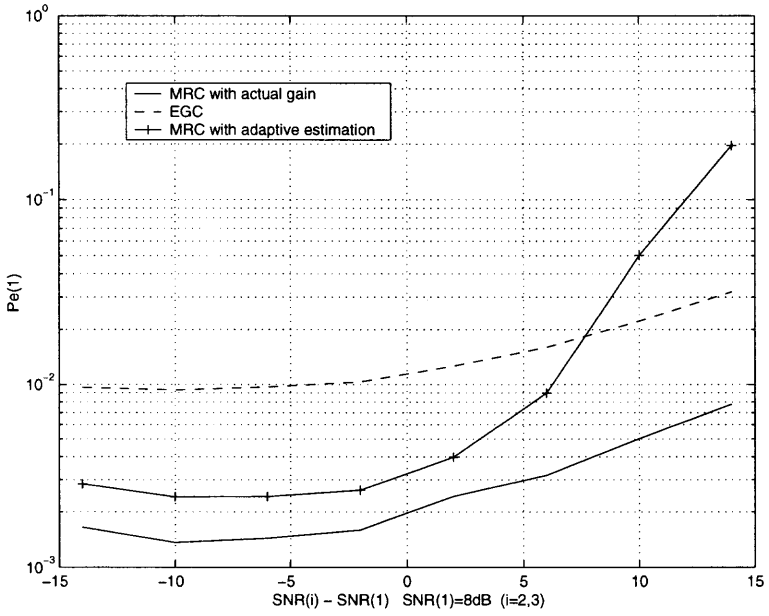

Figure 2.11 Bootstrap with equal gain, maximum ratio combining and combining with estimated channel gain in Rayleigh fading environment. Maximum delay$< 2T$

estimation only works well when the interference is not very high. When the interference SNR is more than 5dB greater than the desired user's SNR, the estimation loop of the desired user's channel gain becomes unstable causing the detection performance to degrade quickly. A reason for such instability is that with stronger interference, the correlation outputs of the adaptive estimator contain a large residue of the interference, which introduces positive feedback into the adaptive estimation process. If MAI at the matched filter output can be reduced before performing channel estimation, the aforementioned instability could be eliminated. It will be shown later that with a minimum variance based channel gain estimator a stable and accurate estimation can be obtained even in a high near-far ratio environment.

CHAPTER 3

M-ARY QAM RECEIVER IN TIME VARIANT FREQUENCY SELECTIVE RAYLEIGH FADING CDMA ENVIRONMENT

Third generation systems with bandwidths as large as 5MHz have been proposed by UMTS/IMT-2000 [45, 46], in which a mix of data transmission types should be supported to provide high data rate services. M-ary quadrature modulation may be used in a CDMA system to achieve high spectral efficiency [47, 31].

The challenge in an asynchronous time variant frequency selective fading environment is that of handling amplitude and phase shift variation caused by the channel. Particularly, with an M-ary modulated signal these variation will distort the original signal constellation and thus deteriorate the receiver performance. To correctly detect the M-ary signals it is essential to recover and use the channel gain and phase shift in the detector.

In this chapter, the focus is on a z-transform based decorrelating detector [48] for M-ary modulated signal detection. Unlike the regular decorrelator which stacks a number of symbols and calculates the inverse of the extended correlation matrix, only the inverse of a partial correlation matrix, which has a reduced dimension, is used. Also, the required truncation of an infinite-impulse-response (IIR) structure, to a practical length finite-impulse-response (FIR) structure causes no significant performance loss. To reduce the phase distortion blindly, the use of a bootstrap phase corrector is proposed. Again, the decision aided channel estimator of Chapter 2 is also used here for MRC combining. However, to avoid possible positive-feedback, it is moved from the input of the bootstrap decorrelator to the output of the FIR decorrelator. This modification results in a stable channel estimate in severe near-far situation, though at the expense of increased complexity of the decorrelator.

3.1 M-ary Quadrature Amplitude Modulated Signal

To mathematically deal with M-ary QAM modulation, the signal will be represented in complex form. The I and Q rails of the signal are spread by different codes and carry independent data streams. The received signal is

$$r(t) = \sum_{n} \sum_{k=1}^{K} b_k(n)\sqrt{a_k} \sum_{l=1}^{L_k} \gamma_{kl}(n) e^{j\theta_{kl}} c_k(t - nT - \tau_{kl}) + v(t), \tag{3.1}$$

where $b_k(n)$ is complex valued with its real and imaginary part belonging to the set $\{-(\sqrt{M}-1), -(\sqrt{M}-3), ..., (\sqrt{M}-3), (\sqrt{M}-1)\}$. In addition, $c_k(t)$ is a complex signature waveform of the form $c_{kI}(t) + jc_{kQ}(t)$, where $c_{kI}(t)$ and $c_{kQ}(t)$ are spreading codes used for the k-th user's I and Q rails. Let θ_{kl} be the phase shift associated with the l-th path of the k-th user. The phase shifts of all paths from one particular user are assumed to be the same, i.e. θ_k. This is reasonable as the difference among these phase shifts, caused by different path delays, can be compensated at the matched filter stage since the delays are assumed known. To fairly evaluate the performance, the real fading coefficient γ_{kl} is normalized [48] such that the signal-to-noise ratio remains unchanged:

$$\sum_{l=1}^{L} E[\gamma_{kl}^2(n)] = 1 \qquad 1 \leq k \leq K.$$

Here, it is assumed that the delays of the received signals, τ_{kl}, are known accurately and that the maximum path delay ($\max \tau_{kl}$) is less than T. The scheme can be extended to larger delay spreads in a straight forward manner. Using a multishot matched filter bank [39], to correlate the received signal during the interval $[\tau_{kl},\ T + \tau_{kl}]$ for each path and each user with the corresponding code, its output is as follows:

$$\begin{aligned} \mathbf{x}(n) \;=\; & P_1^u \Gamma(n-1) A \Theta \mathbf{b}(n-1) + P\Gamma(n) A \Theta \mathbf{b}(n) + P_1^l \Gamma(n+1) A \Theta \mathbf{b}(n+1) \\ & + \mathbf{v}(n), \end{aligned} \tag{3.2}$$

where matrix A is defined in Chapter 2, Γ(n) is a real valued channel gain matrix which contains the amplitudes of the channel gains:

$$\Gamma^T(n) = \begin{bmatrix} \gamma_{11}(n) & \cdots & \gamma_{1L}(n) & & & & & & \\ & & & \gamma_{21}(n) & \cdots & \gamma_{2L}(n) & & & \\ & & & & & & \cdots & & \\ & & & & & & & \gamma_{K1}(n) & \cdots & \gamma_{KL}(n) \end{bmatrix}_{K \times KL} \tag{3.3}$$

And, $\mathbf{x}(n) = [x_{11}(n), ..., x_{1L}(n), ..., x_{K1}(n), ..., x_{KL}(n)]^T$, where x_{kl} is the multi-shot matched filter output of the l-th path of the k-th user. Phase matrix $\Theta = diag(e^{j\theta_1}, e^{j\theta_2}, ..., e^{j\theta_K})$ which is assumed static during adaptive phase correction period.

Assume $\mathbf{c}^T(t) = [c_1(t-\tau_{11}), \cdots, c_1(t-\tau_{1L}), c_2(t-\tau_{21}), \cdots, c_K(t-\tau_{KL}]$, then the correlation matrix is

$$\begin{aligned} P &= \frac{1}{2}\int \mathbf{c}(t)\mathbf{c}^H(t)dt; \\ P_1^u &= \frac{1}{2}\int \mathbf{c}(t-T)\mathbf{c}^H(t)dt = \frac{1}{2}\int \mathbf{c}(t)\mathbf{c}^H(t+T)dt \triangleq P_1; \\ P_1^l &= \frac{1}{2}\int \mathbf{c}(t+T)\mathbf{c}^H(t)dt = P_1^H, \end{aligned} \tag{3.4}$$

and the noise output is

$$\mathbf{v}(n) = \frac{1}{2}\int v(t+nT)\mathbf{c}^H(t)dt, \tag{3.5}$$

where the coefficient "$\frac{1}{2}$" is to normalize the auto-correlation to 1. The channel given in Chapter 1 doesn't fade fast such that $\Gamma(n-1), \Gamma(n)$, and $\Gamma(n+1)$ could be treated as the same, i.e. $\Gamma(n-1) = \Gamma(n+1) = \Gamma(n)$. Taking the Z-transform of equation (3.2), the matched filter output $\mathbf{x}(n)$ then becomes,

$$\mathbf{x}(z) = [P_1^H z + P + P_1 z^{-1}][\Gamma A \Theta \mathbf{b}](z) + \mathbf{v}(z), \tag{3.6}$$

where $[\Gamma A \Theta \mathbf{b}](z)$ is the combined z-transform of $[\Gamma A \Theta \mathbf{b}](n)$. Assuming that each of the received signals corresponding to different propagation paths is independent,

the inverse filter of $[P_1^H z + P + P_1 z^{-1}]$ exists and can be used to decorrelate the matched filter outputs $\mathbf{x}(z)$. That is, the z-transform $\mathbf{y}(z)$ of the output $\mathbf{y}(n) = [y_{11}(n), \cdots, y_{1L}(n), y_{21}(n), \cdots, y_{KL}(n)]^H$ is given by,

$$\mathbf{y}(z) = H(z)\mathbf{x}(z) = [\Gamma A \Theta \mathbf{b}](z) + \mathbf{v}_o(z) \tag{3.7}$$

where $H(z) = [P_1^H z + P + P_1 z^{-1}]^{-1}$ is the decorrelator's transfer function, and $\mathbf{v}_o(z) = H(z)\mathbf{v}(z)$ is the noise output. With an estimate of the channel gain $\Gamma(n)$, the output of the MRC combiner is:

$$\hat{\mathbf{y}}(n) = \Gamma^T(n)\mathbf{y}(n) \tag{3.8}$$

3.2 FIR Decorrelator

Since the correlation matrix P is non-singular, the transfer function $H(z)$ can be expanded into an infinite series form with the relation $(1+a)^{-1} = \sum_{i=0}^{\infty}(-a)^i$:

$$\begin{aligned} H(z) &= \{I + P^{-1}[P_1^H + P_1 z^{-2}]z\}^{-1} \cdot P^{-1} \\ &= (\sum_{i=0}^{\infty}\{-P^{-1}[P_1^H + P_1 z^{-2}]z\}^i) \cdot P^{-1}. \end{aligned} \tag{3.9}$$

It is obvious that the time response of the decorrelator is noncausal. In practice, such a noncausal IIR filter can be replaced by an FIR filter through delay and truncation. This truncated FIR version of the decorrelator is realizable, however, inevitably introduces decision errors which affect its performance.

Let $k_t > 0$ denote the delay for the truncation, then

$$\begin{aligned} z^{-k_t}\mathbf{y}(z) &= z^{-k_t}H(z)\mathbf{x}(z) \\ &\approx z^{-k_t}(\sum_{i=0}^{k_t}\{-P^{-1}(P_1^H + P_1 z^{-2})z\}^i) \cdot P^{-1}\mathbf{x}(z) + z^{-k_t}\mathbf{v}_o(z) \\ &= (\sum_{i=0}^{k_t}\{-P^{-1}(P_1^H + P_1 z^{-2})\}^i z^{-(k_t-i)}) \cdot P^{-1}\mathbf{x}(z) + z^{-k_t}\mathbf{v}_o(z) \\ &= (\sum_{i=0}^{k_t} H_1^i z^{-(k_t-i)}) \cdot P^{-1}\mathbf{x}(z) + z^{-k_t}\mathbf{v}_o(z) \end{aligned} \tag{3.10}$$

This structure is shown in Figure 3.1, and H_1 is shown in Figure 3.2. The choice of k_t is a trade-off between the detector's performance and system complexity. It will be shown that when $k_t = 4$, the detector provides almost flat near-far resistant performance within a wide range of interference energy.

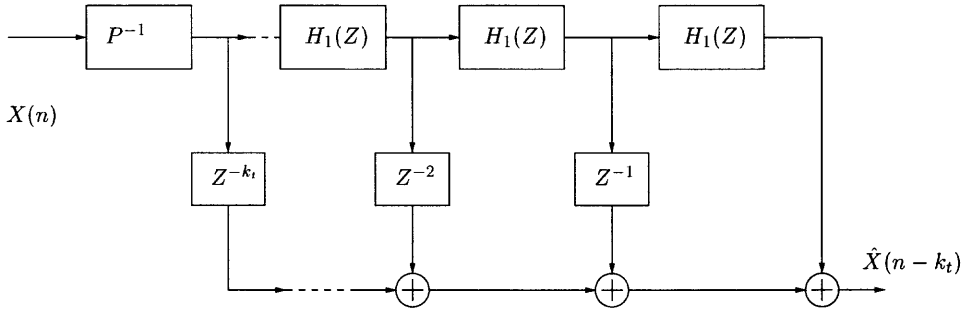

Figure 3.1 FIR decorrelator structure

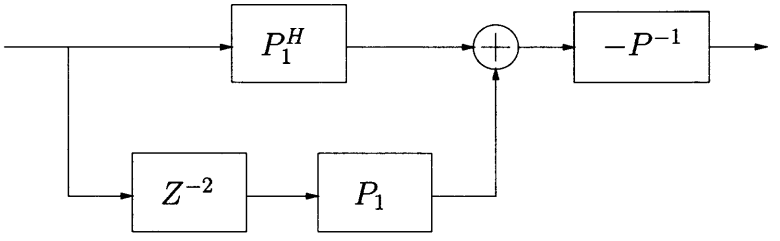

Figure 3.2 H1 structure

3.3 Channel Gain Estimate for M-ary QAM Signals

Here, the channel estimator used in Chapter 2 is extended to M-ary QAM modulated signals. As in Figure 2.5, the estimator uses a correlation between the lth path of the kth user's MF output, x_{kl}, and the MRC output. Here, however, the combining is done at the outputs of the decorrelator (see Figure 3.4). The MRC output is $\hat{b}_k$ with an unknown phase shift θ_k, or $e^{j\theta_k}\hat{b}_k$, such that the output of the correlation is given by,

$$\begin{aligned} E[x_{kl}sgn((e^{j\theta_k}\hat{b}_k)^*)] &= E[\{\int \frac{1}{2}r(t)c_k^*(t-nT-\tau_{kl})dt\}sgn(e^{-j\theta_k})sgn(\hat{b}_k^*)] \\ &= \sqrt{a_k}(\gamma_{kl} + \sum_{m=1,m\neq l}^{L} \rho_{ml}\gamma_{km})E[b_k(n)sgn(\hat{b}_k^*(n))]sgn(e^{-j\theta_k}) \end{aligned}$$

$$= \{\sqrt{a_k}\frac{2}{\sqrt{M/4}}\sum_{i=1}^{\sqrt{M/4}}(2i-1)[1-2Q(\frac{2i-1}{\sigma})]\}$$
$$\cdot(\gamma_{kl}+\sum_{m=1,m\neq l}^{L}\rho_{ml}\gamma_{km})sgn(e^{-j\theta_k}), \tag{3.11}$$

where $sgn(*) = sgn(real(*)) + jsgn(imag(*))$, $Q(x) = \frac{1}{\sqrt{2\pi}}\int_x^\infty e^{-t^2/2}dt$, and the correlation coefficient,

$$\rho_{ml} = \int_{nT}^{(n+2)T}\frac{1}{2}c_k(t-nT-\tau_{km})c_k^*(t-nT-\tau_{kl})dt \tag{3.12}$$

The derivation of (3.11) is given in Appendix A, and uses the fact that data symbols are independent of each other and the noise.

The real part in equation (3.11) can be used to estimate the channel gain of path l of user k if the phase shift θ_k is within $\{-\pi/2, \pi/2\}$. The estimation accuracy is acceptable as long as the correlation, ρ_{ml}, between the different paths is small. A recursive algorithm for $\hat{\gamma}_{kl}$ can be found in equation (2.30).

3.4 Phase Shift Correction

If the phase shift θ_k is not equal to zero, the constellation of the decorrelator's output will be rotated, causing errors in the symbol decision. Hence, to make a correct symbol decision, this phase shift should be removed, before applying it to the decision stage, i.e. the sorter. Let the detector's output be a phase shifted version: $\hat{b}_k e^{j\theta_k}$, where $\hat{b}_k = \hat{b}_{kR} + j\hat{b}_{kI}$ and $e^{j\theta_k} = \alpha_R + j\alpha_I$, then

$$\hat{b}_k e^{\theta_k} = \hat{b}_{kR}\alpha_R - \hat{b}_{kI}\alpha_I + j[\hat{b}_{kR}\alpha_I + \hat{b}_{kI}\alpha_R] \tag{3.13}$$

The bootstrap algorithm has been used in [49] to correct a frequency offset in an OFDM system. Here, it is applied to remove the effect of θ_k. Its structure is shown in Figure 3.3. Assume the bootstrap output $\hat{\hat{b}}_k = \hat{\hat{b}}_{kR} + j\hat{\hat{b}}_{kI}$:

$$\begin{bmatrix}\hat{\hat{b}}_{kR}\\ \hat{\hat{b}}_{kI}\end{bmatrix} = \left(\begin{bmatrix}1 & 0\\ 0 & 1\end{bmatrix} - \begin{bmatrix}0 & w_{12}\\ w_{21} & 0\end{bmatrix}\right)\begin{bmatrix}\hat{b}_{kR}\alpha_R - \hat{b}_{kI}\alpha_I\\ \hat{b}_{kR}\alpha_I + \hat{b}_{kI}\alpha_R\end{bmatrix}$$

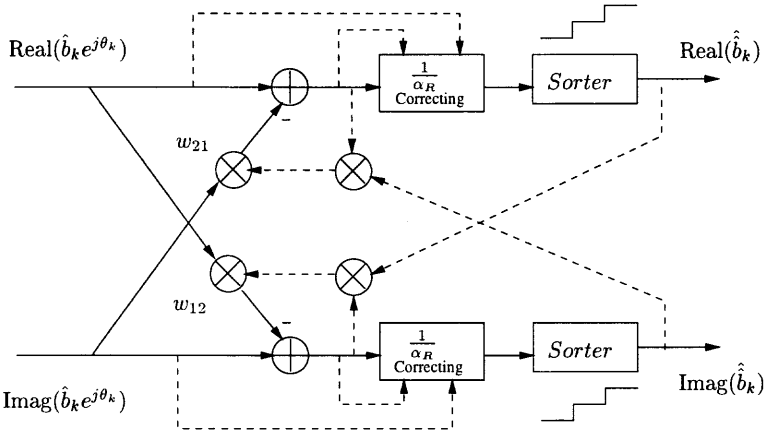

Figure 3.3 Bootstrap phase corrector

$$= \begin{bmatrix} \hat{b}_{kR}(\alpha_R - w_{12}\alpha_I) - \hat{b}_{kI}(\alpha_I + w_{12}\alpha_R) \\ \hat{b}_{kR}(\alpha_I - w_{21}\alpha_R) + \hat{b}_{kI}(\alpha_R + w_{21}\alpha_I) \end{bmatrix} \tag{3.14}$$

If the weight W converges to $w_{12} = -w_{21} = -\frac{\alpha_I}{\alpha_R}$, then, since $\alpha_R^2 + \alpha_I^2 = 1$, the output of the bootstrap becomes,

$$\begin{bmatrix} \hat{\hat{b}}_{kR} \\ \hat{\hat{b}}_{kI} \end{bmatrix} = \frac{1}{\alpha_R} \begin{bmatrix} \hat{b}_{kR} \\ \hat{b}_{kI} \end{bmatrix} \tag{3.15}$$

Equation (3.15) indicates that the phase shift has been eliminated while an amplitude change is introduced. Unlike BPSK, for M-ary QAM modulation, this amplitude change introduces detection errors. For a fading channel, this amplitude distortion can be corrected together with readjusting the channel gain.

The weight W is updated using the following adaptive algorithm:

$$\begin{aligned} w_{12} &= w_{12} + \mu * imag(\hat{\hat{b}}_k) * sorter(real(\hat{\hat{b}}_k)) \\ w_{21} &= w_{21} + \mu * real(\hat{\hat{b}}_k) * sorter(imag(\hat{\hat{b}}_k)). \end{aligned} \tag{3.16}$$

where the $sorter(\cdot)$ gives multi-level hard decision for M-ary signals. It was found that using $sorter(\cdot)$ to replace $sgn(\cdot)$ in [12] results in faster convergence and better performance. A major reason lies in the fact that more information about the desired signals is involved in the sorter's outputs which increase the convergence rate.

3.5 Symbol Sorter

The transmitter and propagation channel's gain is unknown to the receiver. Hence, an M-ary quadrature modulated data symbols' constellation will be distorted in amplitude when they travel over the radio channel. An amplitude equalizer is therefor needed at the receiving side to return the constellation to its original size. Note that, the phase distortion of the channel is compensated separately through phase shift correction. Thus, the only remaining distortion is an unknown amplitude gain g_k for user k. In time-variant fading channel, g_k will be a time-variant coefficient.

Let z_k be the k-th user's input to the sorter, which is an un-equalized complex signal. The unknown factor g_k is equal to

$$g_k = \sqrt{E[|z_k|^2]} \tag{3.17}$$

To estimate g_k in a time-variant environment, a time sliding window with M inputs of z_k is used:

$$\hat{g}_k = \sqrt{\frac{1}{M}\sum_{n=1}^{M}|z_k(n)|^2} \tag{3.18}$$

The constellation is then normalized by dividing z_k by the estimation value $\hat{g}_k$, and the constellation size is corrected to its original value. The detector's structure incorporating all above functions is shown in Figure 3.4.

3.6 Simulation Results and Conclusions

In the simulations, three active users each with three paths are used. Length 31 Gold codes are chosen as the signature waveforms. The signal to noise ratio of the desired user to AWGN is set to 12dB for a 16-QAM signal. Also, random delay spread was

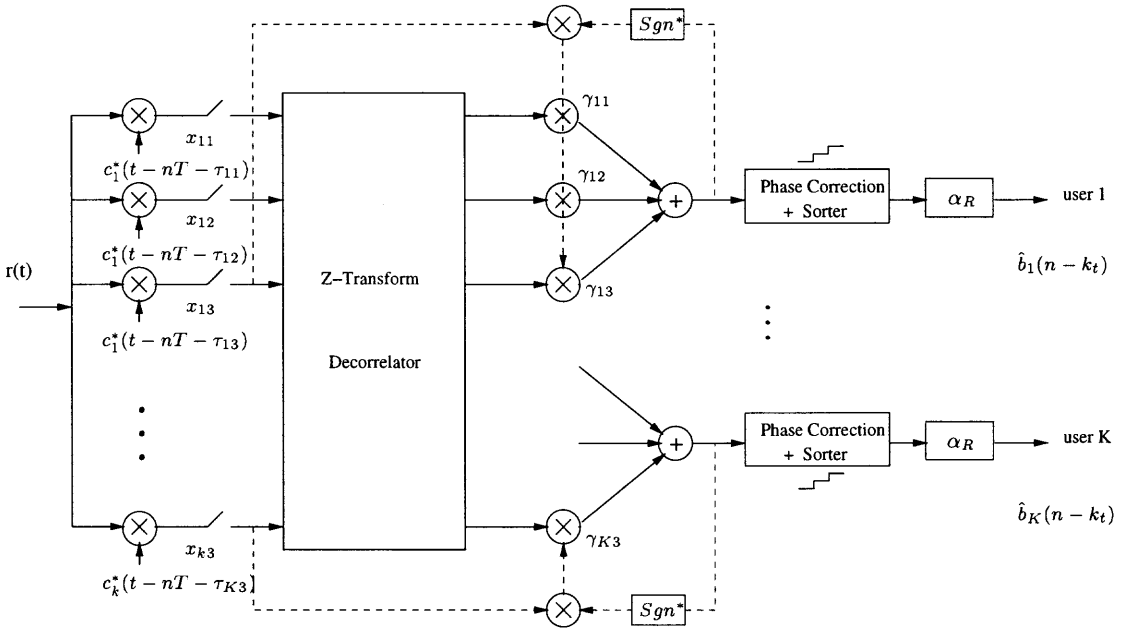

Figure 3.4 Receiver structure

used in simulations with maximum delay within one symbol interval, and the results are based on averaging over the different delays.

Figures 3.5 and 3.6 show the result of phase correction using the bootstrap algorithm, with a phase shift $\theta_k = 0.2rad/s$. The phase was corrected blindly.

Figure 3.7 depicts the near-far property of the proposed FIR detector with phase corrector. The phase shift was set to $\theta_k = 0.2rad/s$. The detector with $k_t = 4$ provides a pretty flat near-far resistance property. With $k_t = 4$, the detector uses two more sub-blocks of $H_1(z)$ than the detector with $k_t = 2$. The computational requirements linearly increases with the number of sub-blocks, and the stored information bits. While due to the need of inverting of the extended correlation matrix, the computational requirements of time domain decorrelator, discussed in the previous chapter, increases exponentially to the stacked data size. Therefore, the

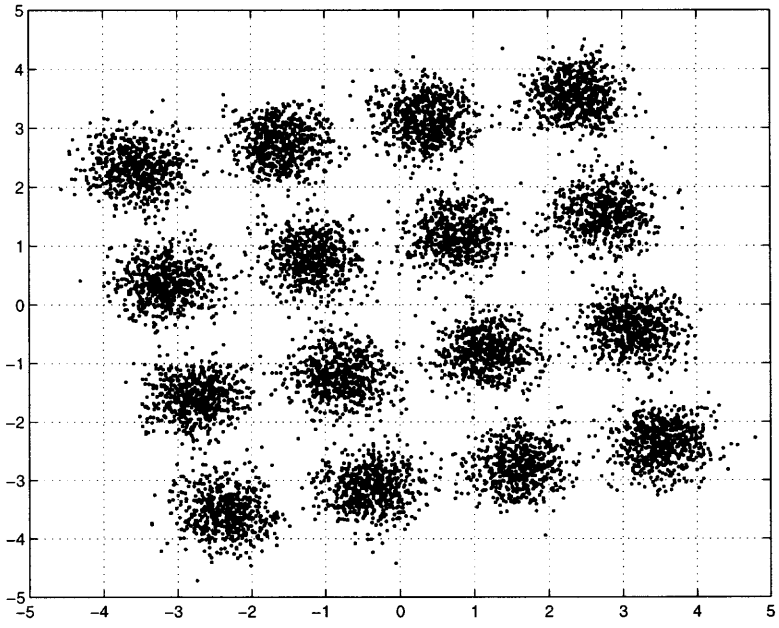

Figure 3.5 Received 16-ary QAM signal before phase correction

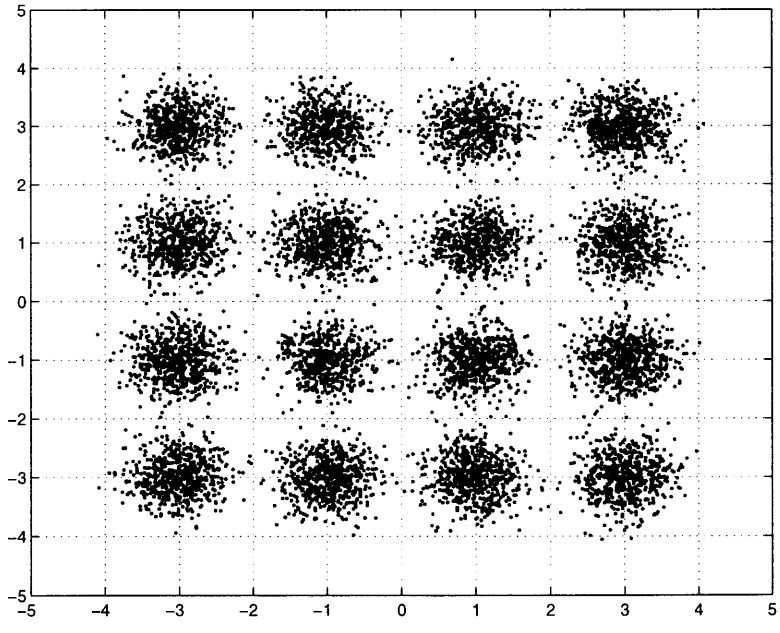

Figure 3.6 Received 16-ary QAM signal after phase correction

detector proposed in this chapter provides a better solution for balancing performance and complexity.

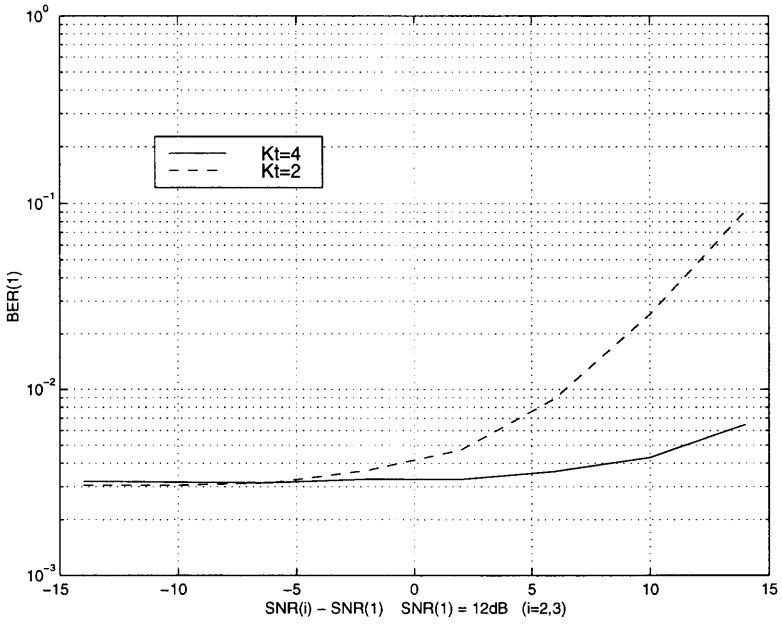

Figure 3.7 BER vs. near-far ratio for a 16-ary QAM signal receiving in Rayleigh fading channel with 0.2rad/s phase shift

In Figure 3.8, interference users' energies were set to be the same as that of the desired user. With both $k_t = 2$ and $k_t = 4$ the detectors present similar performance. This means that, with perfect power control, the performance is less sensitive to k_t than in a severe near-far situation. If the BER performance requirement is not stringent, the detector could use a smaller k_t to obtain a simple implementation.

As the conclusion, the proposed scheme is able to detect M-ary quadrature modulated signals in a time-variant channel with computational complexity increase with the calculation of correlation matrices P and P_1. It brings implementation simplicity when k_t is small. Comparing to Chapter 2, performing MRC combining for decorrelator's outputs presents stable performance under strong interference environment. Obviously, this improvement is at the expense of increased complexity.

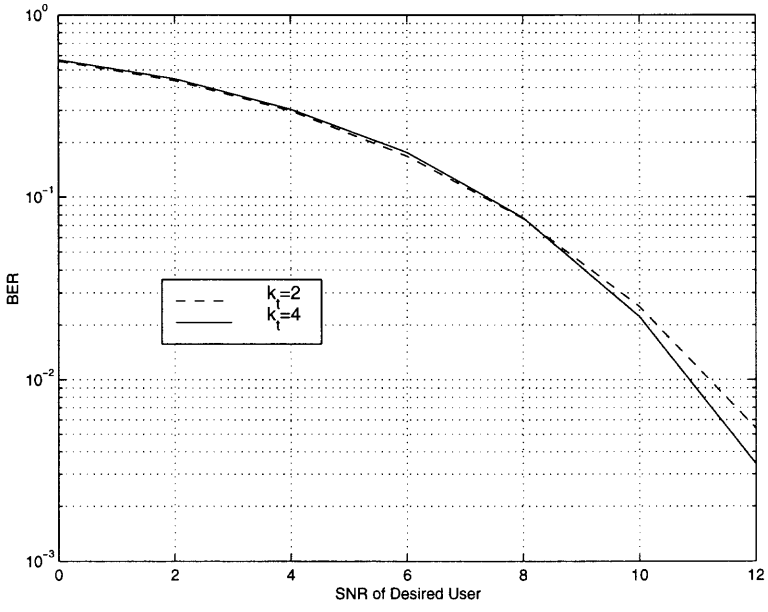

Figure 3.8 BER vs. SNR for 16-ary QAM signal receiving in Rayleigh fading channel with 0.2rad/s phase shift (all signals at same SNR)

CHAPTER 4

MINIMUM VARIANCE DECORRELATING CDMA RECEIVER IN TIME VARIANT FREQUENCY SELECTIVE RAYLEIGH FADING CHANNEL

The minimum variance beamforming criterion has long been applied in adaptive array processing [6, 50]. It minimizes the interference power present in the output, while its constraint allows signal distortion. In [8] on the other hand, a linear decorrelating multipath constraint was used with the goal to separate the desired signal without distortion. A subspace minimum variance decorrelating (MVD) receiver which has reduced complexity by limiting the operation in signal subspace only is derived in [51]. Its performance, however, is sensitive to the estimation accuracy of signal subspace.

An advantage of the MVD receiver is that it requires only a desired user's signature waveform and timing information. It was shown that the MVD receiver, which is in fact a minimum output energy (MOE) [7] based receiver, provides similar performance as an linear MMSE receiver [52] in a quasi-synchronous (delay spread is much smaller than spreading code length) CDMA environment wherein delay is a multiple of chip intervals. However, in practical situations the delay can be much more than just a few chip intervals and non-integer multiples of chip interval. In addition, the channel can suffer deep fading which dramatically deteriorates the performance of the MOE algorithm.

In this chapter, a more general asynchronous situation is considered and it is assumed that the delays are uniformly distributed over one symbol interval. To combat performance loss due to deep channel fading, the MVD based decision aided channel estimator is also derived, which can be shown to be near-far resistant and recover multipath fading if the BER of the decision outputs is small. After decoupling the multipath signals, the transmitted signals can be regenerated using the available information including codewords, delays, and decision outputs. Then, MVD based

adaptive PIC and SIC interference cancellers are applied in this chapter. An MVD based transmit diversity (TD) scheme, named TD-MVD, is also proposed. This scheme enables the multiple transmit antennas to be placed at arbitrary locations even though the signals transmitted from different antennas are asynchronous as long as the path fading remains independent.

4.1 Chip Rate Matched-filter Outputs

Consider the signal model in equation (1.6). It is assumed that the desired signal's delays, τ_{1l}, are limited to within one symbol interval, and not necessarily a multiple of the chip duration. This assumption can be easily extended to more than one symbol interval. Let $\tau_{1l} = (m_l + \delta_l)T_c$ and $\tau_{11} = 0$, where $m_l = \lfloor \frac{\tau_{1l}}{T_c} \rfloor$ is the largest integer no more than $\frac{\tau_{1l}}{T_c}$. And, let $p = \lceil \frac{\tau_{1L}}{T_c} \rceil$, where $\lceil x \rceil$ is the smallest integer which is no less than x. It is assumed that the delays are known at the receiver and that the channel phases are perfectly tracked.

The chip rate MF, which aligns with the first path, samples the entire desired n-th symbol interval $[nT, nT + (N + p)T_c]$ as shown in Figure 4.1.

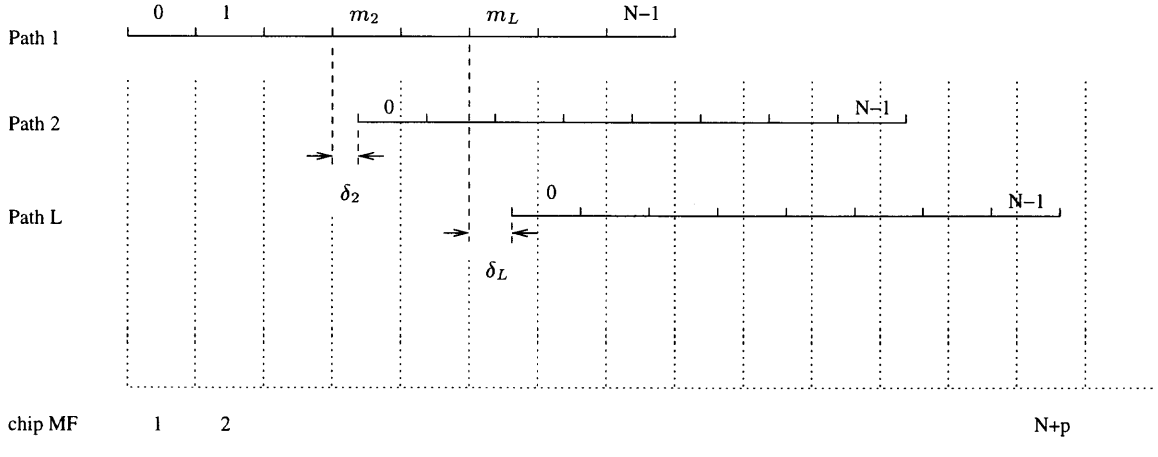

Figure 4.1 Chip rate MF samples of the received signal with misalignment for multipaths except the first path

Then, the output vector $\mathbf{x}(n)$ of the MF at the n-th symbol is given by,

$$\mathbf{x}(n) = C\mathbf{\Gamma}(n)b_1(n) + \mathbf{u}(n), \tag{4.1}$$

where $\mathbf{\Gamma}(n)_{L\times 1}$ is defined as the desired user's channel response vector, which is given as $\mathbf{\Gamma}(n) = [\sqrt{a_1}\gamma_{1,1}(n), \cdots, \sqrt{a_1}\gamma_{1,L}(n)]^T$. Matrix C is the desired signal's code matrix, whose columns are the desired user's code sequences of length N shifted downward by m_l elements, $l = 1, \cdots, L$. It is given as

$$C_{(N+p)\times L} =$$
$$\begin{bmatrix}
g_1(0) & & & \\
\vdots & & & \\
g_1(m_2) & (1-\delta_2)g_1(0) & \cdots & \\
\vdots & (1-\delta_2)g_1(1)+\delta_2 g_1(0) & & \\
g_1(m_L) & \vdots & \cdots & (1-\delta_L)g_1(0) \\
\vdots & \vdots & & (1-\delta_L)g_1(1)+\delta_L g_1(0) \\
g_1(N-1) & \vdots & \cdots & \vdots \\
 & (1-\delta_2)g_1(N-1)+\delta_2 g_1(N-2) & & \vdots \\
 & \delta_2 g_1(N-1) & & (1-\delta_L)g_1(N-1)+\delta_L g_1(N-2) \\
 & & & \delta_L g_1(N-1)
\end{bmatrix}$$

where the coefficients $1-\delta_i$ and δ_i are the misalignment of the chip rate MF with the multipath signals except the first. Each column in the code matrix C contains the propagation delay information corresponding to the related multipath component. Since no multipath signal from one transmit antenna has the same delay, the matrix C has full column rank.

The noise vector $\mathbf{u}(n)$ is composed of ISI, MAI and AWGN. The MVD receiver applies a set of weight coefficients $\mathbf{w}_l$ to decouple the multipaths of the desired signals. That is, the weight matrix $W = [\mathbf{w}_1, \mathbf{w}_2, ..., \mathbf{w}_L]_{(N+p)\times L}$ should satisfy the following linear decorrelating constraint,

$$W^H C = I_{L\times L} \tag{4.2}$$

With condition (4.2), the decorrelator output $\mathbf{y}(n)$ is given by

$$\mathbf{y}(n) = W^H \mathbf{x}(n)$$

$$= \mathbf{\Gamma}(n)b_1(n) + W^H\mathbf{u}(n) \tag{4.3}$$

To achieve the best performance, the weight matrix W, besides satisfying the constraint of (4.2), is chosen to maximize the output SNR. Let

$$\begin{aligned} R_{\mathbf{y}}(n) &= E[\mathbf{y}(n)\mathbf{y}^H(n)] \\ &= \mathbf{\Gamma}(n)\mathbf{\Gamma}^H(n) + W^H R_{\mathbf{u}}(n)W, \end{aligned} \tag{4.4}$$

where it is assumed that the desired symbol of user 1 is uncorrelated with its adjacent information symbols and other users' information symbols. We also defined the noise auto-correlation matrix $R_{\mathbf{u}}(n) = E[\mathbf{u}(n)\mathbf{u}^H(n)]$, and used $E[b_1^2(n)] = 1$ for BPSK modulated signals. The output SNR is obtained from (4.4),

$$SNR = \frac{tr\{\mathbf{\Gamma}(n)\mathbf{\Gamma}^H(n)\}}{tr\{W^H R_{\mathbf{u}}(n)W\}}. \tag{4.5}$$

Since the numerator does not depend on the weight matrix, maximizing the SNR is equivalent to minimizing the noise output energy $tr\{W^H R_{\mathbf{u}}(n)W\}$. From equation (4.4), it is noted that the output energy of the MVD receiver, $tr\{R_{\mathbf{y}}(n)\} = tr\{\mathbf{\Gamma}(n)\mathbf{\Gamma}^H(n)\} + tr\{W^H R_{\mathbf{u}}(n)W\}$. Therefore, minimizing the noise output energy is equivalent to minimizing the decorrelator output energy $tr\{R_{\mathbf{y}}(n)\}$. So, the decorrelating receiver is basically a constrained MOE receiver. Estimation of the matrix $R_{\mathbf{u}}(n)$ requires a desired signal silence period, which needs heavy coordination between the base station and each mobile user. Particularly in a time-variant channel, such coordination should be repeated periodically. Utilizing the claim of the following proposition, instead, $SNR_{\mathbf{x}}$ which includes the desired signal can be used.

Proposition: Assume the SNR of the output of the MVD receiver in the presence of the desired signal is $SNR_{\mathbf{x}}$, and the SNR in the absence of the desired signal is $SNR_{\mathbf{u}}$. Then, with perfect estimation of both $R_{\mathbf{x}}(n)$ and $R_{\mathbf{u}}(n)$, $SNR_{\mathbf{x}} = SNR_{\mathbf{u}}$.

Proof: see Appendix B.

The advantage of using $R_{\mathbf{x}}(n)$ instead of $R_{\mathbf{u}}(n)$ is obvious. Estimation of $R_{\mathbf{x}}(n)$ can be directly obtained from the chip-rate MF output vectors $\mathbf{x}(n)$, which is preferred from an implementation point of view.

From equation (4.3), $R_{\mathbf{y}}(n) = W^H R_{\mathbf{x}}(n) W$. Hence, to maximize the SNR choose W such that,

$$W = arg \min_{W} \{W^H R_{\mathbf{x}}(n) W\} \qquad subject\ to \quad W^H C = I \tag{4.6}$$

Using the Lagrange multipliers as in [6], we define

$$F = W^H R_{\mathbf{x}}(n) W + \lambda (W^H C - I) \tag{4.7}$$

The optimum solution W_o for this constrained minimizing problem is found by taking the derivative of equation (4.7) with respect to W^H and equating to zero:

$$\frac{\partial F}{\partial W^H} = R_{\mathbf{x}}(n) W + \lambda C = 0,$$

which implies,

$$W_o = -R_{\mathbf{x}}^{-1}(n) C \lambda I \tag{4.8}$$

With constraint $W_o^H C = I$,

$$\lambda I = -(C^H R_{\mathbf{x}}^{-1}(n) C)^{-1} \tag{4.9}$$

Replacing λI in equation (4.8) with (4.9), the optimum solution is finally obtained as,

$$W_o = R_{\mathbf{x}}^{-1}(n) C (C^H R_{\mathbf{x}}^{-1}(n) C)^{-1} \tag{4.10}$$

In [8], an adaptive update of W via a standard LMS algorithm was presented. Let the output power of the l-th path

$$J_l(n) = \mathbf{w}_l^H(n) R_{\mathbf{x}}(n) \mathbf{w}_l(n), \qquad l = 1, \cdots, L. \tag{4.11}$$

The gradient of the output power is given by

$$\nabla J_l(n) = 2R_{\mathbf{x}}(n)\mathbf{w}_l(n) \approx 2\mathbf{x}(n)\mathbf{x}^H(n)\mathbf{w}_l(n) \qquad l = 1, \cdots, L \tag{4.12}$$

where, for simplicity, the correlation matrix $R_{\mathbf{x}}(n)$ was approximated by the single sample outer product $\mathbf{x}(n)\mathbf{x}^H(n)$. Considering the constraint $W^H C = I$, the search direction is restricted to the constrained subspace, which is obtained by using the projection of the gradient in (4.12) onto the subspace orthogonal to C. With the orthogonal projection matrix $P^{\perp} = I - C(C^H C)^{-1}C^H$, the recursive algorithm is,

$$\mathbf{w}_l(n+1) = \mathbf{w}_l(n) - \mu P^{\perp}\mathbf{x}(n)\mathbf{x}^H(n)\mathbf{w}_l(n) \qquad l = 1, \cdots, L \tag{4.13}$$

It can be written in matrix form as

$$W(n+1) = W(n) - \mu P^{\perp}\mathbf{x}(n)\mathbf{x}^H(n)W(n) \tag{4.14}$$

It was stated in [8] that using the pseudoinverse of C as the initial value, $W(0)$, $W(n)$ converges to its optimum value (4.10) with probability 1.

The output vector $\mathbf{y}(n)$ consist of the L paths' outputs, which can be combined to obtain a better performance. For MRC combining, the combination coefficients should be found. In [8], the output energies are used as the combination coefficients assuming the output SNRs are very high at all paths.

However, in a time-variant fading channel, using the single sample's outer product $\mathbf{x}(n)\mathbf{x}^H(n)$ to approximate the autocorrelation matrix $R_{\mathbf{x}}(n)$ will introduce a large uncertainty, and dramatically deteriorate the detector's performance. The SNR of the decorrelated multipath outputs can be very low when a channel suffers a deep fade. Thus, using the output energies as combination coefficients will result in performance degradation. As an improvement, here $R_{\mathbf{x}}(n)$ is estimated by an AR low-pass filter with its initial value being $R_{\mathbf{x}}(0) = \mathbf{0}$.

$$\hat{R}_{\mathbf{x}}(n+1) = (1-\mu)\hat{R}_{\mathbf{x}}(n) + \mu\mathbf{x}(n)\mathbf{x}^H(n) \tag{4.15}$$

Therefore, the recursive algorithm for updating $W(n)$ becomes,

$$W(n+1) = W(n) - \mu P^{\perp} \hat{R}_{\mathbf{x}}(n+1) W(n) \tag{4.16}$$

For faster convergence of the recursive updating of weight matrix $W(n)$, the initial value of $W(n)$ is not set to the pseudoinverse of C. Instead, equation (4.10) is used to get the initial value of $W(n)$ after an accurate estimate of $R_{\mathbf{x}}$ is reached using equation (4.15). Thereafter, for every new sample, equation (4.15) is used to update the estimate of $R_{\mathbf{x}}$, and then, $W(n+1)$ is updated according to (4.16).

If channel is steady, i.e. $\hat{R}_{\mathbf{x}}(n+1) = \hat{R}_{\mathbf{x}}(n)$, then

$$\begin{aligned} W(n+1) &= W(n) - \mu[I - C(C^H C)^{-1} C^H] \hat{R}_{\mathbf{x}}(n+1) W(n) \\ &= W(n) - \mu[\hat{R}_{\mathbf{x}}(n+1) \hat{R}_{\mathbf{x}}^{-1}(n) C (C^H \hat{R}_{\mathbf{x}}^{-1}(n) C)^{-1} \\ &\qquad - C(C^H C)^{-1} C^H \hat{R}_{\mathbf{x}}(n+1) \hat{R}_{\mathbf{x}}^{-1}(n) C (C^H \hat{R}_{\mathbf{x}}^{-1}(n) C)^{-1}] \\ &= W(n) \end{aligned} \tag{4.17}$$

The performance is affected by the length of the initial stage to estimate the $R_{\mathbf{x}}$. Also, in [8], using the pseudoinverse of C as the initial value requires an initial stage with $W(n)$ converged to its optimum value. In Figure 4.2, the convergence rate for both schemes is compared. Eight users are assumed, each with the same energy. The SNR is 8dB, and the delays are not an integer multiple of the chip interval. It is shown that the proposed scheme converges faster than the scheme in [8]. In 250 to 300 bits, the BER of the proposed scheme approaches its stable value. Apparently, the improved performance is at the expense of increased computational complexity.

4.2 MVD Based Channel Estimation and MRC Combination

As mentioned before, in [8] the output energy of all paths was combined to approximate MRC under the assumption that the interference and noise were

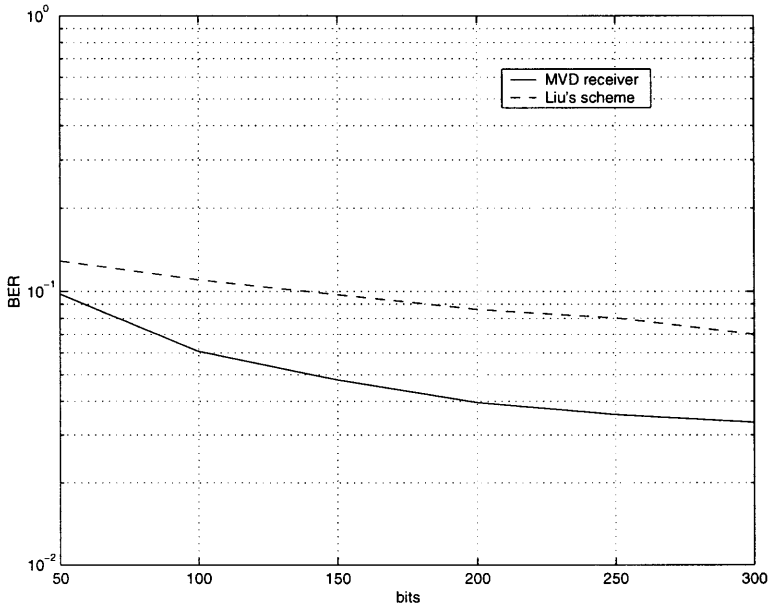

Figure 4.2 Convergence comparison

sufficiently suppressed. However, in a time-variant channel, multipath signals may suffer deep fading, which significantly reduces the output SNR, causing instability in the energy measurement, and hence, deteriorating the combining performance. Instead, a channel gain estimator is derived here to achieve an optimal combination of the outputs.

In equation (4.3), the first term contains the channel response information corresponding to each propagation path. The second term $W^H\mathbf{u}(n)$ consists of the MAI, ISI and background noise, which are uncorrelated with $b_1(n)$ and have zero mean. Due to this extra term, the output energy contains some residue that affects the performance. When applying the decision aided channel estimator, as described in previous chapters (see Section 3.3), a better estimate of the multipath fading coefficients may be obtained, resulting in improved performance.

Let P_e be the output error probability, and consider a BPSK signal. Taking the expectation of the product of $\hat{b}_1(n)$ and the MVD outputs $\mathbf{y}(n)$,

$$E[\mathbf{y}(n)\hat{b}_1(n)] = \mathbf{\Gamma}(n)E[b_1(n)\hat{b}_1(n)] + W^H E[\mathbf{u}(n)\hat{b}_1(n)] \tag{4.18}$$

The second term in equation (4.18) is negligible because different users, symbols, and paths are uncorrelated, resulting in,

$$\begin{aligned} E[\mathbf{y}(n)\hat{b}_1(n)] &\approx \mathbf{\Gamma}(n)E[b_1(n)\hat{b}_1(n)] \\ &= \mathbf{\Gamma}(n)(1-2P_e), \end{aligned} \tag{4.19}$$

where $E[b_1^2(n)] = 1$. If the BER is small, there is an improvement over the results in previous chapters since the ouput contains no fading residues from other multipaths, as is the case in equations (2.29) and (3.11). Therefore, the MVD based channel estimator may be able to provide a more accurate estimate.

The decorrelated desired multipath signals in the output vector $\mathbf{y}(n)$ are combined using the estimated channel gain $\hat{\mathbf{\Gamma}}(n)$. If the desired symbol $b_1(n)$ is a BPSK signal, the final decision is made by

$$\begin{aligned} \hat{b}_1(n) &= sgn\{\hat{\mathbf{\Gamma}}^H(n)\mathbf{y}(n)\} \\ &= sgn\{\hat{\mathbf{\Gamma}}^H(n)W_o^H\mathbf{x}(n)\} \end{aligned} \tag{4.20}$$

For M-ary quadrature modulated signals, a sorter operation should take place. The receiver structure with MRC combining is given in Figure 4.3.

The recursive $\mathbf{\Gamma}(n)$ estimate algorithm is similar to (2.30). Using the correlation in (4.19), it gives

$$\begin{aligned} \hat{\mathbf{\Gamma}}(n+1) &= \lambda\hat{\mathbf{\Gamma}}(n) + \mathbf{y}(n)\hat{b}_1(n) \\ &= \lambda\hat{\mathbf{\Gamma}}(n) + \mathbf{y}(n)sgn\{\hat{\mathbf{\Gamma}}^H(n)\mathbf{y}(n)\} \end{aligned} \tag{4.21}$$

A sample of the estimated channel gain is presented in Figure 4.4, where the ISR is set to 14dB. In initial 200 bits, fading $\hat{\mathbf{\Gamma}}(n)$ is set to be equal for EGC

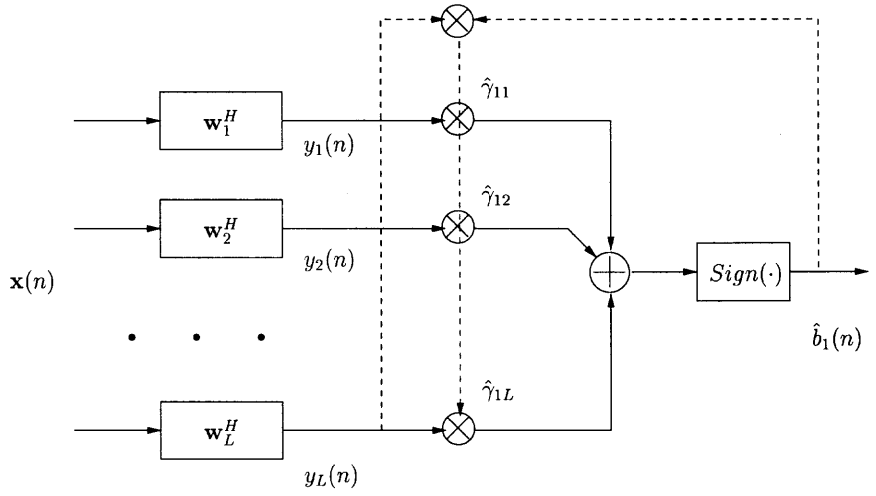

Figure 4.3 Decision feedback estimator and MRC combiner

combining. It shows that the MVD based adaptive algorithm accurately tracks the channel fading. Using an ISR of 14dB suggests that the estimator works well in the presence of MAI. Since the channel estimator provides decorrelated multipath fading, its outputs can be used for further processing, such as signal reconstruction for interference cancellation which will be added later.

In Figure 4.5, a comparison is shown for the proposed MVD receiver using channel estimator outputs or output energy as combining coefficients. The estimate of $R_{\mathbf{x}}$ based on equation (4.15) is used in both schemes. The figure shows that the proposed channel estimator improves the performance in a fading channel.

Note that in the aforementioned discussion, it is assumed that the propagation channel phase response has already been recovered. In case it is not, there are basically two approaches to recover the unknown channel phase shift. One is to periodically use a known sequence instead of the decision output $\hat{b}_1(n)$, which is not available in case of an unknown phase shift exist. This approach requires the channel phase shift to be quasi-static between two training sequences. The other is

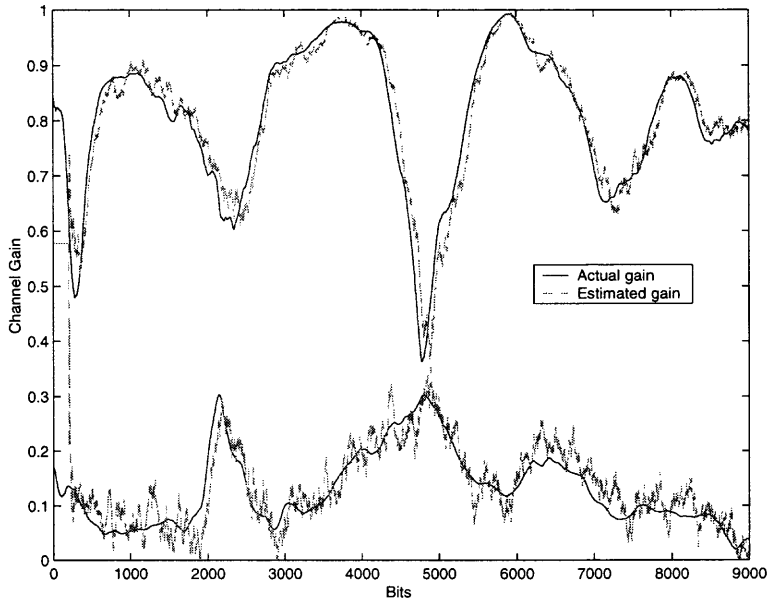

Figure 4.4 Adaptive Channel Gain Estimate (ISR=14dB)

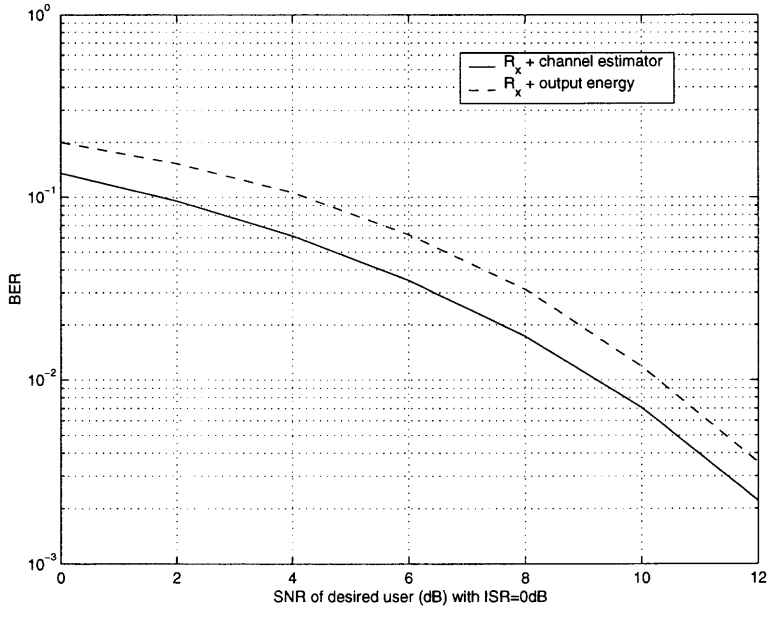

Figure 4.5 Comparison of using channel estimator or output energy in fading channel

to use differentially encoded symbols $b(n)$. This approach, however, may result in a performance loss.

4.3 Performance Comparison

With perfect channel estimation as MRC combining coefficients, and the optimum weight matrix W_o, the MVD receiver's output at the final decision stage is equal to

$$\begin{aligned} z_{MVD} &= \mathbf{\Gamma}^H(n)\mathbf{y}(n) \\ &= \mathbf{\Gamma}^H(n)\mathbf{\Gamma}(n)b_1(n) + \mathbf{\Gamma}^H(n)W_o^H\mathbf{u}(n) \end{aligned} \tag{4.22}$$

Then, the SNR at the output is,

$$\begin{aligned} SNR_{MVD} &= \frac{\|\mathbf{\Gamma}(n)\|^4}{\mathbf{\Gamma}^H(n)W_o^H R_{\mathbf{u}}(n)W_o\mathbf{\Gamma}(n)} \\ &= \frac{\|\mathbf{\Gamma}(n)\|^4}{\mathbf{\Gamma}^H(n)(C^H R_{\mathbf{x}}^{-1}(n)C)^{-1}C^H R_{\mathbf{x}}^{-1}(n)R_{\mathbf{u}}(n)R_{\mathbf{x}}^{-1}(n)C(C^H R_{\mathbf{x}}^{-1}(n)C)^{-1}\mathbf{\Gamma}(n)} \end{aligned} \tag{4.23}$$

The outputs of the conventional matched-filter receiver are obtained by taking the receiver's weight matrix $W_{MF} = C$. Using MRC combining, the output is given as

$$\begin{aligned} z_{MF} &= \mathbf{\Gamma}^H(n)W_{MF}^H\mathbf{x}(n) \\ &= \mathbf{\Gamma}^H(n)C^HC\mathbf{\Gamma}(n)b_1(n) + \mathbf{\Gamma}^H(n)C^H\mathbf{u}(n) \\ &= \|C\mathbf{\Gamma}(n)\|^2 b_1(n) + \mathbf{\Gamma}^H(n)C^H\mathbf{u}(n) \end{aligned} \tag{4.24}$$

The SNR of the MF output is,

$$SNR_{MF} = \frac{\|C\mathbf{\Gamma}(n)\|^4}{\mathbf{\Gamma}^H(n)C^H R_{\mathbf{u}}C\mathbf{\Gamma}(n)} \tag{4.25}$$

Let $\mathbf{w}_{MMSE}$ be the linear MMSE receiver's coefficient vector, which is obtained by minimizing the output mean-square-error (MSE).

$$MSE = E[\|\mathbf{w}_{MMSE}^H\mathbf{x}(n) - b_1(n)\|^2] \tag{4.26}$$

Therefore,

$$\begin{aligned}\mathbf{w}_{MMSE} &= \min_{\mathbf{w}}(MSE) \\ &= \min_{\mathbf{w}} E[(\mathbf{w}^H\mathbf{x}(n) - b_1(n))(\mathbf{w}^H\mathbf{x}(n) - b_1(n))^H] \\ &= \min_{\mathbf{w}}\{\mathbf{w}^H R_{\mathbf{x}}\mathbf{w} - \mathbf{w}^H C\mathbf{\Gamma}(n) - \mathbf{\Gamma}^H(n)C^H\mathbf{w} + 1\} \end{aligned} \tag{4.27}$$

Taking the derivative of the MSE with respect to $\mathbf{w}^*$, and equating the result to zero, it gives

$$\frac{\partial MSE}{\partial \mathbf{w}^*} = R_{\mathbf{x}}\mathbf{w} - C\mathbf{\Gamma}(n) = 0, \tag{4.28}$$

which results in the MMSE solution as

$$\mathbf{w}_{MMSE} = R_{\mathbf{x}}^{-1}(n)C\mathbf{\Gamma}(n) \tag{4.29}$$

So, the output of the linear MMSE is given by,

$$\begin{aligned} z_{MMSE} &= \mathbf{w}_{MMSE}^H\mathbf{x}(n) \\ &= \mathbf{\Gamma}^H(n)C^H R_{\mathbf{x}}^{-1}(n)C\mathbf{\Gamma}(n)b_1(n) + \mathbf{\Gamma}^H(n)C^H R_{\mathbf{x}}^{-1}(n)\mathbf{u}(n) \end{aligned} \tag{4.30}$$

From (4.30), the corresponding output SNR is given by,

$$SNR_{MMSE} = \frac{\|\mathbf{\Gamma}^H(n)C^H R_{\mathbf{x}}^{-1}(n)C\mathbf{\Gamma}(n)\|^2}{\mathbf{\Gamma}^H(n)C^H R_{\mathbf{x}}^{-1}(n)R_{\mathbf{u}}(n)R_{\mathbf{x}}^{-1}(n)C\mathbf{\Gamma}(n)} \tag{4.31}$$

According to [8], the SNR_{MVD} is upper bounded by SNR_{MMSE}, or

$$SNR_{MMSE} \geq SNR_{MVD} \tag{4.32}$$

Comparing equations (4.23) and (4.31), it is found that the equality in equation (4.32) only holds when

$$C^H R_{\mathbf{x}}^{-1}(n)C = \alpha I_{L\times L} \tag{4.33}$$

One particular case assumes only a single path. As a result, the code matrix C becomes the vector $\mathbf{c}_1$, the code word of user 1, and the channel response vector $\mathbf{\Gamma}(n)$

becomes the fading coefficient $\gamma_1(n)$ of this path. Then, using Woodbury's identity

$$\begin{aligned} R_{\mathbf{x}}^{-1}(n) &= \{C\mathbf{\Gamma}(n)\mathbf{\Gamma}^H(n)C^H + R_{\mathbf{u}}(n)\}^{-1} \\ &= R_{\mathbf{u}}^{-1}(n) - \frac{\gamma_1^2(n)R_{\mathbf{u}}^{-1}(n)\mathbf{c}_1\mathbf{c}_1^T R_{\mathbf{u}}^{-1}(n)}{1+\gamma_1^2(n)\mathbf{c}_1^T R_{\mathbf{u}}^{-1}(n)\mathbf{c}_1} \end{aligned} \tag{4.34}$$

Let $\mathbf{c}_1^T R_{\mathbf{u}}^{-1}(n)\mathbf{c}_1 = a$, and consider $\mathbf{c}_1^T\mathbf{c}_1 = 1$, it is easy to show that:

$$\begin{aligned} C^H R_{\mathbf{x}}^{-1}(n)C &= \frac{a}{1+a\gamma_1^2(n)} \\ C^H R_{\mathbf{x}}^{-1}(n)R_{\mathbf{u}}(n)R_{\mathbf{x}}^{-1}(n)C &= \frac{a}{\{1+a\gamma_1^2(n)\}^2} \end{aligned} \tag{4.35}$$

Replacing equations (4.23) and (4.31) with (4.35), it can be shown that both SNR are same, or

$$SNR_{MMSE} = SNR_{MVD} = a\gamma_1^2(n) \tag{4.36}$$

The result is reasonable because, for the single path case, the condition in equation (4.33) is always satisfied. It also implies that the linear MMSE and MVD receiver are equivalent in a single path fading channel.

4.4 Performance Evaluation

In this section the performance of the proposed MVD receiver that uses the estimation of $R_{\mathbf{x}}(n)$ as well as the adaptive channel estimation for MRC combining is compared with several other receivers: MF, MMSE receivers, and Liu's scheme in [8], which employed the output path energies for MRC combining and a single sample's outer product to replace $R_{\mathbf{x}}(n)$. The performance is compared through simulations. Eight simultaneous active users, each with three paths, are used. Length $N = 15$ Gold codes are chosen as the spreading codes. The channel is time-variant using the model described in section 1.1.1. All results are averaged over different combinations of delays that are assumed uniformly distributed in [0,T).

Figures 4.6 and 4.7 show a BER comparisons between the proposed MVD receiver and other receivers as a function of the desired user's SNR. In Figure 4.6

delay is distribution continuous over one symbol interval while in Figure 4.7 the delay is in integer multiples of the chip interval. All interfering users have the same signal energy as the desired user such that the $ISR = 0dB$. Comparing Figures 4.6 and 4.7, shows that the MVD receiver suffers more performance loss than the MMSE receiver when the delays become continuously distributed. However, its performance is still close to the MMSE receiver for both delay distributions, and better than the MF and Liu's scheme [8]. The proposed MVD receiver exploits the same information as the MF receiver, i.e. the desired user's signature waveform and timing information, and does not require a training sequence as is needed by the MMSE receiver.

In Figures 4.8 and 4.9 the receivers' performance is compared in a more severe interference environment where the interference is 14 dB stronger than the desired user. Due to the error in estimating $R_{\mathbf{x}}(n)$ using a single sample, the performance of Liu's scheme [8] deteriorates dramatically while the performance of the proposed MVD receiver remains close to the performance of the MMSE receiver.

4.5 Performance Improvement Using the Modified Autocorrelation Matrix Estimation

The previous section stated that using the autocorrelation matrix $R_{\mathbf{x}}$ instead of $R_{\mathbf{u}}$ is more convenient to implement because $R_{\mathbf{x}}$ can be estimated from the chip MF outputs. It was shown in [53] that the detection performance of the MVD receiver is highly dependent on the estimation accuracy of the autocorrelation matrix. In a time-variant channel, the estimated $R_{\mathbf{x}}$ may suffer a large estimation error due to the limited processing window size, and thus, significantly degrade the receiver's performance.

However, it was shown in [54] that the estimate of the autocorrelation matrix $R_{\mathbf{x}}$ (with the desired signal present) leads to a significant decrease of the SNR at the MVDR output when a limited number of samples is used. With the aid of a

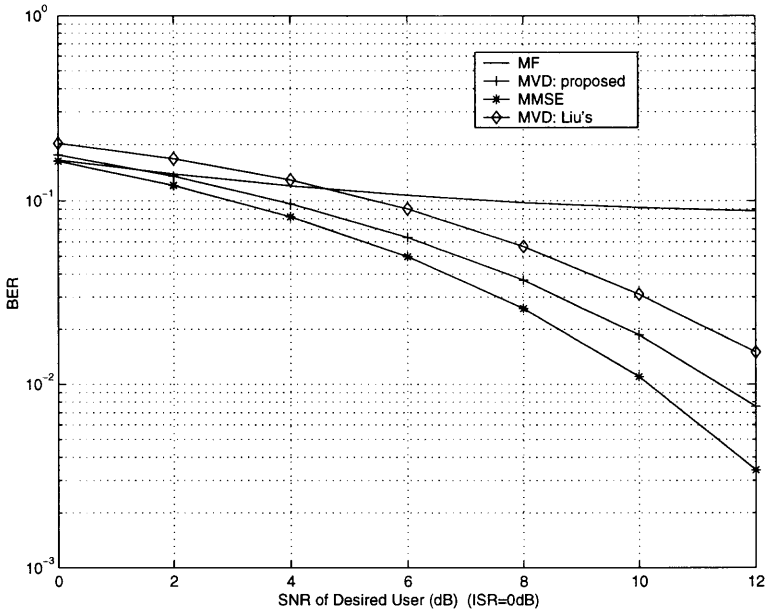

Figure 4.6 Bit error rate vs the desired user's SNR with ISR=0dB (delay not integer multiples of chip interval)

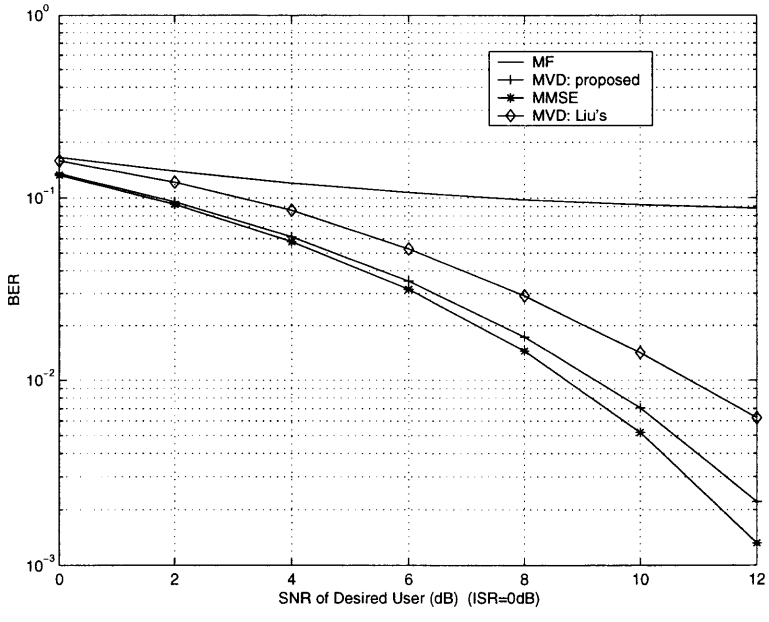

Figure 4.7 Bit error rate vs the desired user's SNR with ISR=0dB (delay being integer multiples of chip interval)

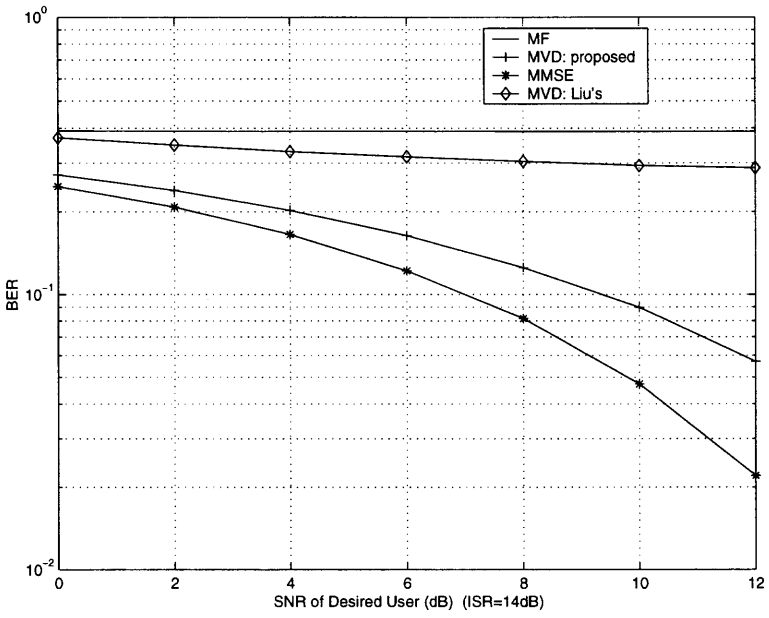

Figure 4.8 Bit error rate vs the desired user's SNR with ISR=14dB (delay not integer multiples of chip interval)

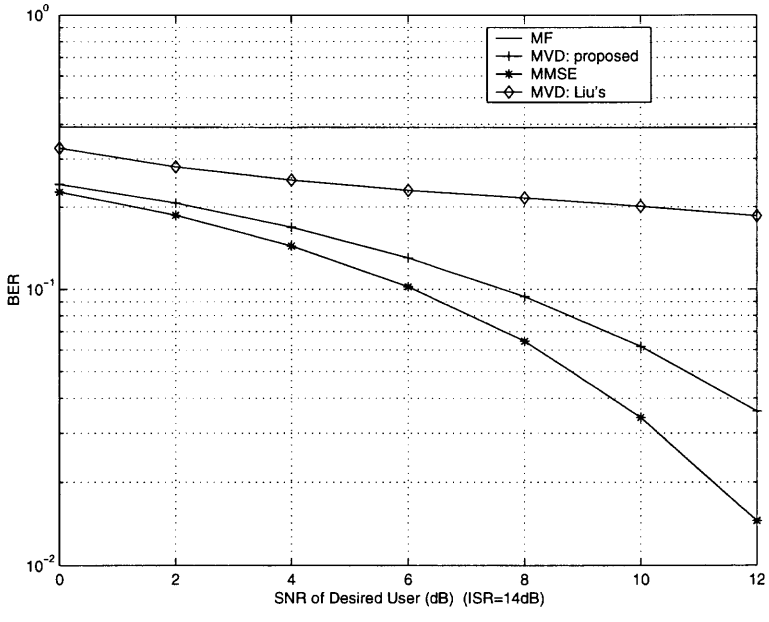

Figure 4.9 Bit error rate vs the desired user's SNR with ISR=14dB (delay being integer multiples of chip intervals)

pilot, the performance was improved by estimating the desired signal absent matrix $R_{\mathbf{u}}$. This motivates the use of the estimation matrix $R_{\mathbf{u}}$ instead of $R_{\mathbf{x}}$ to improve the MVD receiver performance. Obviously, the improvement is at the expense of computational complexity because the estimate of $R_{\mathbf{u}}$ is not obtained directly.

Consider the desired user's multipath fading is provided by the channel estimator, then the desired signal can be reconstructed by exploiting the existing information, which includes the desired signal's spreading code, the multipath delays and the decision outputs. To enhance the performance while minimizing the complexity, it is suggested to not use the estimate of $R_{\mathbf{u}}$ that has to be obtained in the absence of the desired signal. Instead, estimate $R_{\mathbf{x}}$, and therefore the channel response, at an initial stage from which the desired signal is reconstructured. Subtract the estimated desired signal from the received signal to estimate $R_{\mathbf{u}}$. Then, the weight matrix is obtained from $R_{\mathbf{u}}$. This approach removes the complicated coordination between base station and associated subscribers, while making full use of the existing information provided by the proposed MVD receiver. The computational requirements are not significantly increased.

In Figure 4.10, the MVD receiver's performance using an estimated $R_{\mathbf{x}}$ and $R_{\mathbf{u}}$ is compared, where six users are assumed and the delays are integer multiples of the chip interval. The interference energy is equal to the desired signal. Figure 4.10 shows that the proposed $R_{\mathbf{u}}$ estimation scheme provides a performance enhancement in a time-variant fading channel.

The corresponding MVD receiver structure is given in Figure 4.11.

4.6 MVD Based Adaptive Multistage PIC and SIC Detectors

In many references, the building-blocks in multistage structures use rake receivers. Although it is relatively simple, the overall complexity of the receiver is high as it

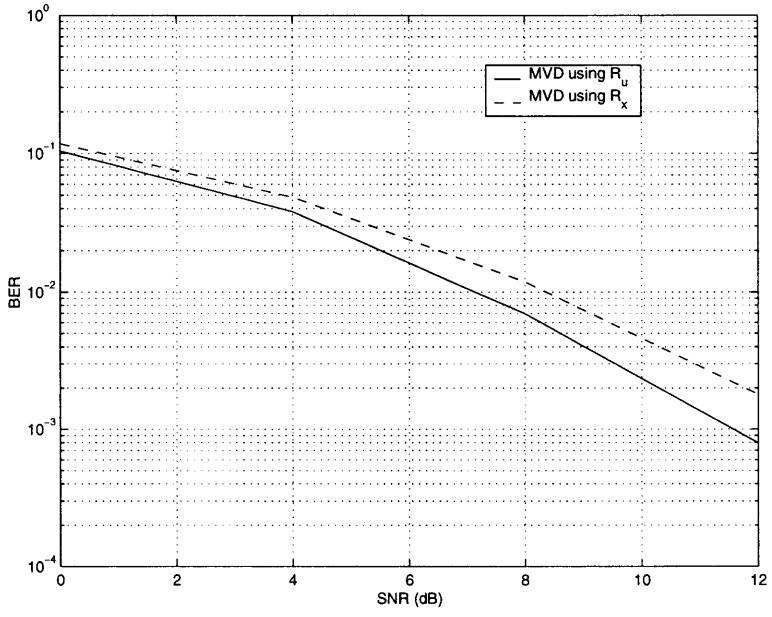

Figure 4.10 Performance comparison with $R_{\mathbf{x}}$ and $R_{\mathbf{u}}$ estimations.

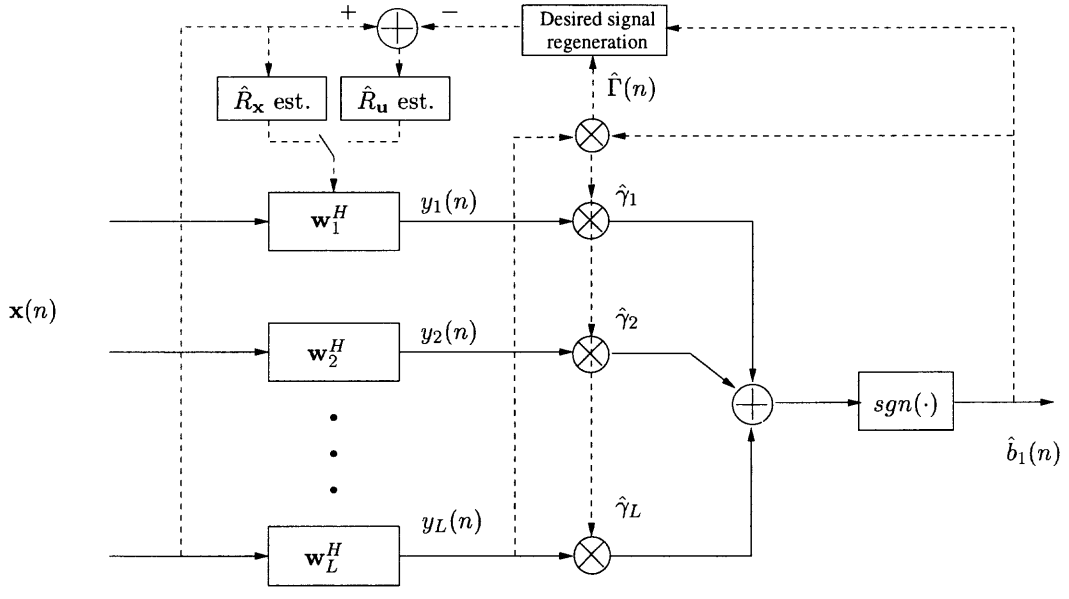

Figure 4.11 MVD receiver with $R_{\mathbf{u}}$ estimation

requires many stages to achieve better performance, due to the inferior performance of the rake receiver in a MAI environment.

Instead, adaptive MVD receiver based multistage IC detectors are proposed here. Since the MVD receiver is a single user detector, and provides an accurate estimate of the multipath fading, it can recover each interfering signal and remove them with an IC scheme. Accurate estimation can be obtained at the first stage as its performance is comparable to a linear MMSE detector. As a result, the following stage will be able to remove a significant amount of interference. Hence, this reduces the number of stages that is required. Also, to keep low implementation complexity, the MVD receiver given in Figure 4.3, not as in Figure 4.11, is used as the building-block.

In this section, after defining the MVD building block, both PIC and SIC based structures are developed separately. Recall that SIC needs to rank the signals in power, which raises a question regarding the use of the SIC structure with perfect power control. In that case, the signal energies of all users are the same, or, equivalently, all SINRs are the same. Hence, there is no significant interference for SIC to cancel first to improve the detection performance for the other users. Therefore, cancellation of any user may not improve the detection performance of the others. Nevertheless, a sufficient condition, for which SIC still performs even with perfect power control will be given in this section.

4.6.1 MVD Building-block Model

Considering the required processing power and the implementation complexity, multistage PIC and SIC schemes are most likely adopted at the base station to simultaneously detect multiple transmitted signals. The channel is then modeled as an asynchronous frequency selective fading channel. For simplicity, it is assumed that the number of resolvable discrete multipaths, L, is the same for all the users.

Delays $0 \leq \tau_{k1} < \tau_{k2} < \cdots < \tau_{kL} < T$, for $k = 1, \cdots, K$, are multiples of the chip interval.

For each user, say user k, the chip rate MF samples the interval in which the n-th symbol is present: $[nT + \tau_{k1}, (n+1)T + \tau_{kL}]$. Then, the output vector $\mathbf{x}(n)$ of the MF at the n-th symbol is given by,

$$\mathbf{x}_k(n) = C_k \mathbf{\Gamma}_k(n) b_k(n) + \mathbf{u}_k(n) \tag{4.37}$$

This is the same as in section 4.1 except that here the code matrix C_k is given by,

$$C_k = \begin{bmatrix} g_k(0) & & \vdots & \\ g_k(1) & & \vdots & \\ \vdots & g_k(0) & \vdots & \\ \vdots & g_k(1) & \vdots & g_k(0) \\ g_k(N-1) & \vdots & \vdots & g_k(1) \\ & g_k(N-1) & \vdots & \vdots \\ & & & g_k(N-1) \end{bmatrix}_{(N+p)\times L} \tag{4.38}$$

with integer $p = (\tau_{kL} - \tau_{k1})/T_c$, $k = 1, \cdots, K$. An MVD receiver, with its structure as shown in Figure 4.3, is then used to detect and re-generate the signal for each user.

4.6.2 PIC Structure

The MVD based multistage PIC structure is shown in Figure 4.12. At the first stage, MVD detectors are employed to detect all user signals. The decision variables $\hat{b}_{1,k}$, $k = 1, \cdots, K$, combined with the channel gain estimates, are used to generate an estimate for every user's signal. All regenerated signal estimates for $i = 1, \cdots, K$, except $i = k$, are subtracted from the received signal $r(t)$. The resulting signal at the i-th branch consists of the i-th user's signal, the background noise, and error noise caused by incorrect interference signal re-generation. This signal is then passed to the next stage for further processing.

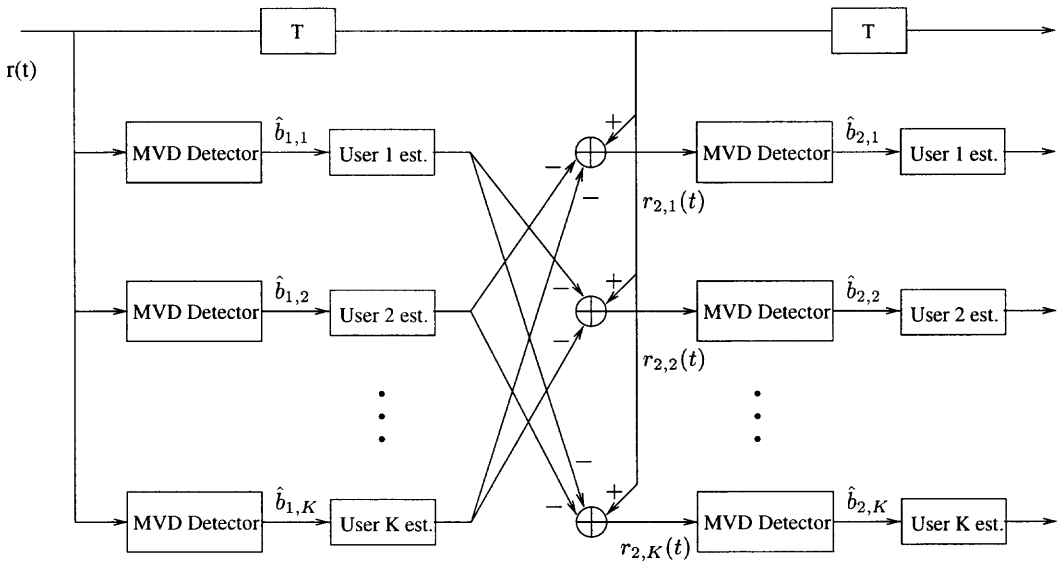

Figure 4.12 PIC structure, each MVD detector with L multipaths.

The input signal to the k-th MVD detector at the m-th stage is

$$r_{m,k}(t) = r(t) - \sum_{i=1,i\neq k}^{K} \sum_{l=1}^{L} \hat{\gamma}_{m-1,il}(n)\hat{b}_{m-1,i}(n)c_i(t - nT - \tau_{il}) \tag{4.39}$$

where $\hat{\gamma}_{m-1,kl}(n)$ is the estimation of the channel gain $\sqrt{a_k}\gamma_{kl}(n)$ at the $(m-1)$-th stage.

With good estimation, it is expected that the SINR in the remainder signal $r_{m,k}(t)$ is improved. Thus, each subsequent stage of the MVD detector is expected to provide better detection performance than the previous one.

Reviewing Figure 4.12, it is clear that the processing delay of every stage is a single symbol interval, and the total delay for an M-stage PIC scheme is M symbol intervals. It is also clear that the processing delay for every user is same.

4.6.3 SIC Structure

The structure of a multistage SIC scheme is given in Figure 4.13, where two successive stages are shown. For the first stage, $r_m(t) = r_1(t) = r(t)$, and other inputs to the adders are set to zero. The signal from every user is detected, re-generated,

and subtracted from the input signal, in a descending order of the different signals' energy, if applicable, or arbitrarily if perfect power control is assumed. After the j-th cancellation at the first stage, what remains are the cancellation noise $\sum_{k=1}^{j}\{s_k(t) - \hat{s}_k(t)\}$, where it is assumed that $s_k(t)$ is the received signal of user k and $\hat{s}_k(t)$ is its estimate, the background Gaussian noise, and the remaining signals. After all K users are canceled, what remains at the outputs of the first stage are the background noise and the compound value of the cancellation errors $\sum_{k=1}^{K}\{s_k(t) - \hat{s}_k(t)\}$. At the following stage, the estimates signal $\hat{s}_k(t)$ of the preceding stage is restored to the input, and the original signal $s_k(t)$ is recovered. However, the total noise is reduced provided accurate cancellation of the interference took place at the preceding stage. Therefore, detection and estimation at the following stage is better, which further reduces the cancellation noise.

In most of the literature dealing with the SIC scheme, the different signals are assumed to have different energy levels. As a result of ordering the interference by energy level, the SIC is supposed to cancel the strongest interference first. Such cancellation is performed in sequence until all the users are detected and canceled. By canceling the strong interference, the detection performance of the weak desired signal is improved.

However, there is an issue in applying such a SIC scheme to a practical systems. To keep the interference plus noise floor as low as possible, so as to maximize the system capacity, current and future CDMA cellular systems designers make efforts on uplink channel to obtain stringent power control. Therefore, received signal energies from all active users are kept the same at base stations, making the aforementioned assumption of having different level signal for SIC invalid.

Since the SINR for every user is the same, their BER performance will be similar. This contrasts with a situation without power control, where the BER for the stronger signal is significantly lower than that of weaker signals. Then, the

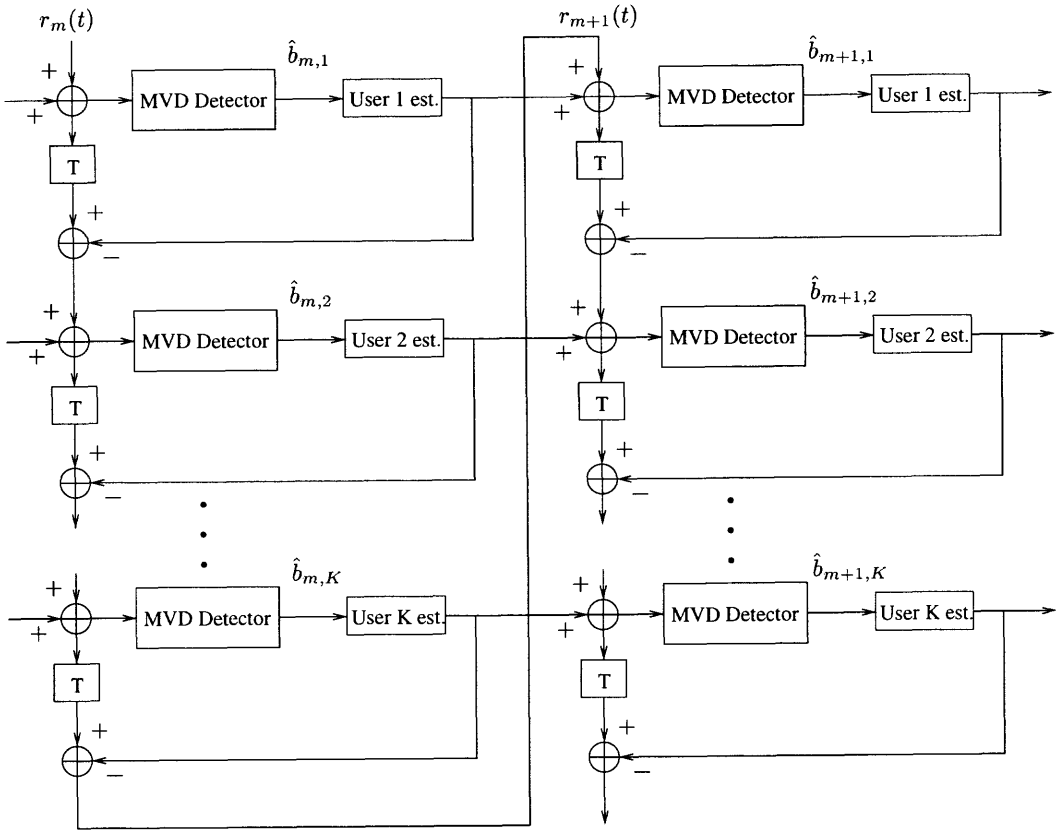

Figure 4.13 SIC structure, each MVD detector with L multipaths.

possibility of incorrect interference cancellation can be ignored. With perfect power control, however, the chance of incorrect interference detection and cancellation is comparable to the BER of the remained users with no cancellation. Thus, it is possible that in such an environment the SIC scheme may not improve the detection performance, but rather could worsen it. For a practical power control systems, this becomes interesting to know if an SIC scheme can improve the performance and under what conditions. A sufficient condition for BER improvement using an SIC scheme in the presence of perfect power control is given next.

Proposition: With perfect power control, that is when all users' received signals have equal energy, or $SINR$. Let the corresponding BER at the output of the detector be $P_{el}(SINR)$, $l = 1, \cdots, K$. The $P_{el}(SINR)$ is not necessarily be equal for all l. Assume user 1 through user $(k-1)$ have been detected and canceled in succession, and assume their corresponding BER after cancellation $\hat{P}_{el}$, $l = 1, \cdots, k-1$ is not worse, i.e. $\hat{P}_{el} \leq P_{el}(SINR)$. If $P_{el}(SINR) << 1$, then a sufficient condition for BER improvement for the k-th user using an SIC scheme is

$$\frac{P_{ek}(SINR) - P_{ek}(SINR_k^c)}{P_{ek}(SINR_k^e) - P_{ek}(SINR_k^c)} > \sum_{l=1}^{k-1} P_{el}(SINR) \tag{4.40}$$

where $P_{ek}(SINR)$ is the k-th user's BER before cancellation. $SINR_k^c$ is the SINR of user k when preceding users (user 1 to user $k-1$) are canceled correctly, while $SINR_k^e$ is the SINR of user k when one of the preceding users is canceled incorrectly.

Proof: see Appendix C.

If the SINR loss due to a single incorrect cancellation can be compensated by all the other correct cancellations for some k, the resulting $SINR_k^e$ is larger than the $SINR$. Then, $P_{ek}(SINR) > P_{ek}(SINR_k^e)$, and the ratio in (4.40) is greater than unity. Therefore, if $P_{el}(SINR) << 1$ is satisfied, their summation is far less than unity, and condition (4.40) is satisfied, meaning performance improvement occurs for the k-th user and beyond using an SIC scheme. With perfect power control, the

value of k is not very large because SINR loss due to one user's error cancellation is easily compensated by a relatively small number of users' correct cancellation.

In general, the BER $P_{ek}(SINR)$ as a function of $SINR$, depends on the codewords and correlation among them, and the delay patterns. A simple example is given here. Assume three synchronous users with equal energy a at the receiver front end, then, the received signal $r(t)$ is

$$r(t) = \sum_{i=1}^{3} \sqrt{a} c_i(t) + n(t) \tag{4.41}$$

where $n(t)$ is the background white Gaussian noise. The MF outputs of user 1 and 2 are given as

$$\begin{aligned} x_1 &= \int_0^T r(t) \cdot c_1(t) dt = \sqrt{a} + \sqrt{a}\rho_{21} + \sqrt{a}\rho_{31} + n_1 \\ x_2 &= \int_0^T r(t) \cdot c_2(t) dt = \sqrt{a} + \sqrt{a}\rho_{12} + \sqrt{a}\rho_{32} + n_2 \end{aligned} \tag{4.42}$$

where the correlation ρ_{31} between code $c_3(t)$ and $c_1(t)$, and ρ_{32} between code $c_3(t)$ and $c_2(t)$ are different which result in different MAI and output SINR of x_1 and x_2, and their BER's are not equal.

When the number of users is large, the interference may be approximated as a Gaussian distributed signal, with the similar MAI output for all users. Then, their detection performance is approximately the same, i.e. $P_{ek}(SINR) = P_e(SINR)$ for every k. In that case, the sufficient condition in equation (4.40) is further simplified to (see Appendix C):

$$\frac{P_e(SINR)}{P_e(SINR_k^c)} > \frac{1-(k-1)P_e(SINR)}{1-(k-1)P_e(SINR_k^e)} \tag{4.43}$$

From equation (4.43), when BER $P_e(SINR) << 1$, and $P_e(SINR_k^e) << 1$, the right hand side approaches unity when k is not extremely large. The condition becomes $P_e(SINR) > P_e(SINR_k^c)$, which is obviously always satisfied. That means that in general an SIC scheme will help to reduce the BER in the presence of perfect power control.

4.6.4 Simulations and Conclusions

To evaluate the proposed non-linear (using hard decision outputs to estimate the signals) MVD based multistage PIC and SIC schemes, three active users are assumed. They are spread by length $N = 7$ goldcodes, with $g_1 = [1, 1, 1, -1, -1, 1, -1]$, $g_2 = [-1, 1, 1, 1, 1, -1, -1]$, and $g_3 = [1, 1, -1, 1, 1, 1, 1]$. The signal of each user is composed of three independent Rayleigh fading channels. The delays are integer multiples of the chip interval and the maximum delay is less than a single symbol interval. The BER of user 1 is evaluated and averaged over these different delays. For the PIC scheme, interference cancellation is performed at the outputs of the first stage which may improve the performance for the following stages except the first.

The performance of the PIC scheme is shown in Figures 4.14 and 4.15, where the SNR of user 1 is set to 8dB. Users 2 and 3 are equally strong with the ISR set to 0dB, and 8dB, for Figures 4.14 and 4.15 respectively. With interference cancellation, the second and third stages provide a lower BER than the first stage, where no interference cancellation is performed before detection. With strong interference situation, as in Figure 4.15, the second and third stages exhibit a comparable performance that is close to the single user bound. This implies that using an MVD receiver as the ICU, the interference can be effectively canceled with a small number of stages.

Figure 4.16 depicts the near-far resistance performance of PIC. It shows that the proposed scheme has excellent near-far resistance performance when the ISR is higher, and the BER gets close to the single user bound. When the ISR is less than 0dB, desired user 1 is stronger than user 2 and 3. In that case, the estimate of user 2 and 3 are poor at the first stage, which results in a large cancellation noise at user 1's input to the second stage. However, the noise is low at the inputs of user 2 and 3 due to better estimation and cancellation of the strongest signal, i.e. user 1. The second stage is then able to provide better detection and estimation for user 2 and

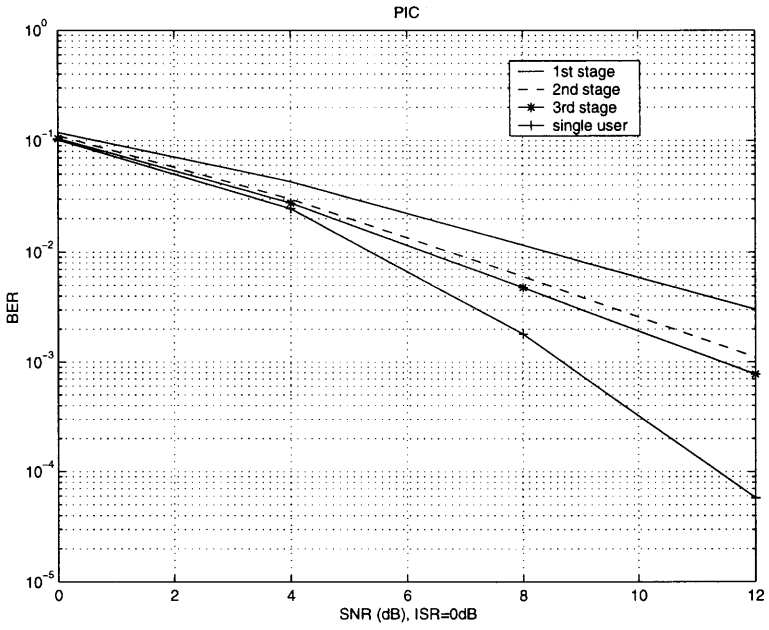

Figure 4.14 BER of User 1 vs. SNR for PIC scheme with ISR=0dB

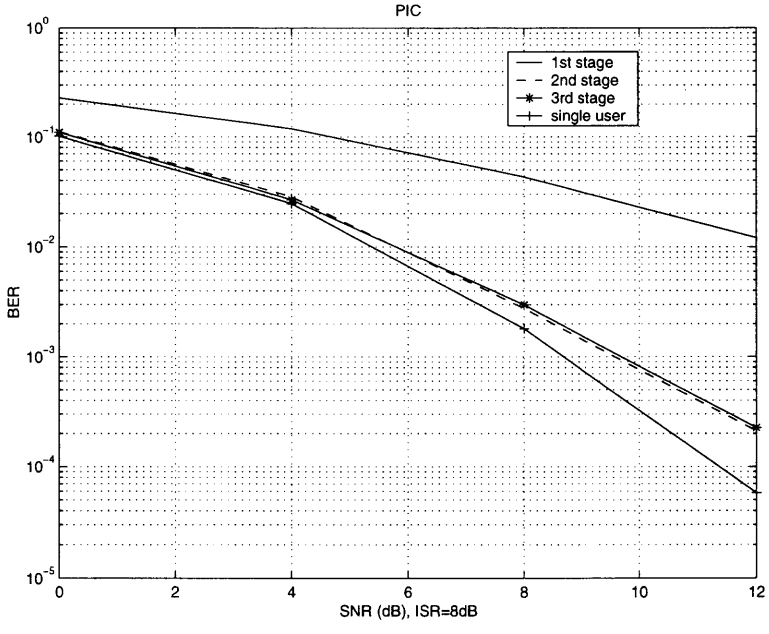

Figure 4.15 BER of User 1 vs. SNR for PIC scheme with ISR=8dB

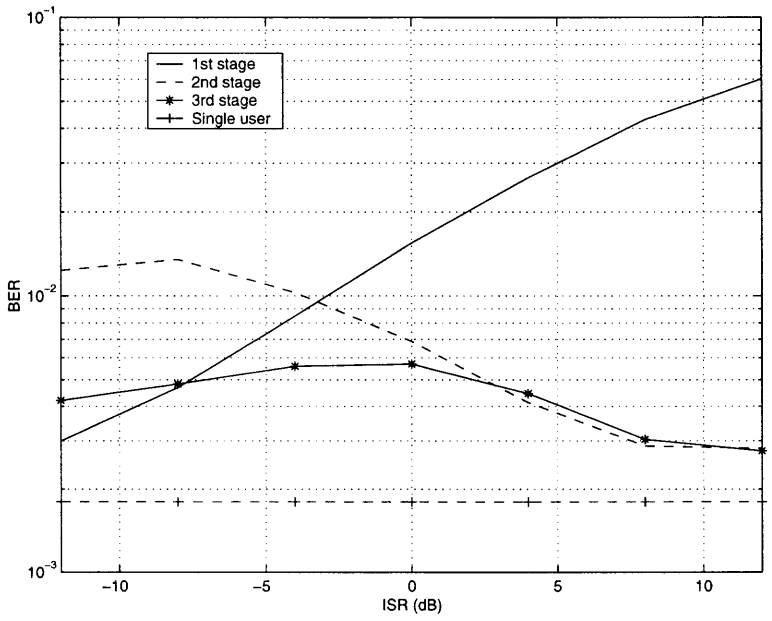

Figure 4.16 Near-far resistance performance of user 1 for PIC scheme (SNR=8dB)

3. Consequently, the third stage provides better detection of user 1's signal than the second stage due to the reduced cancellation noise.

In Figures 4.17 and 4.18, the detection performance of user 1 is investigated for different positions in the SIC structure. The ISR is set to $0dB$ and $8dB$ for Figures 4.17 and 4.18 respectively. In these figures, "One user canceled" means only user 2 is canceled before the desired signal, user 1, is detected, and "Two users canceled" means both user 2 and 3 are canceled before detecting user 1. Compared to Figures 4.14 and 4.15, SIC scheme with one stage ("Two users canceled, 1st stage") provides comparable performance to PIC scheme with two stages ("2nd stage"). Also, the performance of SIC with "Two users canceled, 2nd stage" is close to PIC with "3rd stage". Therefore, SIC is more robust.

However, an advantage of multistage PIC over multistage SIC is that PIC has less processing delay, M symbols delay for an M-stage PIC. In comparison, the processing delay for an M-stage SIC scheme, varies between $(M-1)K+1$ and

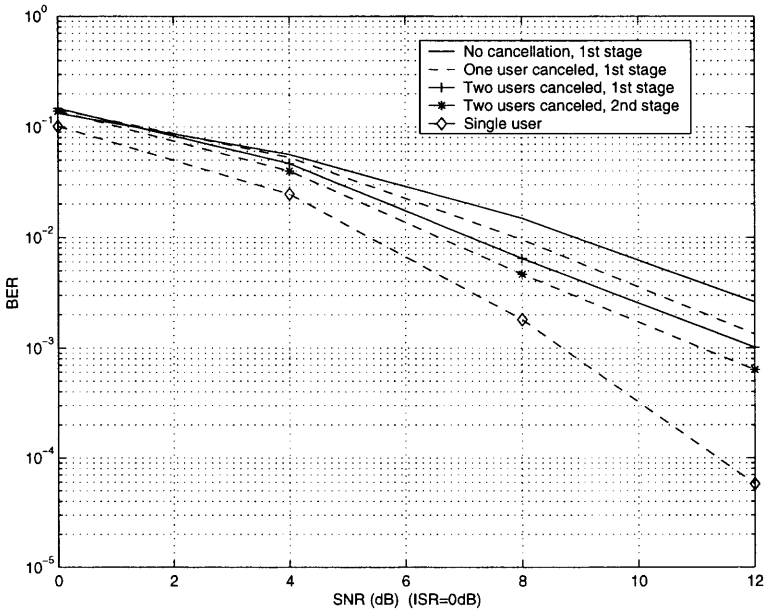

Figure 4.17 BER of User 1 vs. SNR for SIC scheme with ISR=0dB

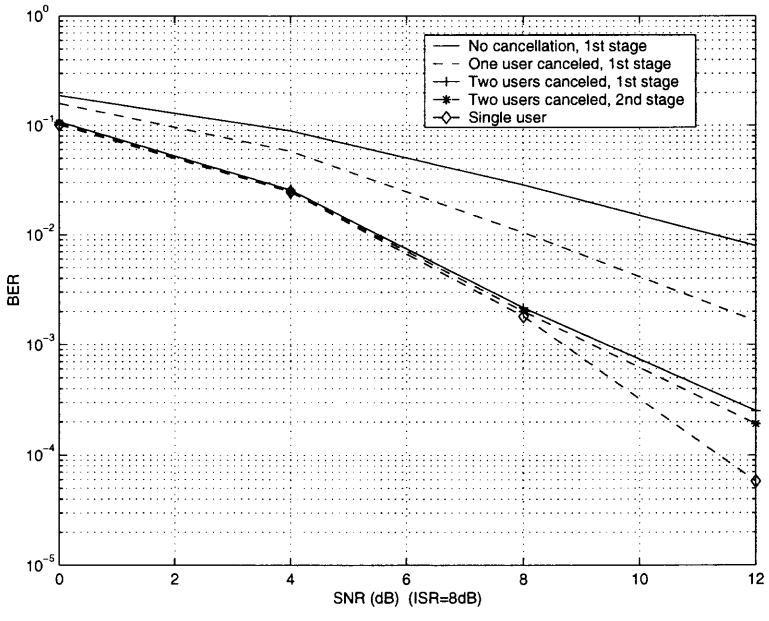

Figure 4.18 BER of User 1 vs. SNR for SIC scheme with ISR=8dB

MK symbol intervals depending on where the particular user's detection takes place. This delay increases linearly with the total number of users and stages. Therefore, a multistage PIC scheme is more suitable when the application demands a small delay, especially when the number of users is large.

Reviewing Figure 4.17, where all users are equally strong, shows that when the SNR is high (about 4dB or more), the BER is much smaller than unity. Thus, the detection performance is improved with each cancellation. However, for low SNR, a performance improvement with the SIC scheme is not guaranteed, which is in agreement with the sufficient condition for SIC with perfect power control stated earlier.

4.7 TD-MVD Transmit Diversity Scheme

In existing systems, power control and multiple receiving antennas are employed to increase the uplink capacity. Multiple antenna reception at the mobile side is impractical due to its limited physical size. However, multiple antenna transmission from the base stations is easily implemented for the downlink. As a result, transmit diversity at the base stations is an alternative solution to balance the capacity of the downlink and uplink.

To maximize the spatial diversity gain, independent transmission, i.e. fading independent, among different transmit antennas and propagation paths is required. For this, the transmit antennas should be mounted far apart. In some cases, antennas that belong to different base stations can be used to achieve TD. For example, current IS-95 systems have the ability to support such a transmission scheme when a subscriber initializes soft handover.

It is obvious that synchronization is an essential condition for existing TD schemes to operate. However, with the distant location of the transmit antennas, the downlink propagation channels are no longer synchronous, but rather asynchronous,

and frequency selective. The presence of multipaths will further destroy the orthogonality between the transmitted signals and hence, the receiver performance is degraded. Therefore, many existing TD techniques are not able to deliver the suggested performance.

To combat the loss of orthogonality, due to the asynchronous frequency selective characteristics of the TD downlink, it is suggested to use a simulcasting transmit diversity (STD) scheme. Since orthogonality can't be maintained in an asynchronous environment, the simulcasting information symbol is spread by linearly independent Gold codes at each transmission branch instead of using orthogonal codes to separate different antenna transmissions. As will be shown, such a structure will lead to a code matrix with a full column rank. The cross correlation property of the Gold codes allows the receiver to distinguish between duplicate transmissions of the desired signal in an asynchronous multipath propagation channel. At the receiver, the MVD receiver is proposed for these different transmissions. To obtain a better receiving performance, the MVD receiver uses the structure based on desired signal absence autocorrelation matrix $R_{\mathbf{u}}$ as given in Section 4.5.

4.7.1 TD-MVD System Model

Consider a wireless communication system with 2 transmit antennas at the base station, and single receive antenna at the mobile. Each information symbol $b_k(n)$ of user k is copied to both transmission branches, spread by a different codeword $c_k^{(i)}, i = 1, 2$, for each branch and added to the signals intended for other users, before being transmitted by the corresponding antennas, as shown in Figure 4.19.

The signal model needs to be modified for multiple transmit antenna applications. In a downlink scenario, the signals of different users originating from the same antenna suffer the same fading and path delay as they travel through the same propagation channel. Consequently, they have an identical number of multipath

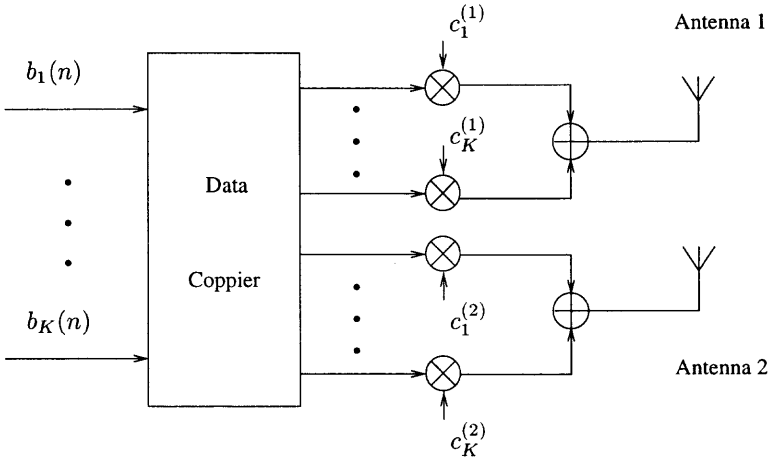

Figure 4.19 Two antennas simulcasting transmit diversity system structure.

components. The transmitted signal at the n-th symbol of user k from antenna i is given by

$$s_{k,n}^{(i)}(t) = \sqrt{a_k^{(i)}} b_k(n) c_k^{(i)}(t - nT) \qquad i = 1, 2 \tag{4.44}$$

where $a_k^{(i)}$ is the energy of the transmitted signal on antenna i. The spreading codes c are different at each antenna.

Let L_i be the number of resolvable discrete multipath components from the i-th antenna, and integer $p = max\{\tau_{L_1}^{(1)}, \tau_{L_2}^{(2)}\}/T_c$. The output vector $\mathbf{x}_{(N+p)\times 1}(n)$ of chip rate MF at the n-th symbol has the same form as in equation (4.1), with a modified $\mathbf{\Gamma}(n) = [\sqrt{a_1^{(1)}}\gamma_1^{(1)}(n), \cdots, \sqrt{a_1^{(1)}}\gamma_{L_1}^{(1)}(n), \sqrt{a_1^{(2)}}\gamma_1^{(2)}(n), ..., \sqrt{a_1^{(2)}}\gamma_{L_2}^{(2)}(n)]^T$, and code matrix $C_{(N+p)\times(L_1+L_2)}$ as

$$C = \begin{bmatrix} g_1^{(1)}(0) & & & g_1^{(2)}(0) & \\ g_1^{(1)}(1) & & & g_1^{(2)}(1) & \\ \vdots & \vdots & g_1^{(1)}(0) & \vdots & \\ g_1^{(1)}(N-1) & \vdots & g_1^{(1)}(1) & \vdots & \vdots \; g_1^{(2)}(0) \\ & \vdots & \vdots & g_1^{(2)}(N-1) & \vdots \; g_1^{(2)}(1) \\ & & g_1^{(1)}(N-1) & & \vdots \\ & & & & g_1^{(2)}(N-1) \end{bmatrix}_{(N+p)\times(L_1+L_2)} \tag{4.45}$$

For better receiving performance, the structure of the MVD receiver shown in Figure 4.11 is used to interpret the TD signals. As a result, $R_{\mathbf{u}}$ estimation is performed. Corresponding to the transmission structure, the weight matrix W has a dimension $(N+p) \times (L_1 + L_2)$, and is obtained as in section 4.1.

The receiver's structure with the decision aided channel estimator, MRC combining and $R_{\mathbf{u}}$ estimation is given in Figure 4.20, where, BPSK signals are assumed such that decision making is implemented with $sgn(\cdot)$. For M-ary quadrature modulated signals, a $sorter(\cdot)$ will be used.

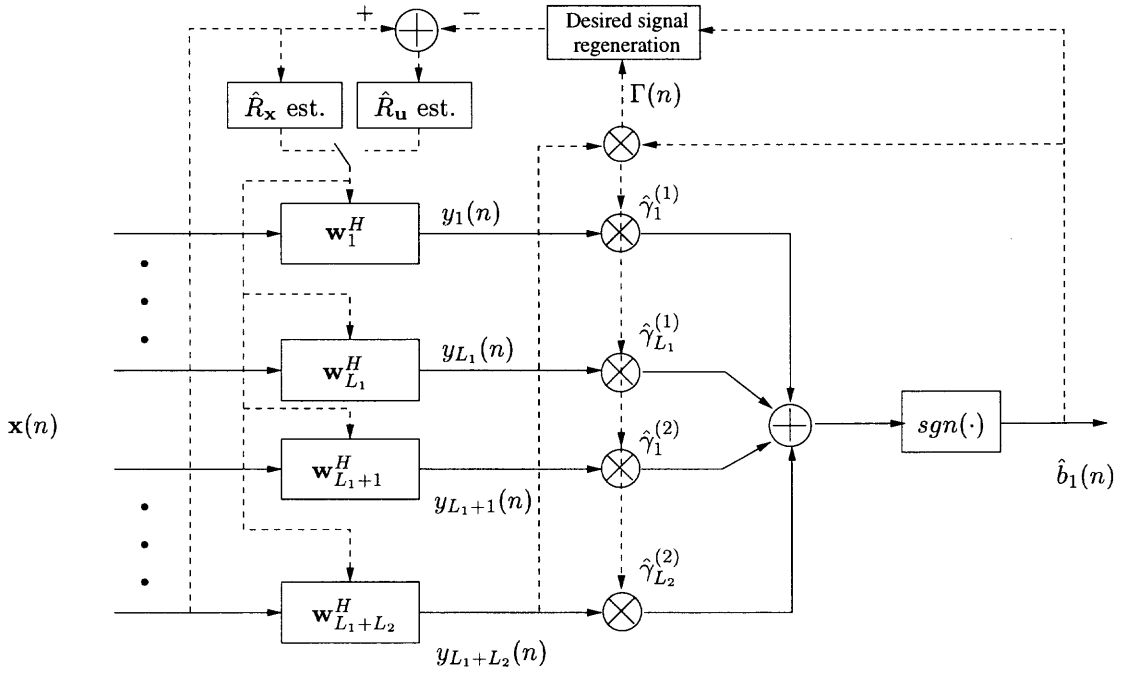

Figure 4.20 Decorrelator structure with channel response estimator and MRC combiner

4.7.2 Numerical Study and Simulation

To evaluate the performance of the proposed two antenna TD-MVD scheme in an asynchronous receiving TD fading channel, length $N = 15$ Gold codes are used as spreading signatures for different users and different antennas. Five simultaneously active users are assumed and the signals transmitted from each antenna experience

independent multipath channels with two paths, i.e. $L_1 = L_2 = 2$. It is assumed that the transmission of all users is with the same signal energy. The receiver performance is obtained by averaging over a random selection of delays, of the paths from all antennas, chosen within one symbol interval $[0, T)$.

For a fair comparison between receivers' performance, the corresponding Rayleigh fading coefficients, $\gamma_l^{(i)}$ are normalized such that the total received power remains the same,

$$\sum_{i=1}^{2} \sum_{l=1}^{L_i} E\{\gamma_l^{(i)}(n)[\gamma_l^{(i)}(n)]^*\} = 1 \tag{4.46}$$

Besides the method shown in (4.15), another most common estimation algorithm for $\hat{R}_{\mathbf{x}}$ and $\hat{R}_{\mathbf{u}}$ estimation is the sample outer product averaging algorithm. Suppose there are M samples of the vector $\mathbf{x}(n)$, the estimate $\hat{R}_{\mathbf{x}}$ is given by

$$\hat{R}_{\mathbf{x}} = \frac{1}{M} \sum_{n=1}^{M} \mathbf{x}(n)\mathbf{x}^H(n) \tag{4.47}$$

Under the assumption that the received samples of $\mathbf{x}(n)$ are independent, identically distributed (iid), the averaging algorithm is the maximum likelihood estimation [55].

The effect of processing window size M on the receiver's performance is further investigated by using the $R_{\mathbf{x}}$ estimation given in equation (4.47). The channel is assumed to be static during the processing window. This is a reasonable approximation for a wideband channel as long as M is sufficiently small. Moreover, if the proposed scheme results in a performance that is not sensitive to the size of the processing window, it may also be applied to a time-variant channel because the use of a shorter window size will not cause significant performance loss.

In Figure 4.21, the performance of the proposed system, as given in Figure 4.20, is depicted, and compared to the same system except for an MLE based channel estimator, both for $M = 20N$ and $30N$. In both cases the estimated channel responses were used to reconstruct the desired signals. Judging from the results,

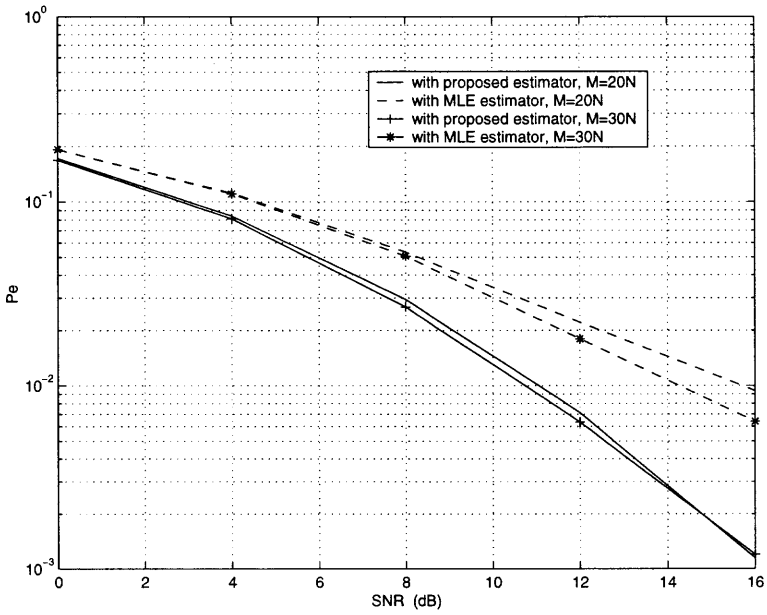

Figure 4.21 Performance comparison using different channel estimators.

it is concluded that the proposed decision aided channel estimator makes better use of the information on the desired signal than the MLE estimator, which is simply based on the received random signal vectors.

It is found that the performance using $\hat{R}_{\mathbf{u}}$ is not as sensitive to M as when an MLE channel estimator is used. The effect of different estimation window sizes, $M = 10N$, $20N$ and $30N$, on the BER performance is further investigated in Figures 4.22 and 4.23, using $R_{\mathbf{x}}$ and $R_{\mathbf{u}}$ respectively. It is clear that using a larger window size results in better performance due to more accurate estimation of the autocorrelation matrix. Also, it is found that, besides a lower BER, the proposed TD-MVD scheme using $R_{\mathbf{u}}$ exhibits a performance that is less sensitive to the estimation window size. In other words, its performance is more robust to the estimation error of $R_{\mathbf{u}}$, and thus, preferable for application in a time-variant channel.

Spatial diversity gain, using the proposed TD scheme, is evaluated in Figure 4.24. Three transmit diversity scenarios are compared: two transmit antennas, each with

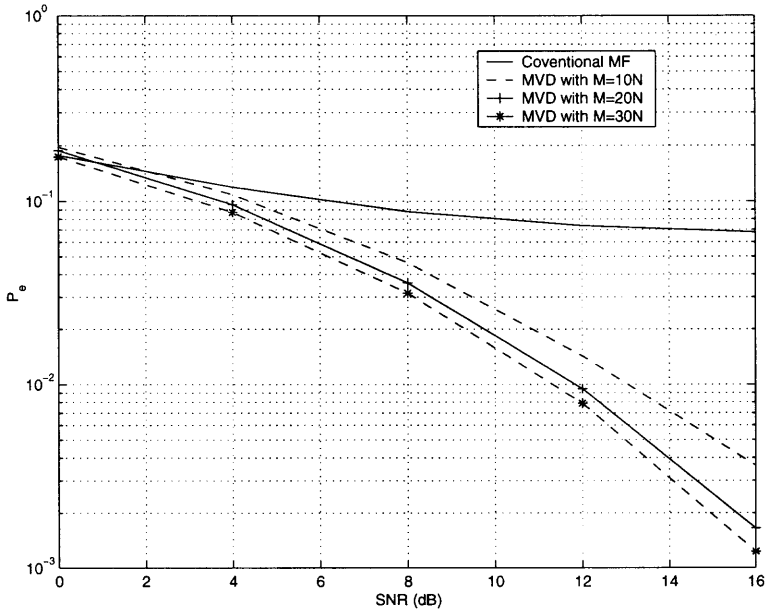

Figure 4.22 Comparison with difference window sizes using $R_{\mathbf{u}}$ as described. Decision aided channel estimator is employed for $R_{\mathbf{u}}$ estimation.

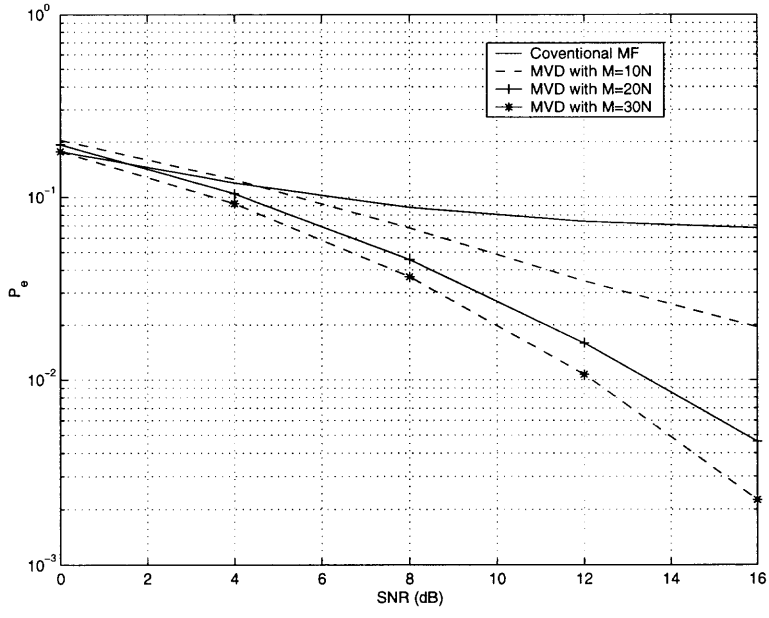

Figure 4.23 Comparison with difference window sizes using $R_{\mathbf{x}}$

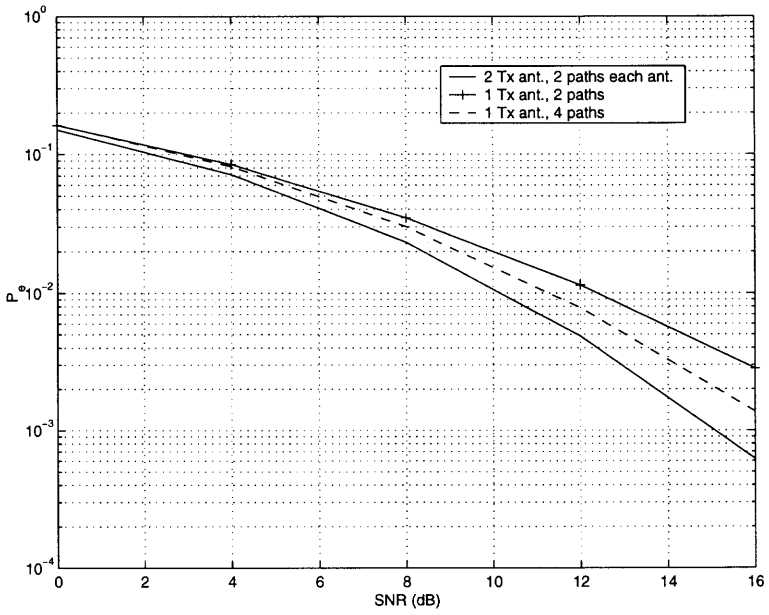

Figure 4.24 Spatial diversity comparison.

two propagation paths; one transmit antenna with two propagation paths; and one transmit antenna with four propagation paths. All multipath channel fading is assumed independent. In the first scenario, one of the propagation paths from each transmit antenna is dominant. The fading profile of the two multipath channels for both antennas follows the assumed distribution $[1, 0.5]$. In the second scenario, the same fading profile is used for the sole transmit antenna. In the third scenario, one dominant path is assumed and the fading profile of $[1, 0.5, 0.28, 0.2]$. Clearly, as shown in the figure, both scenario 1 and 3 should present better performance than scenario 2 due to larger diversity gain. However, in scenario 1, there are two dominant paths compared with only one dominant path in scenario 3. Therefore, the latter is more sensitive to the channel fading and thus, the former has better performance. In the figure, when P_e is about 10^{-2}, the first scenario provides more than 1dB diversity gain over scenario 3, and more than 2dB diversity gain over scenario 2.

As a conclusion, the proposed TD-MVD is suitable for practical application of TD techniques, with low implementation complexity for frequency selective fading channel. Other existing TD schemes have degraded performance in such channel due to a loss of synchronization. The TD-MVD can be extended to more transmit antennas, to obtain larger diversity gain, in a straightforward manner.

CHAPTER 5

EFFECT OF SYNCHRONIZATION ERROR ON THE PERFORMANCE OF ADAPTIVE BOOTSTRAP MULTIUSER DETECTION

In the previous chapters, it was assumed, as is customary, that the MF has perfect knowledge of the signal timing information, and either bit rate or chip rate MF's are well aligned with the received signal timing. However, almost all timing estimation algorithms, for example [33], can not satisfy such a strict assumption. As a result, the detector's performance deteriorates due to residual ISI and MAI. For a practical implementation it is crucial to evaluate the effect of delay estimation errors on the detector's performance to design reliable detectors.

In this section an analytical evaluation of the performance of the adaptive bootstrap detector, in the presence of timing estimation errors, is presented. This performance is compared with the performance of a linear MMSE detector with the same timing errors. It is shown that the performance of both detectors remain comparable when timing estimation errors exist. This proves that the performance of the adaptive bootstrap detector remains near optimal in a linear sense in the presence of a timing synchronization error. In addition, the bootstrap detector has the ability to perform blind detection. Furthermore, a modification of the bootstrap algorithm is proposed, which minimizes the residual ISI caused by timing errors.

5.1 Signal Reception in the Presence of a Timing Error

Consider a downlink frequency flat fading channel. Then, signal delays from all users are the same, i.e. $\tau_k = \tau$, for $k = 1, \cdots K$, and the estimated delay $\hat{\tau} = \tau + \delta$, with error $0 \leq \delta < T_c$. In fact, most timing algorithms will provide delay estimate with an error far smaller than T_c. The MF bank then correlates the received signal within the time interval $[\tau + \delta, T + \tau + \delta]$, as shown in Figure 5.1 for $\tau = 0$.

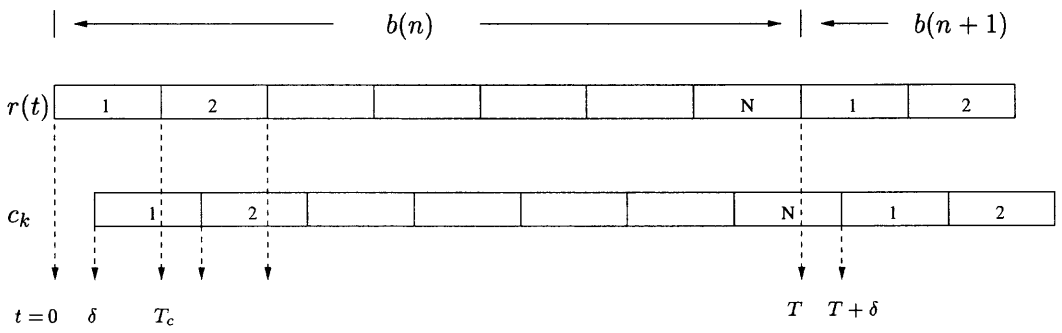

Figure 5.1 Signal misalignment at MF

Assume, without loss of generality, that $\tau = 0$. Then, the MF output $x_k(n)$ for user k is,

$$\begin{aligned}
x_k(n) &= \int_{\delta}^{T+\delta} r(t)c_k(t-\delta)dt \\
&= \sum_{l=1}^{K} \sqrt{a_l}\gamma_l b_l(n)[\int_{\delta}^{T_c} c_l(t)c_k(t-\delta)dt + \cdots + \int_{(N-1)T_c+\delta}^{NT_c} c_l(t)c_k(t-\delta)dt] \\
&\quad + \sum_{l=1}^{K} \sqrt{a_l}\gamma_l b_l(n)[\int_{T_c}^{T_c+\delta} c_l(t)c_k(t-\delta)dt + \cdots + \int_{(N-1)T_c}^{(N-1)T_c+\delta} c_l(t)c_k(t-\delta)dt] \\
&\quad + \sum_{l=1}^{K} \sqrt{a_l}\gamma_l b_l(n+1)[\int_{NT_c}^{NT_c+\delta} c_l(t-LT_c)c_k(t-\delta)dt] + v_k(n) \\
&= \sum_{l=1}^{K} \sqrt{a_l}\gamma_l b_l(n)(1-\frac{\delta}{T_c})\int_0^T c_l(t)c_k(t)dt \\
&\quad + \sum_{l=1}^{K} \sqrt{a_l}\gamma_l b_l(n)\frac{\delta}{T_c}\int_0^{(N-1)T_c} c_l(t+T_c)c_k(t)dt \\
&\quad + \sum_{l=1}^{K} \sqrt{a_l}\gamma_l b_l(n+1)\frac{\delta}{T_c}\int_0^{T_c} c_l(t)c_k(t+(N-1)T_c)dt + v_k(n) \qquad (5.1)
\end{aligned}$$

This can be written in matrix form as,

$$\mathbf{x}(n) = \bar{P}A\mathbf{b}(n) + \bar{Q}A\mathbf{b}(n+1) + \mathbf{v}(n), \qquad (5.2)$$

where $A = diag(\sqrt{a_1}\gamma, \sqrt{a_2}\gamma, ..., \sqrt{a_k}\gamma)$. Here, the channel fading γ is assumed to be constant. $\bar{P} = (1-\frac{\delta}{T_c})P + \frac{\delta}{T_c}P_1$ is the modified correlation matrix with P_1 introducing inter chip distortion

$$P(i,j) = \int_0^T c_j(t)c_i(t)dt;$$

$$P_1(i,j) = \int_0^{(L-1)T_c} c_j(t+T_c)c_i(t)dt; \tag{5.3}$$

and $\bar{\mathbf{Q}}$ is given by,

$$\bar{Q}(i,j) = \frac{\delta}{T_c}\int_0^{T_c} c_j(t)c_i(t+(L-1)T_c)dt. \tag{5.4}$$

In general, the matrix $\bar{P}$ is not Hermitian. The noise vector $\mathbf{v} \sim N(\mathbf{0}, \sigma^2 P)$. If δ is negative, matrices $\bar{P}$ and $\bar{Q}$ are replaced by their transpose, and $\mathbf{b}(n+1)$ becomes $\mathbf{b}(n-1)$.

5.2 Adaptive Bootstrap Detector

Bootstrap detectors suppress MAI by applying a matrix $V = I - W$ to equation (5.2). Then,

$$\mathbf{y}(n) = V\mathbf{x}(n) = V\bar{P}A\mathbf{b}(n) + V\bar{Q}A\mathbf{b}(n+1) + \boldsymbol{\xi}(n), \tag{5.5}$$

where the additive Gaussian noise $\boldsymbol{\xi} \sim N(\mathbf{0}, \sigma^2 VPV^H)$. The elements of matrix W are chosen according to the decorrelating criterion:

$$E[y_k(n)sgn(\mathbf{y}_k(n))] = \mathbf{0} \qquad k = 1, \cdots, K \tag{5.6}$$

where $\mathbf{y}_k(n)$ is the vector $\mathbf{y}(n)$ without the k-th element. Assuming the SINR is large, or $sgn(y_k(n)) \simeq b_k(n)$ for any k, the above equation becomes:

$$E[y_k(n)\mathbf{b}_k(n)] = \mathbf{0}, \tag{5.7}$$

where $\mathbf{b}_k(n)$ is $\mathbf{b}(n)$ without the k-th element. Such a condition will be termed SINR in the limit (LSINR). From equation (5.5),

$$y_k(n) = x_k(n) - \mathbf{w}_k^T\mathbf{x}_k(n), \tag{5.8}$$

where $\mathbf{w}_k^T$ is the k-th row of W without the k-th element. $\mathbf{x}_k$ is $\mathbf{x}$ without k-th element, and

$$\begin{aligned} x_k(n) &= \sqrt{a_k}b_k(n)\bar{P}(k,k) + \hat{\mathbf{p}}_k A_k \mathbf{b}_k(n) + \mathbf{q}_k A\mathbf{b}_k(n+1) + v_k(n) \\ \mathbf{x}_k(n) &= A(k,k)b_k(n)\bar{\mathbf{p}}_k + \bar{P}_k A_k \mathbf{b}_k(n) + \bar{Q}_k A\mathbf{b}_k(n+1) + \mathbf{v}_k(n), \end{aligned} \tag{5.9}$$

where $\hat{\mathbf{p}}_k$ is the k-th row of $\bar{P}$ without the k-th element. The vector $\mathbf{q}_k$ is the k-th row of $\bar{Q}$. The matrices $\bar{P}_k, A_k$ and $\bar{Q}_k$ are the corresponding matrices without their k-th row and column. The vector $\bar{\mathbf{p}}_k$ is the k-th column of $\bar{P}$ without the k-th element. The vector $\mathbf{v}_k$ is the noise vector $\mathbf{v}$ without the k-th element.

The matrix W can be derived by applying equations (5.8) and (5.9) into (5.7) and assuming that the data information from different users is uncorrelated as well as uncorrelated for different symbol intervals of one particular user:

$$\mathbf{w}_k^T = \hat{\mathbf{p}}_k \bar{P}_k^{-1} \qquad k = 1, \cdots, K \tag{5.10}$$

Then, the signal energy of the desired bits of all users is given by,

$$\begin{aligned} E_s &= E[\{(I-W)\bar{P}A\mathbf{b}(n)\}\{(I-W)\bar{P}A\mathbf{b}(n)\}^H] \\ &= (I-W)\bar{P}A^2\bar{P}^H(I-W)^H \\ &= diag\{a_1\gamma^2(\bar{P}(1,1) - \underline{\hat{\mathbf{p}}}_1^T\bar{P}_1^{-1}\underline{\bar{\mathbf{p}}}_1)^2, \cdots, a_k\gamma^2(\bar{P}(k,k) - \underline{\hat{\mathbf{p}}}_k^T\bar{P}_k^{-1}\underline{\bar{\mathbf{p}}}_k)^2\}, \end{aligned} \tag{5.11}$$

where the fact is used that $I-W$ diagonalizes the correlation matrix $\bar{P}$. The energy E_i of the MAI and ISI, and the energy E_n of the noise are given by

$$E_i = (I-W)\bar{Q}A^2\bar{Q}^H(I-W)^H \tag{5.12}$$

$$E_n = \sigma^2(I-W)P(I-W)^H \tag{5.13}$$

Then, the SINR of desired user 1, is given as

$$SINR(1) = \frac{a_1\gamma^2(\bar{P}(1,1) - \hat{\mathbf{p}}_1\bar{P}_1^{-1}\bar{\mathbf{p}}_1)^2}{E_i(1,1) + E_n(1,1)} \tag{5.14}$$

From equation (5.5) and (5.10),

$$y_1(n) = \sqrt{a_1}\gamma(\bar{P}(1,1) - \hat{\mathbf{p}}_1\bar{P}_1^{-1}\bar{\mathbf{p}}_1)b_1(n) + \hat{\mathbf{w}}_1^T\bar{Q}A\mathbf{b}(n+1) + \xi_1(n), \tag{5.15}$$

where $\hat{\mathbf{w}}_1^T = [1, -\hat{\mathbf{p}}_1\bar{P}_1^{-1}]$. The bit error rate of user 1 is

$$Pe(1) = \frac{1}{2}\{P_r(y_1(n) < 0 | b_1(n) = 1; \mathbf{b}(n+1)) \cdot P_r(\mathbf{b}(n+1))$$

$$
\begin{aligned}
&+P_r(y_1(n) > 0 | b_1(n) = -1; \mathbf{b}(n+1)) \cdot P_r(\mathbf{b}(n+1))\} \\
= \; & \frac{1}{2^{k+1}} \sum_{\mathbf{b}(n+1)} \{Q(\frac{\sqrt{a_1}\gamma_1(\bar{P}(1,1) - \hat{\mathbf{p}}_1\bar{P}_1^{-1}\bar{\mathbf{p}}_1) + \hat{\mathbf{w}}_1^T\bar{Q}A\mathbf{b}(n+1)}{\sigma_{\xi_1}} | b_1(n) = 1) \\
& +Q(\frac{\sqrt{a_1}\gamma_1(\bar{P}(1,1) - \hat{\mathbf{p}}_1\bar{P}_1^{-1}\bar{\mathbf{p}}_1) - \hat{\mathbf{w}}_1^T\bar{Q}A\mathbf{b}(n+1)}{\sigma_{\xi_1}} | b_1(n) = -1)\} \quad (5.16)
\end{aligned}
$$

where $Q(x) = \frac{1}{\sqrt{2\pi}} \int_x^\infty e^{-\frac{x^2}{2}} dx$.

5.3 Performance of a Linear MMSE Detector with Timing Error

Let the signal vector $\boldsymbol{\theta}(n) = A\mathbf{b}(n)$, then the linear MMSE based multiuser detector decisions are given by [14]:

$$\hat{\mathbf{b}}(n) = sign(\hat{\boldsymbol{\theta}}(n)), \tag{5.17}$$

with the linear MMSE estimator $\hat{\boldsymbol{\theta}}$ obtained from [56]:

$$\hat{\boldsymbol{\theta}}(n) = E(\boldsymbol{\theta}(n)) + C_{\theta\mathbf{x}}C_{\mathbf{xx}}^{-1}[\mathbf{x}(n) - E(\mathbf{x}(n))], \tag{5.18}$$

where $\mathbf{x}(n)$ is defined in (5.2), and from which,

$$
\begin{aligned}
& E(\boldsymbol{\theta}(n)) = AE[\mathbf{b}(n)] = \mathbf{0} \\
& E(\mathbf{x}(n)) = \bar{P}AE[\mathbf{b}(n)] + \bar{Q}AE[\mathbf{b}(n+1)] + E[\mathbf{v}(n)] = \mathbf{0} \\
& C_{\theta\mathbf{x}} = E[\boldsymbol{\theta}(n)\mathbf{x}^H(n)] = E[A\mathbf{b}(n)\mathbf{b}^H(n)A^H\bar{P}^H] = A^2\bar{P}^H \\
& C_{\mathbf{xx}} = E[\mathbf{x}(n)\mathbf{x}^H(n)] \\
& \quad = E[\bar{P}A\mathbf{b}(n)\mathbf{b}^H(n)A^H\bar{P}^H] + E[\bar{Q}A\mathbf{b}(n+1)\mathbf{b}^H(n+1)A^H\bar{Q}^H] + E[\mathbf{v}(n)\mathbf{v}^H(n)] \\
& \quad = \bar{P}A^2\bar{P}^H + \bar{Q}A^2\bar{Q}^H + \sigma^2 P
\end{aligned}
$$

With these terms, equation (5.18) becomes

$$
\begin{aligned}
\hat{\boldsymbol{\theta}}(n) &= A^2\bar{P}^H[\bar{P}A^2\bar{P}^H + \bar{Q}A^2\bar{Q}^H + \sigma^2 P]^{-1}\mathbf{x}(n) \\
&= \underbrace{[\bar{P} + (\bar{Q}A^2\bar{Q}^H + \sigma^2 P)(A^2\bar{P}^H)^{-1}]^{-1}}_{W_o}\mathbf{x}(n)
\end{aligned}
$$

and with (5.2), it becomes

$$\hat{\boldsymbol{\theta}}(n) = W_o \bar{P} A \mathbf{b}(n) + W_o \bar{Q} A \mathbf{b}(n+1) + \boldsymbol{\zeta}(n) \tag{5.19}$$

where the noise $\boldsymbol{\zeta}(n) \sim N(\mathbf{0}, \sigma^2 W_o P W_o^H)$.

Using Woodbury's identity [57], $(\mathcal{E} + \mathcal{BCD})^{-1} = \mathcal{E}^{-1} - \mathcal{E}^{-1}\mathcal{B}(\mathcal{D}\mathcal{E}^{-1}\mathcal{B} + \mathcal{C}^{-1})^{-1}\mathcal{D}\mathcal{E}^{-1}$, and letting $\mathcal{E} = \bar{P}$, $\mathcal{B} = \bar{Q}A^2\bar{Q}^H + \sigma^2 P$, $\mathcal{C} = I$, and $\mathcal{D} = (A^2\bar{P}^H)^{-1}$, W_o can be re-written as

$$\begin{aligned}
W_o &= \bar{P}^{-1} - \bar{P}^{-1}(\bar{Q}A^2\bar{Q}^H + \sigma^2 P)[(A^2\bar{P}^H)^{-1}\bar{P}^{-1}(\bar{Q}A^2\bar{Q}^H + \sigma^2 P) + I]^{-1} \\
&\quad \cdot (A^2\bar{P}^H)^{-1}\bar{P}^{-1} \\
&= \bar{P}^{-1} - [(\bar{Q}A^2\bar{Q}^H + \sigma^2 P)^{-1}\bar{P}]^{-1}[(A^2\bar{P}^H)^{-1}\bar{P}^{-1}(\bar{Q}A^2\bar{Q}^H + \sigma^2 P) + I]^{-1} \\
&\quad \cdot (A^2\bar{P}^H)^{-1}\bar{P}^{-1} \\
&= \bar{P}^{-1} - [(A^2\bar{P}^H)^{-1} + (\bar{Q}A^2\bar{Q}^H + \sigma^2 P)^{-1}\bar{P}]^{-1}(A^2\bar{P}^H)^{-1}\bar{P}^{-1} \\
&= \bar{P}^{-1} - [(\bar{Q}A^2\bar{Q}^H + \sigma^2 P)(A^2\bar{P}^H)^{-1} + \bar{P}]^{-1}(\bar{Q}A^2\bar{Q}^H + \sigma^2 P)(A^2\bar{P}^H)^{-1}\bar{P}^{-1} \\
&= \bar{P}^{-1} - W_o(\bar{Q}A^2\bar{Q}^H + \sigma^2 P)(A^2\bar{P}^H)^{-1}\bar{P}^{-1}
\end{aligned} \tag{5.20}$$

Hence, (5.19) is given by

$$\hat{\boldsymbol{\theta}}(n) = \boldsymbol{\theta}(n) \underbrace{-W_o(\bar{Q}A^2\bar{Q}^H + \sigma^2 P)(A\bar{P}^H)^{-1}\mathbf{b}(n) + W_o\bar{Q}A\mathbf{b}(n+1)}_{bias(n)} + \boldsymbol{\zeta}(n) \tag{5.21}$$

When detecting user 1, the desired signal, an error can happen in two scenarios,

$$\begin{aligned}
\hat{\theta}_1(n) &= \theta_1(n) + bias_1(n) + \zeta_1(n) < 0 \quad when \quad b_1(n) = 1 \\
\hat{\theta}_1(n) &= \theta_1(n) + bias_1(n) + \zeta_1(n) > 0 \quad when \quad b_1(n) = -1
\end{aligned}$$

where $bias_1(n)$ is the first element of the bias vector in equation (5.21). Thus, the bit error rate of the desired user is given as follows

$$\begin{aligned}
P_e(1) &= \frac{1}{2}\{P_r(\hat{\theta}_1(n) < 0 | b_1(n) = 1) + P_r(\hat{\theta}_1(n) > 0 | b_1(n) = -1)\} \\
&= \frac{1}{2}\{\frac{1}{2^{2K-1}} \sum_{\mathbf{b}_1(n), \mathbf{b}(n+1)} P_e(\hat{\theta}_1(n) < 0 | b_1(n) = 1; \mathbf{b}_1(n); \mathbf{b}(n+1))
\end{aligned}$$

$$+\frac{1}{2^{2K-1}}\sum_{\mathbf{b}_1(n),\mathbf{b}(n+1)} P_e(\hat{\theta}_1(n)>0|b_1(n)=-1;\mathbf{b}_1(n);\mathbf{b}(n+1))\}$$

$$= \frac{1}{2^{2K}}\sum_{\mathbf{b}_1(n),\mathbf{b}(n+1)} \{Q(\frac{\sqrt{a_1}\gamma+bias_1(n)}{\sigma_{\zeta_1}}|b_1(n)=1;\mathbf{b}_1(n);\mathbf{b}(n+1))$$

$$+ Q(\frac{\sqrt{a_1}\gamma-bias_1(n)}{\sigma_{\zeta_1}}|b_1(n)=-1;\mathbf{b}_1(n);\mathbf{b}(n+1))\}, \quad (5.22)$$

where $\mathbf{b}_1(n)$ is vector $\mathbf{b}(n)$ without $b_1(n)$. σ_{ζ_1} is the variance of the first element of vector $\boldsymbol{\zeta}(n)$, which is equal to $\sigma^2\mathbf{w}_{o1}P\mathbf{w}_{o1}^H$, and $\mathbf{w}_{o1}$ is the first row of W_o.

5.4 Improved Adaptive Detector

It is clear from equation (5.2) that the MF outputs in the presence of a timing synchronization error will contain ISI. The effect of ISI can be minimized by stacking three or more bit sequences and choosing the mid-term which suffers minimum bias. That is,

$$\begin{bmatrix} \mathbf{x}(n-1) \\ \mathbf{x}(n) \\ \mathbf{x}(n+1) \end{bmatrix} = \underbrace{\begin{bmatrix} \bar{P} & \bar{Q} & \mathbf{0} \\ \mathbf{0} & \bar{P} & \bar{Q} \\ \mathbf{0} & \mathbf{0} & \bar{P} \end{bmatrix}}_{\mathcal{P}} \begin{bmatrix} A\mathbf{b}(n-1) \\ A\mathbf{b}(n) \\ A\mathbf{b}(n+1) \end{bmatrix} + \underbrace{\begin{bmatrix} \mathbf{0} \\ \mathbf{0} \\ \bar{Q}A\mathbf{b}(n+2) \end{bmatrix}}_{bias} + \mathbf{v} \quad (5.23)$$

The bootstrap detector can then be applied to detect the whole sequence. This structure is also applicable for a negative timing estimation error, δ. In that case the block correlation matrix $\mathcal{P}$ becomes its transpose and the first element of bias in (5.23) is replaced by $\bar{\mathbf{Q}}A\underline{\mathbf{b}}(n-2)$, while the last term becomes $\mathbf{0}$. The middle term $\mathbf{x}(n)$ is used as the output as it suffers the minimum bias for either positive or negative timing error.

5.5 Results and Conclusion

In the simulations length $N = 31$ Gold codes were used and the fading was assumed constant. The analytical performance of the bootstrap detector was evaluated and simulated within the LSINR situation, i.e. condition in (5.7) is valid for all signals.

Figure 5.2 shows the analytical performance of bootstrap detector and linear MMSE detector as a function of delay error, and compared to the simulation results. Figure 5.3 depicts the analytical performance of bootstrap detector and linear MMSE detector as a function of desired user's SNR, and the performance of bootstrap detector is compared to the simulation results in Figure 5.4. It is found that the analytical performance of the bootstrap detector is almost the same as the performance of the linear MMSE detector even when a timing estimation error exists. For the bootstrap algorithm, the numerical simulation results match the mathematical analysis. It is clear from the figures that a smaller timing estimation error is important as the performance deteriorates approximately an order of magnitude for every 0.2 chips.

Results for the modified bootstrap detector are shown in Figure 5.5. The improvement is noticeable, particularly when the code length is 15. That is, with short codes, the improved detector is robust to a delay estimation error. If a longer code (N=31 or greater) is used, the improvement is smaller because the ISI part in (5.2) becomes smaller compared to the desired signal at the MF output.

In conclusion, it is noted that with a timing error δ, the MF desired bit output is reduced in amplitude and contains ISI and inter chip distortion P_1. When the timing error is large, the detector's performance will become unacceptable due to excessive ISI and a significant reduction in amplitude of the desired signal. However, as shown in this work, when the timing error remains sufficiently small in comparison to the chip interval, the bootstrap detector can still provide comparable performance to a linear MMSE for the LSINR situation.

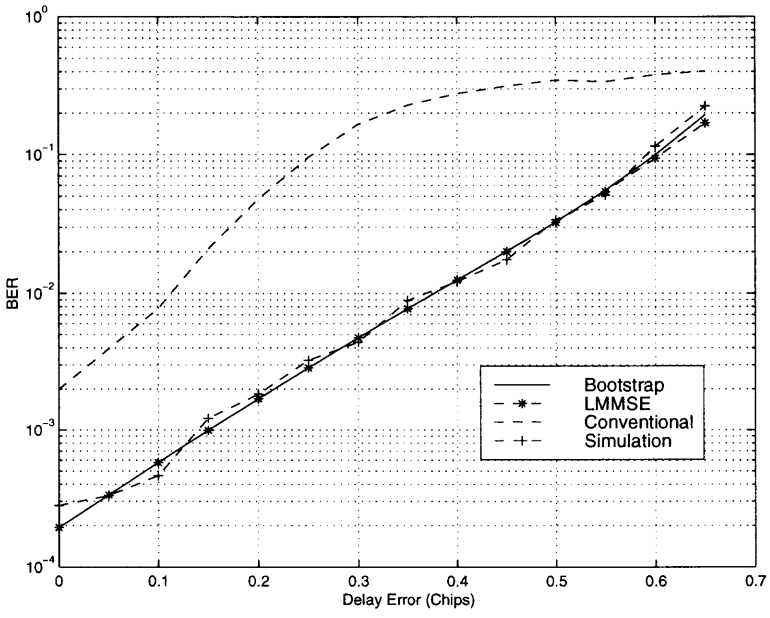

Figure 5.2 Performance versus Delay Error (3 users, desired user's SNR=8dB, ISR ratio=14dB). Simulation was conducted for Bootstrap detector.

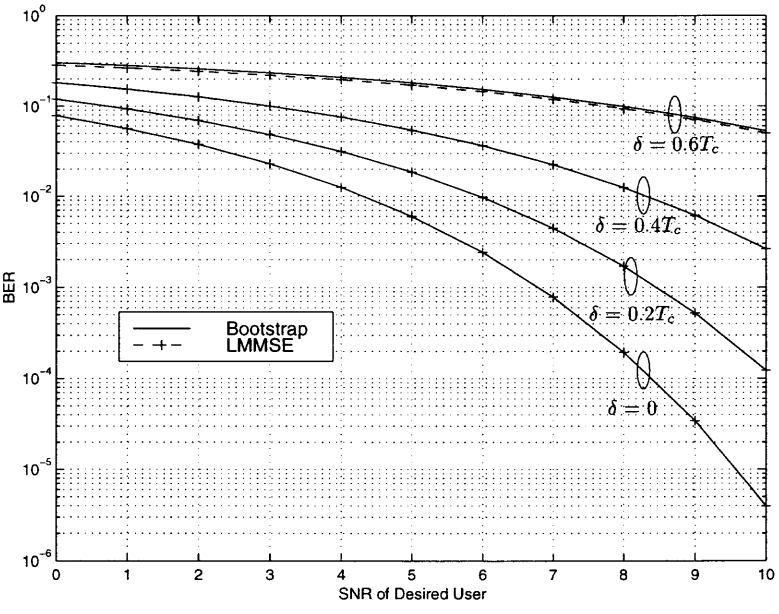

Figure 5.3 BER versus SNR (3 users, SNR(i)-SNR(1)=14dB, (i=2,3 are interference users))

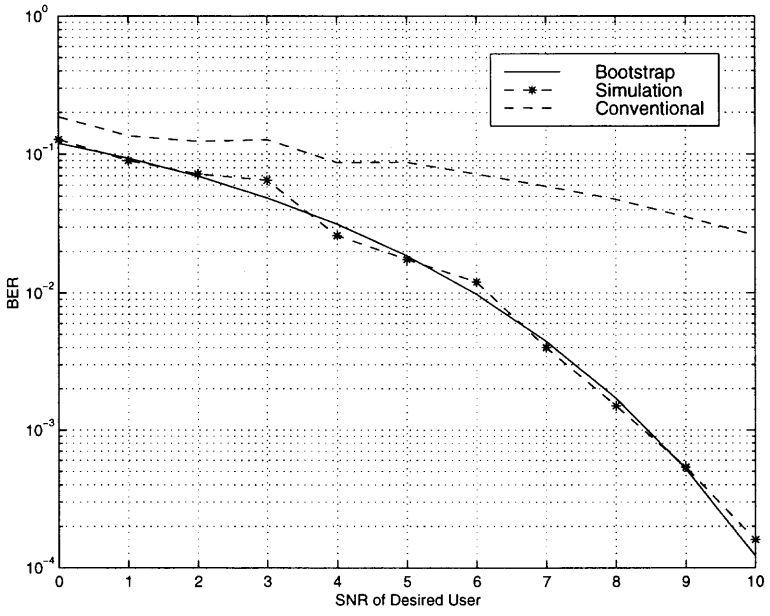

Figure 5.4 Bootstrap detector with three bits stack using different code lengths (3 users, near-far ratio=14dB, $\delta = 0.2T_c$)

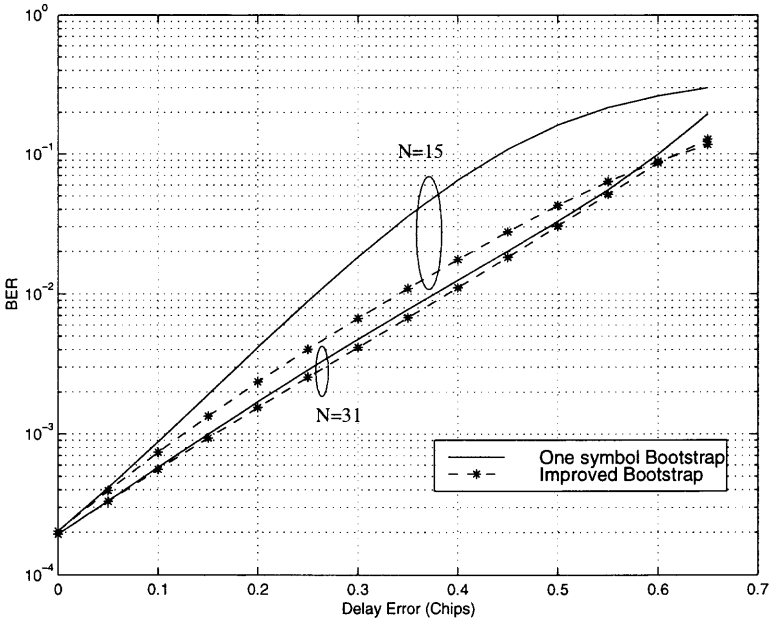

Figure 5.5 Comparison of bootstrap detectors with different code length (N=15, 31)

CHAPTER 6

MAXIMUM LIKELIHOOD DELAY AND CHANNEL ESTIMATION WITH LIMITED SAMPLES

As discussed in the previous chapter, a timing error can significantly reduce the output SINR. The BER performance of the bootstrap and linear MMSE detectors deteriorates approximately an order of magnitude for every 0.2 chips. Therefore, the key issue for any timing algorithm is to provide an estimation error that is as small as possible. In a time-variant channel, usually only a limited number of samples are available. Therefore, how to develop a fast, and sufficiently accurate timing algorithm is a very important topic for practical applications.

As a result of the asymptotically uncorrelated property of the received signal in the frequency domain, as shown in [58, 59], the observation samples become asymptotically uncorrelated and Gaussian distributed in the frequency domain. Due to the uncorrelated property, it is proposed, in this chapter, to use a diagonal matrix approximation (DMA) to improve the performance of the maximum likelihood estimation (MLE) in a time-variant environment. In addition, the computational complexity of the inverse covariance matrix is reduced to the order of the sample dimension, or only O(N) operations.

Another advantage of DMA is the possibility for the estimator to use a singular covariance matrix. This is particularly useful for over sampling techniques. With an over sampling factor of Q, theoretically Q times more samples are required to keep the covariance matrix full rank. Thus, the computational burden of the matrix inverse increases exponentially with Q. So, the increased signal dimension, $N \times Q$, and the number of required samples, prevent the application of over sampling techniques to a time-variant environment.

However, using DMA eliminates the conflict between fast channel estimation and the singularity problem. One can use insufficient samples to estimate the

covariance matrix while keeping the estimation performance close to the CRLB. DMA provides an effective way to overcome the conflict between estimation speed, complexity and accuracy.

6.1 MF Output with Unknown Path Delay

Since multipath delays and the associated channel response are unknown to the receiver, the multipath signals are customarily treated the same as signals from different users. As a result, the channel used in the estimation scheme is described as asynchronous frequency flat fading. Without loss of generality, all delays are assumed within one symbol interval, or $0 \leq \tau_k < T$, for $k = 1, \cdots, K$.

The unknown parameters include the desired user's channel response γ_1, delay τ_1 and information symbols b_1. The joint estimation of these unknown parameters is extremely complicated, and practically impossible. To reduce the estimation burden, it is assumed that the desired user transmits identical data symbol during the channel acquisition period. The channel is assumed quasi-static such that the channel fading can be approximated as a constant within the channel acquisition period, provided this period is short enough.

To simplify the mathematical expression with over sampling, a new spreading codeword of user 1, $\mathbf{s}_1$, is defined as $\mathbf{s}_1 = \mathbf{c}_1 \otimes \mathbf{1}$. "$\otimes$" is Kronecker product and $\mathbf{1}$ is an all 1's vector with dimension $Q \times 1$. For code $\mathbf{c}_1 = [g_1(0), g_1(1), \cdots, g_1(N-1)]^T$, and $Q = 2$, $\mathbf{s}_1$ is the vector $[g_1(0), g_1(0), g_1(1), g_1(1), \cdots, g_1(N-1), g_1(N-1)]^T$ with dimension of $2N \times 1$. Then, for a given starting point $t = 0$, τ_1 is defined as the propagation delay of user 1 corresponding to this point, which can be written as $\tau_1 = (m_1 + \delta_1)\frac{T_c}{Q}$, where $m_1 = \lfloor \frac{\tau_1}{T_c/Q} \rfloor$ denotes the largest integer not greater than $\frac{\tau_1}{T_c/Q}$, and $0 \leq \delta_1 < 1$. It is equivalent to $(m_1 + \delta_1)$ chips delay of codeword $\mathbf{s}_1$.

The MF samples the received signal over one symbol interval $[0, T)$ at a sampling rate of $N \times Q$ starting from $t = 0$ as shown in Figure 6.1.

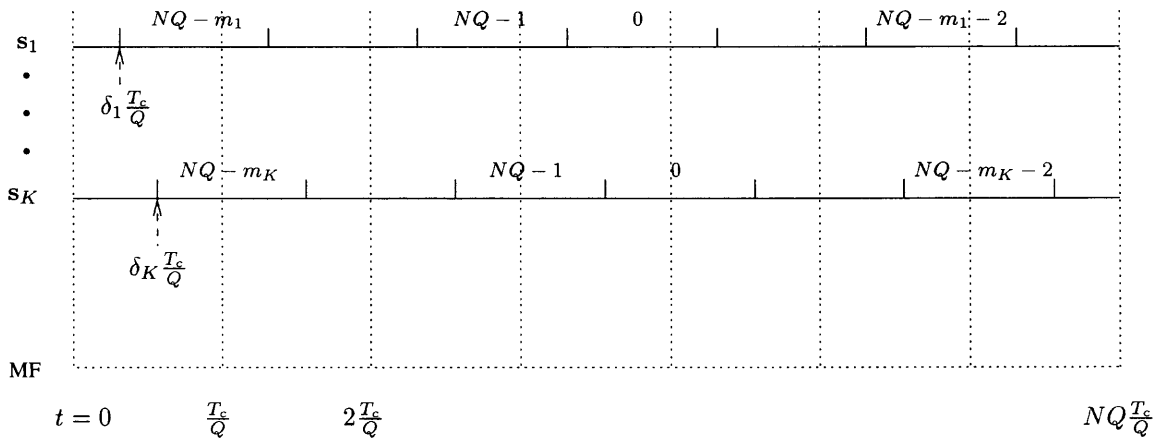

Figure 6.1 Received data frame at chip matched-filter with an over sampling factor Q

The output of the MF contains the cycshift version of $\mathbf{s}_1$. To express such shift in an equation, a permutation matrix $\mathbf{D}^m$ is defined as,

$$\mathbf{D}^m = \begin{bmatrix} \mathbf{0}_{m\times(NQ-m)} & I_{m\times m} \\ I_{(NQ-m)\times(NQ-m)} & \mathbf{0}_{(NQ-m)\times m} \end{bmatrix}_{NQ\times NQ} \tag{6.1}$$

which, when muliplied by $\mathbf{s}_1$, rotates downwards the vector $\mathbf{s}_1$ by m chips. Then the MF output vector $\mathbf{x}(n)$ is given as,

$$\begin{aligned} \mathbf{x}(n) &= \sqrt{a_1}\gamma_1 b_1[\delta_1 \mathbf{D}^{m_1+1}\mathbf{s}_1 + (1-\delta_1)\mathbf{D}^{m_1}\mathbf{s}_1] + \mathbf{u}(n) \\ &= h_1[\delta_1 \mathbf{D}^{m_1+1} + (1-\delta_1)\mathbf{D}^{m_1}]\mathbf{s}_1 + \mathbf{u}(n) \end{aligned} \tag{6.2}$$

where $h_1 = \sqrt{a_1}\gamma_1 b_1$ is the complex channel response corresponding to the desired user. The values δ_1 and $(1-\delta_1)$ result from the partial occurrence of $\mathbf{s}_1$ at each MF sampling output.

Vector $\mathbf{u}(n)$ is comprised of noise and MAI from other users. In general, $\mathbf{u}(n)$ is not Gaussian distributed, particularly when the number of MAI users is small. Also, these elements are correlated in time due to asynchronous transmission and over sampling.

To exploit the asymptotically uncorrelated property of the signal in the frequency domain, $\mathbf{x}(n)$ is converted to the frequency domain using the DFT. Define

the DFT transform matrix as $\mathcal{W} = [\mathbf{w}_0, \mathbf{w}_1, \cdots, \mathbf{w}_{NQ-1}]$, where $\mathbf{w}_i = [1, e^{j\omega i}, \cdots, e^{j\omega i(NQ-1)}]^T$, and $\omega = -\frac{2\pi}{NQ}$. Then, the DTF transform of $\mathbf{s}_1$ is

$$\mathbf{s}_1 \xrightarrow{DFT} \mathcal{W}\mathbf{s}_1$$

Using circular time shift properties, the DFT of the cycshift vesion of $\mathbf{s}_1$, $\mathbf{D}^{m_1}\mathbf{s}_1$, is given by

$$\mathbf{D}^{m_1}\mathbf{s}_1 \xrightarrow{DFT} diag(\mathbf{w}_{m_1})\mathcal{W}\mathbf{s}_1$$

where "$diag(\mathbf{w}_{m_1})$" produces a diagonal matrix with diagonal elements equal to the vector $\mathbf{w}_{m_1}$.

With the above relations, the NQ-point DFT (which can be efficiently implemented using an FFT algorithm) of equation (6.2) can be expressed as

$$\begin{aligned} \tilde{\mathbf{x}}_n &= \mathcal{W}\mathbf{x}(n) \\ &= h_1[\delta_1 diag(\mathbf{w}_{m_1+1}) + (1-\delta_1)diag(\mathbf{w}_{m_1})]\mathcal{W}\mathbf{s}_1 + \tilde{\mathbf{u}}_n \\ &\triangleq h_1\tilde{\mathbf{s}}(\tau_1) + \tilde{\mathbf{u}}_n \end{aligned} \tag{6.3}$$

where $\tilde{\mathbf{x}}_n$ and $\tilde{\mathbf{u}}_n$ are the DFT of $\mathbf{x}(n)$ and $\mathbf{u}(n)$ respectively. The delay information is contained in $\tilde{\mathbf{s}}(\tau_1)$.

The additive noise $\tilde{\mathbf{u}}$ is asymptotically (with increasing NQ) uncorrelated among its frequency components, and approximately Gaussian distributed: $\tilde{\mathbf{u}} \sim N(\mathbf{0}, \mathcal{C})$, with the diagonal elements of $\mathcal{C}$, $\sigma^2_{\tilde{\mathbf{u}}}(l)$, $l = 0, 1, ..., NQ-1$, equal to [58]:

$$\begin{aligned} \sigma^2_{\tilde{\mathbf{u}}}(l) &= \tilde{\mathbf{u}}_n(l)\tilde{\mathbf{u}}^*_n(l) \\ &= |\mathbf{u}^T(n)\mathbf{w}_l|^2 \end{aligned} \tag{6.4}$$

where, "$*$" is conjugate. The approximated Gaussian distribution property allows estimation of the channel using an MLE algorithm.

6.2 Maximum Likelihood Channel Estimate

To use an ML algorithm to estimate the unknown channel parameters, one should first find the pdf of the received signal. Utilizing the Gaussian distribution approximation, the pdf of $\tilde{\mathbf{x}}_n$ is given as

$$p(\tilde{\mathbf{x}}_n) = \frac{1}{\pi^{NQ} \mid \mathcal{C} \mid} exp\{-[\tilde{\mathbf{x}}_n - h_1\tilde{\mathbf{s}}(\tau_1)]^H \mathcal{C}^{-1}[\tilde{\mathbf{x}}_n - h_1\tilde{\mathbf{s}}(\tau_1)]\} \tag{6.5}$$

The desired user's unknown channel response h_1 can be found by equating the partial derivative of the log-likelihood function to zero:

$$\frac{\partial ln[p(\tilde{\mathbf{x}}_n)]}{\partial h_1} = 0. \tag{6.6}$$

This results in the estimate of channel response h_1 as

$$\hat{h}_1 = \frac{\tilde{\mathbf{s}}^H(\tau_1)\mathcal{C}^{-1}}{\tilde{\mathbf{s}}^H(\tau_1)\mathcal{C}^{-1}\tilde{\mathbf{s}}(\tau_1)}\tilde{\mathbf{x}}_n, \tag{6.7}$$

and the MLE of the delay τ_1 is given by [6]

$$\hat{\tau}_1 = arg \min_{\tau_1} \frac{|\tilde{\mathbf{s}}^H(\tau_1)\mathcal{C}^{-1}\tilde{\mathbf{x}}_n|^2}{\tilde{\mathbf{s}}^H(\tau_1)\mathcal{C}^{-1}\tilde{\mathbf{s}}(\tau_1)}. \tag{6.8}$$

Usually, a global search using equation (6.8) is required to find the delay. The channel response $\hat{h}_1$ can be obtained by replacing τ_1 with the estimated $\hat{\tau}_1$ in equation (6.7). The unknown covariance matrix $\mathcal{C}$ should be determined before estimating the delay $\hat{\tau}_1$ and channel gain $\hat{h}_1$. Assume $\tilde{\mathbf{x}}_n, n = 1, ..., M$, are received signal sample vectors of M-symbol intervals. Then, considering identical information symbols are transmitted through desired user's channel, one can obtain an estimation of the mean of the desired signal $h_1\tilde{\mathbf{s}}(\tau_1)$ by sample averaging:

$$\hat{\mathbf{m}}_{\tilde{\mathbf{x}}} = \frac{1}{M}\sum_{n=1}^{M}\tilde{\mathbf{x}}_n \tag{6.9}$$

and the MLE of $\mathcal{C}$ using a sample covariance matrix is:

$$\hat{\mathcal{C}} = (\frac{1}{M}\sum_{n=1}^{M}\tilde{\mathbf{x}}_n\tilde{\mathbf{x}}_n^H) - \hat{\mathbf{m}}_{\tilde{\mathbf{x}}}\hat{\mathbf{m}}_{\tilde{\mathbf{x}}}^H \tag{6.10}$$

As mentioned previously, the interference and noise samples $\tilde{\mathbf{u}}_n$ become approximately uncorrelated Gaussian distributed variables. That implies that the covariance matrix $\mathcal{C}$ is approximately a diagonal matrix, with its diagonal elements equal to $\sigma^2_{\tilde{\mathbf{u}}}(0), \sigma^2_{\tilde{\mathbf{u}}}(1)$, ..., $\sigma^2_{\tilde{\mathbf{u}}}(NQ-1)$. Thus, the estimation of covariance matrix $\mathcal{C}$ in (6.10) can be simplified by estimating its diagonal elements only. Then, the non-diagonal elements are set equal to zero. As a result, the DMA may cause loss of information, borne by the non-diagonal elements, because they are in fact non-zero. However, when M is small, insufficient observation samples used to estimate $\mathcal{C}$ will unavoidably introduce error. Particularly, when the SNR is low, a larger estimation error in $\hat{\mathbf{m}}_{\tilde{\mathbf{x}}}$ can result in a significant estimation bias for the non-diagonal elements because these elements are very small due to the uncorrelating property. In many cases, the errors may even be larger than the actual values of these non-diagonal elements. Therefore, ignoring the non-diagonal elements can result in improved estimation performance besides having the advantage of lower computational complexity.

With DMA, the matrix $\mathcal{C}$ is replaced by its diagonal elements. The computational complexity of its inverse matrix, and the estimation algorithms in (6.7) and (6.8) are then reduced to the order of its dimension, NQ. Considering a total of M samples, to get a better estimate, the average of $\tilde{\mathbf{x}}_n$ is used to replace the signle vector in equations (6.7) and (6.8). Then, they are simplified as follows:

$$\hat{\tau}_1 = arg \min_{\tau_1} \frac{|\sum_{l=0}^{NQ-1} \sigma^{-2}_{\tilde{\mathbf{u}}}(l)\tilde{s}^*(\tau_1, l)\tilde{x}(l)|^2}{\sum_{l=0}^{NQ-1} \sigma^{-2}_{\tilde{\mathbf{u}}}(l)|\tilde{s}(\tau_1, l)|^2} \tag{6.11}$$

and

$$\hat{h}_1 = \frac{\sum_{l=0}^{NQ-1} \sigma^{-2}_{\tilde{\mathbf{u}}}(l)\tilde{s}^*(\hat{\tau}_1, l)\tilde{x}(l)}{\sum_{l=0}^{NQ-1} \sigma^{-2}_{\tilde{\mathbf{u}}}(l)|\tilde{s}(\hat{\tau}_1, l)|^2} \tag{6.12}$$

where $\tilde{s}(\tau_1, l)$ is the l-th element of vector $\tilde{\mathbf{s}}(\tau_1)$, and $\tilde{x}(l)$ is the l-th element of the averaged vector $\tilde{\mathbf{x}} = \frac{1}{M}\sum_{n=1}^{M} \tilde{\mathbf{x}}_n$. The noise variance $\sigma^2_{\tilde{\mathbf{u}}}(l)$ is obtained by

$$\sigma^2_{\tilde{\mathbf{u}}}(l) = \frac{1}{M}\{\sum_{n=1}^{M} |\tilde{x}_n(l)|^2 - \frac{1}{M}|\sum_{n=1}^{M} \tilde{x}_n(l)|^2\} \qquad l = 0, 1, \cdots, NQ-1, \tag{6.13}$$

where $\tilde{x}_n(l)$ is the l-th element of the observation sample vector $\tilde{\mathbf{x}}_n$.

6.3 Cramer-Rao Bound

From the signal model in equation (6.3), the MAI plus noise vector $\tilde{\mathbf{u}}_n$ is assumed independent from the desired signal and satisfies the uncorrelated condition:

$$E[\tilde{\mathbf{u}}_{n_1}\tilde{\mathbf{u}}_{n_2}^H] = \mathcal{C}\delta_{n_1 n_2} \qquad n_1, n_2 = 1, ..., M \tag{6.14}$$

where $\delta_{n_1 n_2}$ is Kronecker delta. Estimation is based on a sample vector $\tilde{\mathbf{x}}_n$, $n = 1, 2, ..., M$. Let $\mathcal{X} = [\tilde{\mathbf{x}}_1^T, \tilde{\mathbf{x}}_2^T, ..., \tilde{\mathbf{x}}_M^T]^T$, and using equation (6.5), the log-likelihood function of $\mathcal{X}$ is given by [33](eq.10):

$$\begin{aligned} lnL(\mathcal{X}) &= Const. - Mln|\mathcal{C}| - \sum_{n=1}^{M}(\tilde{\mathbf{x}}_n - h_1\tilde{\mathbf{s}})^H \\ &\quad \cdot\mathcal{C}^{-1}(\tilde{\mathbf{x}}_n - h_1\tilde{\mathbf{s}}) \end{aligned} \tag{6.15}$$

The unknown parameters of the likelihood function include the desired user's complex amplitude $h_1 = \sqrt{a_1}\gamma_1 b_1$, propagation delay τ_1, and noise covariance matrix $\mathcal{C}$.

If only the vector $\beta = [h_1, \tau_1]^T$ is considered unknown, and it is assume that the channel h_1 is real, otherwise its phase should be considered as another unknown, the gradient $\partial lnL(\mathcal{X})/\partial\beta$ is:

$$\frac{\partial lnL(\mathcal{X})}{\partial\beta} = \begin{bmatrix} \frac{\partial lnL(\mathcal{X})}{\partial h_1} \\ \frac{\partial lnL(\mathcal{X})}{\partial \tau_1} \end{bmatrix} \tag{6.16}$$

The gradient is given as

$$\begin{aligned} \frac{\partial lnL(\mathcal{X})}{\partial h_1} &= -\sum_{n=1}^{M}\{\frac{\partial(\tilde{\mathbf{x}}_n - h_1\tilde{\mathbf{s}})^H}{\partial h_1}\mathcal{C}^{-1}(\tilde{\mathbf{x}}_n - h_1\tilde{\mathbf{s}}) + (\tilde{\mathbf{x}}_n - h_1\tilde{\mathbf{s}})^H\mathcal{C}^{-1}\frac{\partial(\tilde{\mathbf{x}}_n - h_1\tilde{\mathbf{s}})}{\partial h_1}\} \\ &= -2\sum_{n=1}^{M} Re\{\frac{\partial(\tilde{\mathbf{x}}_n - h_1\tilde{\mathbf{s}})^H}{\partial h_1}\mathcal{C}^{-1}(\tilde{\mathbf{x}}_n - h_1\tilde{\mathbf{s}})\} \\ &= 2\sum_{n=1}^{M} Re\{\tilde{\mathbf{s}}^H\mathcal{C}^{-1}\tilde{\mathbf{u}}_n\} \end{aligned} \tag{6.17}$$

$$\begin{aligned}\frac{\partial lnL(\mathcal{X})}{\partial \tau_1} &= -2\sum_{n=1}^{M} Re\{\frac{\partial(\tilde{\mathbf{x}}_n - h_1\tilde{\mathbf{s}})^H}{\partial \tau_1}\mathcal{C}^{-1}(\tilde{\mathbf{x}}_n - h_1\tilde{\mathbf{s}})\} \\ &= 2\sum_{n=1}^{M} Re\{h_1\frac{\partial \tilde{\mathbf{s}}^H}{\partial \tau_1}\mathcal{C}^{-1}\tilde{\mathbf{u}}_n\} \end{aligned} \tag{6.18}$$

The derivative with respect to τ_1 in equation (6.18) is equivalent to a derivative with respect to δ_1, which yields,

$$\frac{\partial \tilde{\mathbf{s}}^H}{\partial \tau_1} = \mathbf{s}_1^T W^H D^H \qquad \delta_1 \neq 0 \tag{6.19}$$

where the diagonal matrix $D = diag(\mathbf{w}_{m_1+1} - \mathbf{w}_{m_1})$. If $\delta_1 = 0$, the derivative gives zero, meaning equation (6.18) is not suitable for such a case. Considering delays with $\delta_1 = 0$ are very scarce in simulations, the CRLB can still be used for performance evaluation. Using equation (6.19), equation (6.18) becomes

$$\frac{\partial lnL(\mathcal{X})}{\partial \tau_1} = 2\sum_{n=1}^{M} Re\{h_1\mathbf{s}_1^T W^H D^H \mathcal{C}^{-1}\tilde{\mathbf{u}}_n\} \tag{6.20}$$

Then, the corresponding Fisher information matrix is

$$I(\beta) = \begin{bmatrix} E[\frac{\partial lnL(\mathcal{X})}{\partial h_1}\frac{\partial lnL(\mathcal{X})}{\partial h_1}] & E[\frac{\partial lnL(\mathcal{X})}{\partial h_1}\frac{\partial lnL(\mathcal{X})}{\partial \tau_1}] \\ E[\frac{\partial lnL(\mathcal{X})}{\partial \tau_1}\frac{\partial lnL(\mathcal{X})}{\partial h_1}] & E[\frac{\partial lnL(\mathcal{X})}{\partial \tau_1}\frac{\partial lnL(\mathcal{X})}{\partial \tau_1}] \end{bmatrix} \tag{6.21}$$

To obtain the matrix I, first it is noticed that for any complex vector $\mathbf{p}$ and $\mathbf{q}$, the following general expression is valid:

$$\begin{aligned} & E[\sum_{n=1}^{M} Re\{\mathbf{p}^H\tilde{\mathbf{u}}_n\}\cdot\sum_{m=1}^{M} Re\{\mathbf{q}^H\tilde{\mathbf{u}}_m\}] \\ &= \sum_{n=1}^{M} E[\frac{\mathbf{p}^H\tilde{\mathbf{u}}_n + \tilde{\mathbf{u}}_n^H\mathbf{p}}{2}\cdot\frac{\mathbf{q}^H\tilde{\mathbf{u}}_n + \tilde{\mathbf{u}}_n^H\mathbf{q}}{2}] \\ &= \frac{1}{4}\sum_{n=1}^{M} E[\mathbf{p}^H\tilde{\mathbf{u}}_n\mathbf{q}^H\tilde{\mathbf{u}}_n + \mathbf{p}^H\tilde{\mathbf{u}}_n\tilde{\mathbf{u}}_n^H\mathbf{q} + \tilde{\mathbf{u}}_n^H\mathbf{p}\mathbf{q}^H\tilde{\mathbf{u}}_n + \tilde{\mathbf{u}}_n^H\mathbf{p}\tilde{\mathbf{u}}_n^H\mathbf{q}] \end{aligned} \tag{6.22}$$

If assuming uncorrelated noise, that is $E[\tilde{\mathbf{u}}_n(i)\tilde{\mathbf{u}}_n^*(j)] = 0$, for $i \neq j$, and without loss of generality assuming that the real and imaginary part of $\tilde{\mathbf{u}}_n(i)$ are uncorrelated with same variance, it is easily shown that $E[\tilde{\mathbf{u}}_n(i)\tilde{\mathbf{u}}_n(i)] = 0$. Then, the first and fourth terms in $E[\cdot]$ of (6.22) become zero. Then, the expection becomes,

$$E[\sum_{n=1}^{M} Re\{\mathbf{p}^H\tilde{\mathbf{u}}_n\}\cdot\sum_{m=1}^{M} Re\{\mathbf{q}^H\tilde{\mathbf{u}}_m\}] = \frac{1}{4}\sum_{n=1}^{M} E[\mathbf{p}^H\tilde{\mathbf{u}}_n\tilde{\mathbf{u}}_n^H\mathbf{q} + \mathbf{q}^H\tilde{\mathbf{u}}_n\tilde{\mathbf{u}}_n^H\mathbf{p}]$$

$$= \frac{1}{2}\sum_{n=1}^{M} Re\{\mathbf{p}^H \mathcal{C}\mathbf{q}\} \tag{6.23}$$

From equations (6.17), and using the relation in (6.23), it is easy to show that

$$\begin{aligned} I_{h_1h_1} &= E[\frac{\partial lnL(\mathcal{X})}{\partial h_1}\frac{\partial lnL(\mathcal{X})}{\partial h_1}] = 4E[\sum_{n=1}^{M} Re\{(\mathcal{C}^{-1}\tilde{\mathbf{s}})^H\tilde{\mathbf{u}}_n\}\sum_{m=1}^{M} Re\{(\mathcal{C}^{-1}\tilde{\mathbf{s}})^H\tilde{\mathbf{u}}_m\}] \\ &= 2\sum_{n=1}^{M} Re\{(\mathcal{C}^{-1}\tilde{\mathbf{s}})^H\mathcal{C}(\mathcal{C}^{-1}\tilde{\mathbf{s}})\} = 2\sum_{n=1}^{M} Re\{\tilde{\mathbf{s}}^H\mathcal{C}^{-1}\tilde{\mathbf{s}}\} \end{aligned} \tag{6.24}$$

Similarly, using equations (6.20), it can be shown that

$$\begin{aligned} I_{h_1\tau_1} &= E[\frac{\partial lnL(\mathcal{X})}{\partial h_1}\frac{\partial lnL(\mathcal{X})}{\partial \tau_1}] = 2\sum_{n=1}^{M} Re\{h_1\tilde{\mathbf{s}}^H\mathcal{C}^{-1}DW\mathbf{s}_1\} \\ I_{\tau_1\tau_1} &= E[\frac{\partial lnL(\mathcal{X})}{\partial \tau_1}\frac{\partial lnL(\mathcal{X})}{\partial \tau_1}] = 2\sum_{n=1}^{M} h_1^2 Re\{\mathbf{s}_1^T W^H D^H\mathcal{C}^{-1}DW\mathbf{s}_1\} \end{aligned} \tag{6.25}$$

If the propagation delay τ_1 is the only unknown, the Cramer-Rao bound for estimation of τ_1 is given as

$$CRLB(\tau_1) = \frac{1}{\sqrt{I_{\tau_1\tau_1}}} \tag{6.26}$$

A different derivation of the CRLB could be found in [60], which is based on the extended Bang's formula for the generalized covariance matrix $\mathcal{C}$ case, and results in the same solutions as (6.25). It should be noted that the bound in (6.26) becomes poorer when more unknown parameters are taken into consideration, for instance the channel gain h_1 and the noise covariance matrix $\mathcal{C}$.

6.4 Performance Evaluation

Defining the root mean square (RMS) estimation error σ_ϵ as

$$\sigma_\epsilon = \sqrt{E[\{\hat{\tau}_1 - \tau_1\}^2]} \tag{6.27}$$

As shown in the previous chapter, the detector's performance deteriorates approximately an order of magnitude for every 0.2 chips timing error. To minimize the performance loss, it is decided that a delay acquisition error occurred when the

estimation error $\epsilon > \epsilon_{max} = 0.2T_c$. Then, the acquisition probability is the percentage of estimations with $\epsilon \leq 0.2T_c$ among all the independent simulation runs.

In the simulations, the code length N was set to 15. The channel fading was assumed to be quasi-static within the channel training period. The desired user's SNR per symbol was equal to $8dB$. All users transmit the same energy as the desired user, i.e. $ISR = 0dB$. A total of 500 Monte Carlo runs, each with a different delay profile, were performed for each simulation. The results were averaged and investigated.

In Figures 6.2 and 6.3, the acquisition probability and the RMS estimation error as a function of the number of users, respectively is depicted for two sampling factor values: Q =1 and 2. The length of the training sequence was set to 50 bits. The proposed DMA scheme which uses the diagonal covariance matrix outperforms the scheme which uses the whole matrix $\mathcal{C}$. So, besides its lower computational complexity, the DMA approach effectively reduces the timing error caused by erroneous non-diagonal elements.

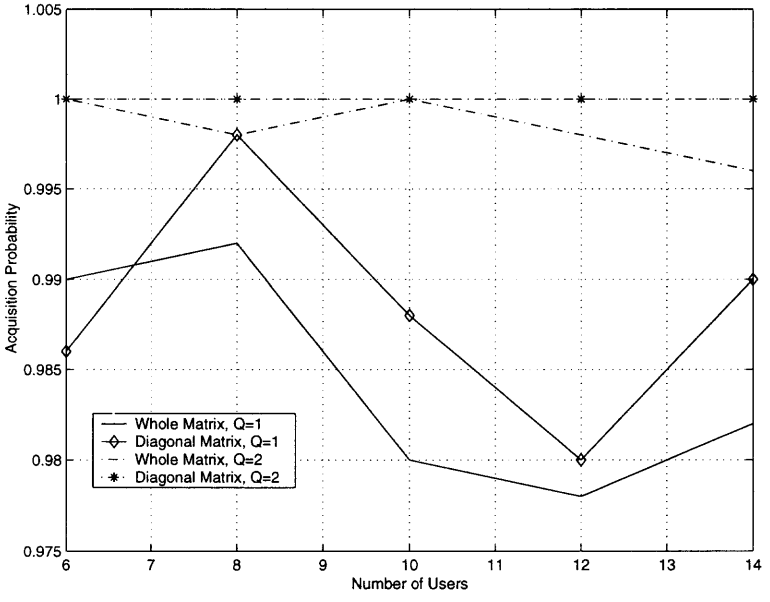

Figure 6.2 Acquisition probability vs different number of users.

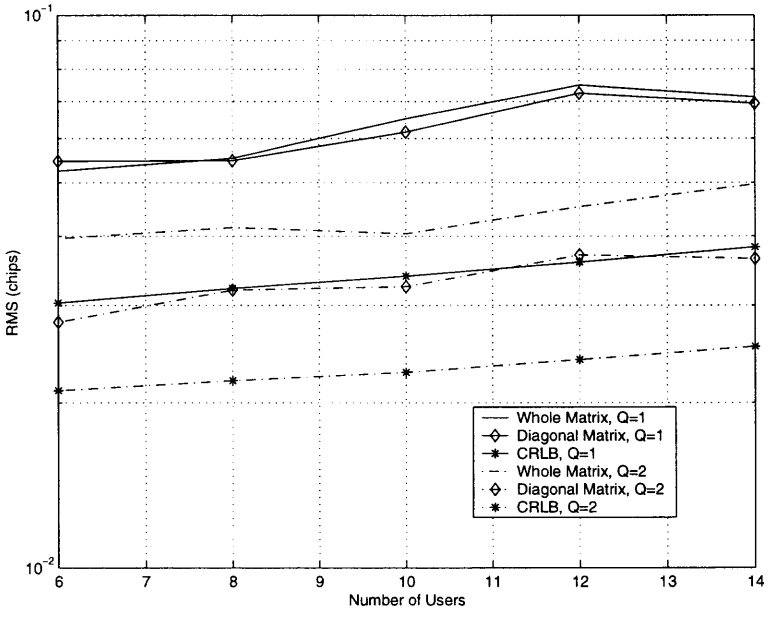

Figure 6.3 RMS estimation error vs different number of users.

In Figures 6.4 and 6.5, the acquisition probability and RMS timing error are shown as a function of the SNR. For the simulation, six users and 50 bits of acquisition time were assumed. For $Q = 1$, the RMS of DMA is smaller than that of the full matrix scheme in the low SNR region, i.e. 8dB and less. An increased SNR results in a better estimation of $\mathcal{C}$, and thus, estimation performance using the whole matrix outperforms DMA for higher SNR. However, with an over sampling factor, $Q = 2$, the output SNR of the MF is reduced due to the shorter integration interval, making the estimate of the non-diagonal elements unreliable. Consequently, the region where DMA exhibits better performance was extended to 14dB. Therefore, DMA with the over sampling technique improves the performance even when the SNR is high.

In Figures 6.6 and 6.7, the acquisition probability and the RMS estimation error, respectively as a function of the acquisition time is shown. Six users were assumed and SNR was set to 8dB. The size M should be sufficiently large such that for the full matrix scheme, the estimated $\mathcal{C}$ remains non-singular. Otherwise,

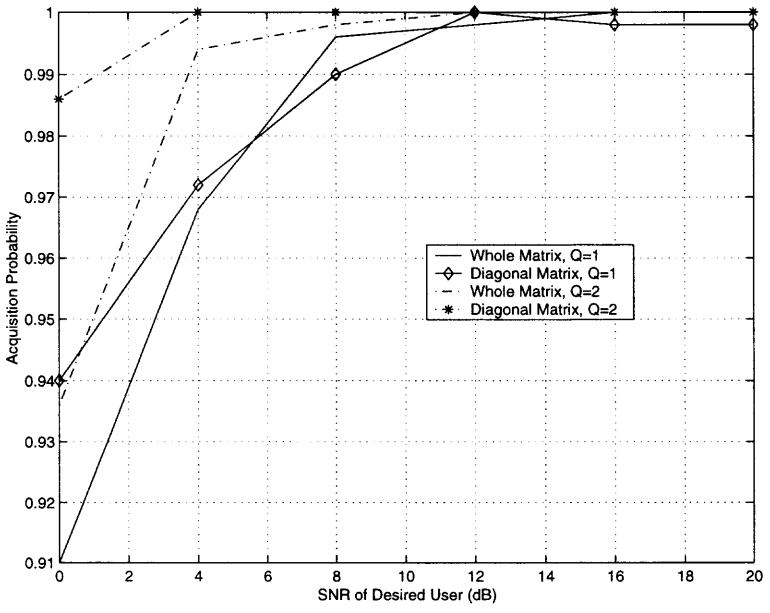

Figure 6.4 Acquisition probability vs SNR of desired user.

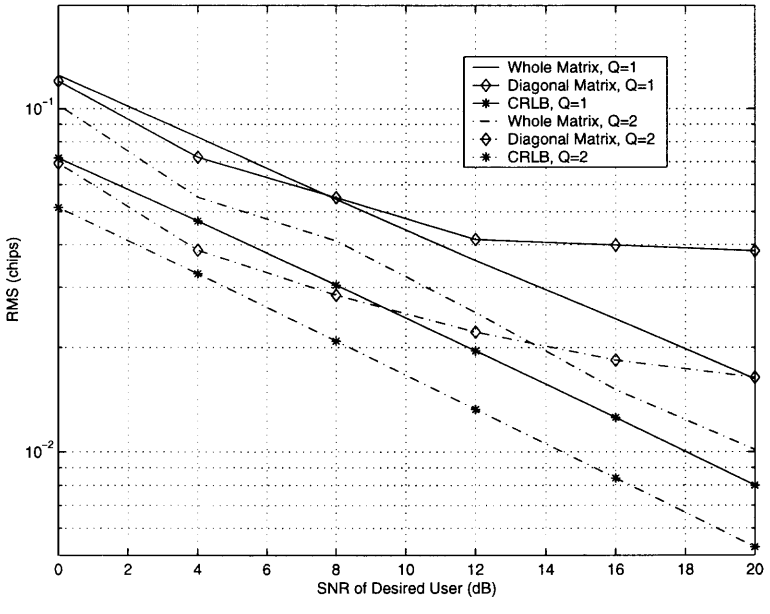

Figure 6.5 RMS estimation error vs SNR of desired user.

the singularity of $\mathcal{C}$ can severely deteriorate the estimation performance. From equation (6.10), the theoretical minimum number of samples required for a non-singular $\mathcal{C}$ is $M = NQ$. In practice, M should be somewhat larger than NQ. Figures 6.6 and 6.7 show that the full matrix scheme, using over sampling $Q = 2$, has poor performance when $M \leq 30$ bits because in this case, the minimum number of samples required is $15 \times 2 = 30$. However, the DMA still works well even for M as small as 20 bits. This is because by treating $\mathcal{C}$ as a diagonal matrix, it remains non-singular, even when M is less than NQ. Therefore, the DMA scheme provides the capability to estimate the delay with a short acquisition time as well as improved performance with over sampling.

It is worth mentioning that the CRLB's given in the figures were derived assuming the propagation delay was the only unknown parameter. The actual CRLB's should be even closer to the corresponding RMS curves because the channel response was also unknown in the simulations.

As a conclusion, the proposed DMA ML estimator, together with over sampling, provides faster and more accurate delay estimation compared to the regular ML estimator. Hence, it is more suitable for timing acquisition in a time-variant channel.

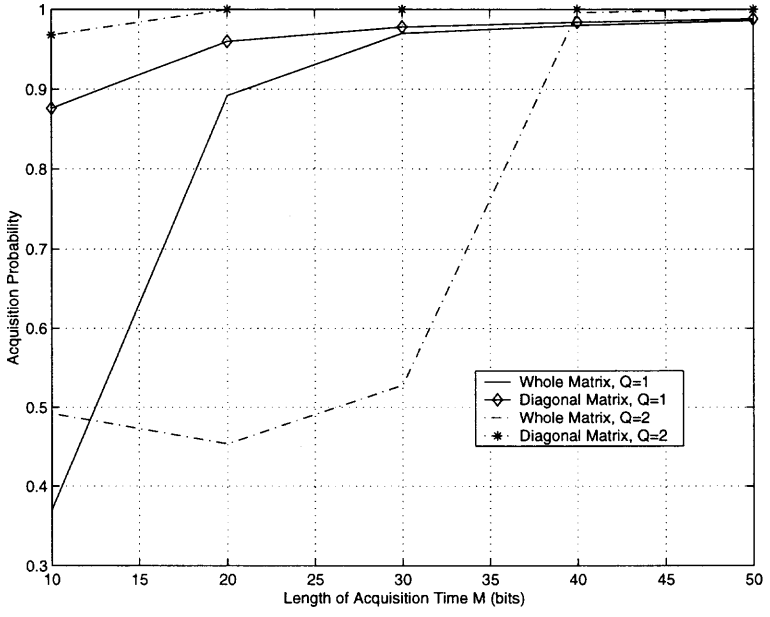

Figure 6.6 Acquisition probability vs length of acquisition time.

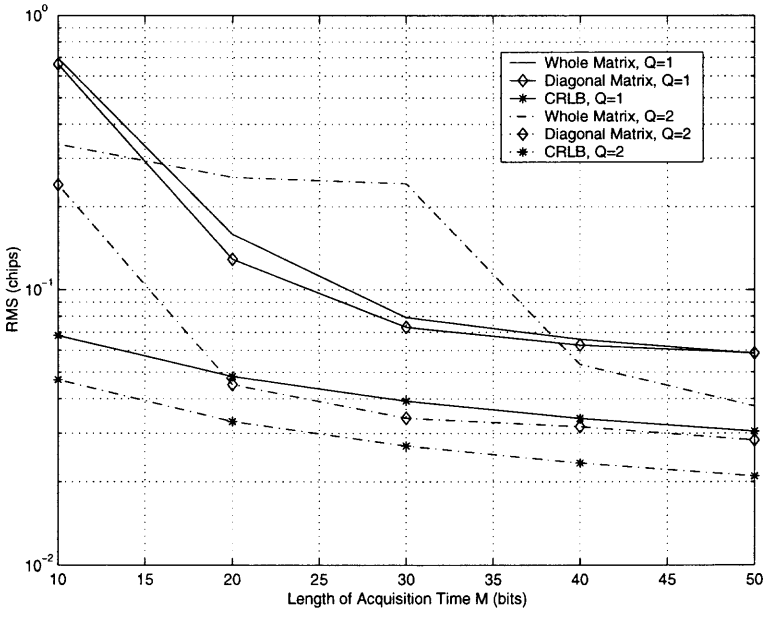

Figure 6.7 RMS estimation error vs length of acquisition time.

CHAPTER 7
CONCLUSIONS

With high data rate communications, higher chip rates are used. The increased chip rate results in increased delay spread in terms of the chip interval, in a multipath environment. Also, due to the higher data rates the channel fading becomes slow in terms of the symbol interval. Most of multiuser detectors consider only small delay spread, usually less than one symbol interval. Although some of them can be extended to a large delay spread situation, the increased computational complexity may restrict such applications. As a result, the reduced complexity detector was proposed that is simplified by exploiting the diagonal dominant property of the correlation matrix. The so-called de-biasing technique significantly reduces the computational redundency without performance loss. The adaptive bootstrap algorithm was also used to combat the large delay spread problem. It was shown to provide good near-far resistance with EGC or MRC without a requirement for a training sequence, a promising approach for adaptive implementation in a time-variant fading environment for channel variation tracking.

M-ary quadrature modulation is another common approach to achieve high data rate transmission. A paramount advantage of M-ary quadrature modulation is that the increase in information data rate is not at the expense of greater bandwidth. However, the detection of M-ary quadrature modulated signals in a time-variant fading channel becomes more challenging as the modulation order increases. The transmitted signal constellation could be distorted and rotated due to the channel. The proposed detector, which is based on an FIR digital filter, jointly with an adaptive channel gain estimator and phase corrector, was shown to provide promising performance for any M-ary quadrature modulated signal with relatively low complexity. The signal distortion was effectively removed by the proposed detector. It should be mentioned that the phase corrector may not blindly

compensate an arbitrary phase shift. In case the phase shift is outside the correction range, additional measurements should be taken, for example employing a training sequence.

The proposed Minimum Variance Decorrelating (MVD) receiver presents performance close to the linear MMSE receiver in a time-variant fading channel. Its implementation is relatively simple and has the ability to detect the signal blindly. The MVD receiver focuses on single user detection and provides decoupled multipath fading. These features enable the MVD detector to be applied to various situations. As a consequence, it was extended to adaptive interference cancellation, and transmit diversity applications.

With the decoupling of multipath signals, the MVD receiver provides an efficient way to estimate and regenerate the interfering signals, and remove them from the received signals. Although the complexity of each building block is increased, compared to linear Parallel Interference Canceler (PIC) and Succesive Interference Canceler (SIC), the MVD based adaptive multistage PIC and SIC reduce the complexity of the receiver by keeping the number of stages at a minimum. As was shown, the whole receivers with 1 to 2 stages give the performance close to the single user bound because the MVD receiver provides an accurate estimate of the interference signals at the earliest stage.

Unlike other Transmit Diversity (TD) schemes, the proposed TD-MVD scheme can work in asynchronous channels, which is more practical. As a result, TD can be conveniently implemented for the downlink because the transmit antennas can be mounted at any place, even in different base stations, to obtain full spatial diversity gain without careful coordination of the multiple transmissions for synchronous reception. The proposed scheme is also robust to variations in the number of multipaths. The dominant multipath signals coming from each transmitted antenna will be selected and decorrelated. This selection can be dynamic, i.e. the number

of multipaths selected and associated with each antenna can vary to maximize the receiver performance. In addition to the convenience and flexibility provided by the MVD detector, the performance is further improved by using $R_{\mathbf{u}}$ instead of $R_{\mathbf{x}}$ without a significant increase in complexity. Moreover, the performance is less sensitive to the estimation accuracy of $R_{\mathbf{u}}$, which enables the MVD receiver to operate with a small number of samples, a nice property for applications in a time-variant channel.

It is shown that MLE with Diagonal Matrix Approximation (DMA) results in fast path delay estimation and channel acquisition. The estimation accuracy approaches the CRLB using an oversampling technique, while the computational complexity is reduced to the order of signal dimension. Another important property is that the requirement for a non-singular covariance matrix is relaxed. So, the estimator can work using smaller number of samples while keeping the performance close to the CRLB. It implies that the proposed estimator is suitable for quick channel acquisition, and thus, suitable for a time-variant fading channel environment.

APPENDIX A

DERIVATION OF QAM CHANNEL ESTIMATION

Assume an M-ary QAM signal of user k, $b_k = b_{kR} + jb_{kS}$, where b_{kR} and b_{kS} take values from the set $\{1, 3, ..., \sqrt{M} - 1\}$. The estimated $\hat{b}_k = \hat{b}_{kR} + j\hat{b}_{kS}$ is the output of decorrelator.

$$\begin{aligned} E[b_k * sgn(\hat{b}_k^*)] &= E[b_{kR}sgn(\hat{b}_{kR}) + b_{kS}sgn(\hat{b}_{kS})] \\ &+ jE[-b_{kR}sgn(\hat{b}_{kS}) + b_{kS}sgn(\hat{b}_{kR})] \\ &= E[b_{kR}sgn(\hat{b}_{kR}) + b_{kS}sgn(\hat{b}_{kS})] \end{aligned} \tag{A.1}$$

since b_{kR} and $\hat{b}_{kS}$, as well as b_{kS} and $\hat{b}_{kR}$ are assumed uncorrelated. Also,

$$\begin{aligned} &E[b_{kR}sgn(\hat{b}_{kR})] \\ &= E\{E[b_{kR}sgn(\hat{b}_{kR})|b_{kR}]\} \\ &= \frac{1}{\sqrt{M/4}} \sum_{i=1}^{\sqrt{M/4}} E[b_{kR}sgn(\hat{b}_{kR})|b_{kR} = 2i - 1] \\ &= \frac{1}{\sqrt{M/4}} \sum_{i=1}^{\sqrt{M/4}} (2i - 1)E[sgn(\hat{b}_{kR})|b_{kR} = 2i - 1] \end{aligned} \tag{A.2}$$

If the noise in the I and Q branches is AWGN with zero mean and variance σ^2, then the outcome of

$$sgn(\hat{b}_{kR})|(b_{kR} = 2i - 1) = \begin{cases} 1 & with probability \quad 1 - Q(\frac{2i-1}{\sigma}) \\ -1 & with probability \quad Q(\frac{2i-1}{\sigma}) \end{cases} \tag{A.3}$$

so,

$$E[b_{kR}sgn(\hat{b}_{kR})] = \frac{1}{\sqrt{M/4}} \sum_{i=1}^{\sqrt{M/4}} (2i - 1)[1 - 2Q(\frac{2i - 1}{\sigma})], \tag{A.4}$$

Also, $E[b_{kS}sgn(\hat{b}_{kS})]$ will have the same result:

$$E[b_k * sgn(\hat{b}_k^*)] = \frac{2}{\sqrt{M/4}} \sum_{i=1}^{\sqrt{M/4}} (2i - 1)[1 - 2Q(\frac{2i - 1}{\sigma})]. \tag{A.5}$$

APPENDIX B

PERFORMANCE EVALUATION USING $R_{\mathbf{X}}$ AND $R_{\mathbf{U}}$

According to equation (4.10), the SNR with the optimal solution of the weight matrix for both cases is given as

$$SNR_{\mathbf{x}} = \frac{|\mathbf{\Gamma}(n)|^4}{\mathbf{\Gamma}^H(n)(C^H R_{\mathbf{x}}^{-1}(n)C)^{-1}C^H R_{\mathbf{x}}^{-1}(n)R_{\mathbf{u}}(n)R_{\mathbf{x}}^{-1}(n)C(C^H R_{\mathbf{x}}^{-1}(n)C)^{-1}\mathbf{\Gamma}(n)} \quad \text{(B.1)}$$

$$SNR_{\mathbf{u}} = \frac{|\mathbf{\Gamma}(n)|^4}{\mathbf{\Gamma}^H(n)(C^H R_{\mathbf{u}}^{-1}(n)C)^{-1}\mathbf{\Gamma}(n)} \quad \text{(B.2)}$$

From equation (4.1) it is clear that

$$R_{\mathbf{x}}(n) = C\mathbf{\Gamma}(n)\mathbf{\Gamma}^H(n)C^H + R_{\mathbf{u}}(n) \quad \text{(B.3)}$$

Using Woodbury identity $(A + \mathbf{b}\mathbf{b}^H)^{-1} = A^{-1} - \frac{A^{-1}\mathbf{b}\mathbf{b}^H A^{-1}}{1+\mathbf{b}^H A^{-1}\mathbf{b}}$, and let $\mathbf{b} = C\mathbf{\Gamma}(n)$, we have

$$R_{\mathbf{x}}^{-1}(n) = R_{\mathbf{u}}^{-1}(n) - \frac{R_{\mathbf{u}}^{-1}(n)C\mathbf{\Gamma}(n)\mathbf{\Gamma}^H(n)C^H R_{\mathbf{u}}^{-1}(n)}{1 + \mathbf{\Gamma}^H(n)C^H R_{\mathbf{u}}^{-1}(n)C\mathbf{\Gamma}(n)} \quad \text{(B.4)}$$

Let $T_{\mathbf{x}} = C^H R_{\mathbf{x}}^{-1}(n)C$ and $T_{\mathbf{u}} = C^H R_{\mathbf{u}}^{-1}(n)C$, and multiply equation (B.4) on the left side by C^H and on the right side by C, it becomes

$$T_{\mathbf{x}} = T_{\mathbf{u}} - \frac{T_{\mathbf{u}}\mathbf{\Gamma}(n)\mathbf{\Gamma}^H(n)T_{\mathbf{u}}}{1 + \mathbf{\Gamma}^H(n)T_{\mathbf{u}}\mathbf{\Gamma}(n)} \quad \text{(B.5)}$$

Comparing equation (B.1) and (B.2) shows that the difference is in the inner part of their denominators. Their relation is obtained following

$$\begin{aligned}
& C^H R_{\mathbf{x}}^{-1}(n)R_{\mathbf{u}}(n)R_{\mathbf{x}}^{-1}(n)C \\
= \; & C^H[R_{\mathbf{u}}^{-1}(n) - \frac{R_{\mathbf{u}}^{-1}(n)C\mathbf{\Gamma}(n)\mathbf{\Gamma}^H(n)C^H R_{\mathbf{u}}^{-1}(n)}{1 + \mathbf{\Gamma}^H(n)T_{\mathbf{u}}\mathbf{\Gamma}(n)}]R_{\mathbf{u}}(n)[R_{\mathbf{u}}^{-1}(n) \\
& -\frac{R_{\mathbf{u}}^{-1}(n)C\mathbf{\Gamma}(n)\mathbf{\Gamma}^H(n)C^H R_{\mathbf{u}}^{-1}(n)}{1 + \mathbf{\Gamma}^H(n)T_{\mathbf{u}}\mathbf{\Gamma}(n)}]C \\
= \; & T_{\mathbf{u}} - 2\frac{T_{\mathbf{u}}\mathbf{\Gamma}(n)\mathbf{\Gamma}^H(n)T_{\mathbf{u}}}{1 + \mathbf{\Gamma}^H(n)T_{\mathbf{u}}\mathbf{\Gamma}(n)} + \frac{T_{\mathbf{u}}\mathbf{\Gamma}(n)\mathbf{\Gamma}^H(n)T_{\mathbf{u}}\mathbf{\Gamma}(n)\mathbf{\Gamma}^H(n)T_{\mathbf{u}}}{(1 + \mathbf{\Gamma}^H(n)T_{\mathbf{u}}\mathbf{\Gamma}(n))^2} \\
= \; & T_{\mathbf{u}} - 2\frac{T_{\mathbf{u}}\mathbf{\Gamma}(n)\mathbf{\Gamma}^H(n)T_{\mathbf{u}}}{1 + \mathbf{\Gamma}^H(n)T_{\mathbf{u}}\mathbf{\Gamma}(n)} + \frac{T_{\mathbf{u}}\mathbf{\Gamma}(n)\mathbf{\Gamma}^H(n)T_{\mathbf{u}}}{1 + \mathbf{\Gamma}^H(n)T_{\mathbf{u}}\mathbf{\Gamma}(n)}T_{\mathbf{u}}^{-1}\frac{T_{\mathbf{u}}\mathbf{\Gamma}(n)\mathbf{\Gamma}^H(n)T_{\mathbf{u}}}{1 + \mathbf{\Gamma}^H(n)T_{\mathbf{u}}\mathbf{\Gamma}(n)}
\end{aligned} \quad \text{(B.6)}$$

Equation (B.5) can be rewritten as

$$\frac{T_{\mathbf{u}}\mathbf{\Gamma}(n)\mathbf{\Gamma}^H(n)T_{\mathbf{u}}}{1+\mathbf{\Gamma}^H(n)T_{\mathbf{u}}\mathbf{\Gamma}(n)} = T_{\mathbf{u}} - T_{\mathbf{x}} \tag{B.7}$$

Replace equation (B.6) using equation (B.7),

$$\begin{aligned} C^H R_{\mathbf{x}}^{-1}(n) R_{\mathbf{u}}(n) R_{\mathbf{x}}^{-1}(n) C &= T_{\mathbf{u}} - 2(T_{\mathbf{u}} - T_{\mathbf{x}}) + (T_{\mathbf{u}} - T_{\mathbf{x}}) T_{\mathbf{u}}^{-1} (T_{\mathbf{u}} - T_{\mathbf{x}}) \\ &= T_{\mathbf{x}} T_{\mathbf{u}}^{-1} T_{\mathbf{x}} \end{aligned} \tag{B.8}$$

Apply equation (B.8) to equation (B.1), which gives

$$\begin{aligned} SNR_{\mathbf{x}} &= \frac{|\mathbf{\Gamma}(n)|^4}{\mathbf{\Gamma}^H(n) T_{\mathbf{x}}^{-1} C^H R_{\mathbf{x}}^{-1}(n) R_{\mathbf{u}}(n) R_{\mathbf{x}}^{-1}(n) C T_{\mathbf{x}}^{-1} \mathbf{\Gamma}(n)} \\ &= \frac{|\mathbf{\Gamma}(n)|^4}{\mathbf{\Gamma}^H(n) T_{\mathbf{x}}^{-1} T_{\mathbf{x}} T_{\mathbf{u}}^{-1} T_{\mathbf{x}} T_{\mathbf{x}}^{-1} \mathbf{\Gamma}(n)} \\ &= \frac{|\mathbf{\Gamma}(n)|^4}{\mathbf{\Gamma}^H(n) (C^H R_{\mathbf{u}}^{-1}(n) C)^{-1} \mathbf{\Gamma}(n)} \\ &= SNR_{\mathbf{u}} \end{aligned} \tag{B.9}$$

APPENDIX C

SUFFICIENT CONDITION FOR SIC WITH PERFECT POWER CONTROL

1. The BER for the 1st user is $P_{e1}(SINR)$.

2. For the 2nd user, its $SINR$ has two possible values:

   - $SINR_2^c$ ($> SINR$) with probability 1-$P_{e1}(SINR)$ when the 1st user is detected and canceled correctly.
   - $SINR_2^e$ ($< SINR$) with probability $P_{e1}(SINR)$ when the 1st user is detected and canceled incorrectly.

   The BER $\hat{P}_{e2}$ is given as

   $$\hat{P}_{e2} = P_{e2}(SINR_2^c)[1 - P_{e1}(SINR)] + P_{e2}(SINR_2^e)P_{e1}(SINR) \qquad \text{(C.1)}$$

   To improve performance with SIC, it is required that $\hat{P}_{e2} < P_{e2}(SINR)$. Or

   $$\frac{P_{e2}(SINR) - P_{e2}(SINR_2^c)}{P_{e2}(SINR_2^e) - P_{e2}(SINR_2^c)} > P_{e1}(SINR) \qquad \text{(C.2)}$$

3. For the 3rd user, its $SINR$ has four possible values. They are

   - $SINR_3^c$ ($> SINR$) with probability $[1 - P_{e1}(SINR)][1 - \hat{P}_{e2}] = 1 - P_{e1}(SINR) - \hat{P}_{e2} + o(P_e^2)$ when both the 1st and 2nd users are detected and canceled correctly.
   - $SINR_3^{e1}$ with probability $P_{e1}(SINR)[1-\hat{P}_{e2}] = P_{e1}(SINR)+O(P_e^2)$ when detection and cancellation for 1st user is incorrect but correct for 2nd user.
   - $SINR_3^{e2}$ with probability $[1 - P_{e1}(SINR)]\hat{P}_{e2} = \hat{P}_{e2} + O(P_e^2)$ when detection and cancellation for the 1st user is correct but incorrect for the 2nd user.

- $SINR_3^{ea}$ ($< SINR$) with probability $P_{e1}(SINR)\hat{P}_{e2} = O(P_e^2)$ when both the 1st and 2nd users are detected and canceled incorrectly.

With perfect power control, canceling either the 1st or 2nd user's signal will equally enhance or reduce the SINR of user 3. Thus, it is assumed that $SINR_3^{e1} = SINR_3^{e2} = SINR_3^e$. Ignoring the higher order items, we get the BER $\hat{P}_{e3}$ of user 3 as

$$\begin{aligned}
\hat{P}_{e3} &\approx P_{e3}(SINR_3^c)[1 - P_{e1}(SINR) - \hat{P}_{e2}] + P_{e3}(SINR_3^e)P_{e1}(SINR) \\
&\quad + P_{e3}(SINR_3^e)\hat{P}_{e2} \\
&= P_{e3}(SINR_3^c)[1 - P_{e1}(SINR)] + P_{e3}(SINR_3^e)P_{e1}(SINR) \\
&\quad + [P_{e3}(SINR_3^e) - P_{e3}(SINR_3^c)]\hat{P}_{e2} \\
&\leq P_{e3}(SINR_3^c)[1 - P_{e1}(SINR)] + P_{e3}(SINR_3^e)P_{e1}(SINR) \\
&\quad + [P_{e3}(SINR_3^e) - P_{e3}(SINR_3^c)]P_{e2}(SINR) \\
&< P_{e3}(SINR) \qquad \text{(C.3)}
\end{aligned}$$

Rewriting equation (C.3), it becomes

$$\frac{P_{e3}(SINR) - P_{e3}(SINR_3^c)}{P_{e3}(SINR_3^e) - P_{e3}(SINR_3^c)} > \sum_{l=1}^{2} P_{el}(SINR) \qquad \text{(C.4)}$$

4. The same proof applies in the case of more users.

If the BER performance is assumed the same for all users, the subscript k in P_{ek} can be dropped. Then, equation (4.40) becomes

$$\frac{P_e(SINR) - P_e(SINR_k^c)}{P_e(SINR_k^e) - P_e(SINR_k^c)} > (k-1)P_e(SINR) \qquad \text{(C.5)}$$

With simple manipulation, we can re-write equation (C.5) as

$$\frac{P_e(SINR)}{P_e(SINR_k^c)} > \frac{1 - (k-1)P_e(SINR)}{1 - (k-1)P_e(SINR_k^e)} \qquad \text{(C.6)}$$

REFERENCES

1. N. P. Shein, "An algorithm for generating nonuniformly spaced correlated samples for simulating a nonselective rayleigh fading channel," in *Proc. of MILCOM'91*, pp. 291–294, 1991.

2. S. Verdu, "Minimum probability of error for asynchronous gaussian multiple access channel," *IEEE trans. Info. Theory*, vol. IT-32, no. 1, pp. 85–96, 1986.

3. R. Lupas and S. Verdu, "Linear multiuser detector for asynchronous code division multiple access channels," *IEEE trans. Info. Theory*, vol. IT-35, no. 1, pp. 123–136, 1989.

4. R. Lupas and S. Verdu, "Near-far resistance of multiuser detectors in asynchronous channels," *IEEE trans. Comm.*, vol. COM-38, no. 4, pp. 496–508, 1990.

5. S. Verdu, "Adaptive multiuser detection," in *ISSSTA '94., IEEE Third International Symposium on Spread Spectrum Techniques and Applications*, vol. 1, pp. 43–50, 1994.

6. D. H. Johnson and D. E. Dudgeon, *Array Signal Processing: Concepts and Techniques*, Prentice Hall, Englewood Cliffs, N.J., 1993.

7. M. Honig, U. Madhow, and S. Verdu, "Blind adaptive multiuser detection," *IEEE Trans. on Info. Theory*, vol. 41, no. 4, pp. 944–960, July 1995.

8. H. Liu and K. Li, "A decorrelating rake receiver for cdma communications over frequency-selective fading channels," *IEEE Trans. on Communications*, vol. 47, no. 7, pp. 1036–1045, July 1999.

9. Y. Bar-Ness and J. Rokach, "Cross-coupled bootstrapped adaptive interference canceler," in *International Conference on Antennas and Propagation*, Los Angeles, CA, pp. 292–295, Jun. 1981.

10. Y. Bar-Ness, J. W. Carlin, and M. L. Steinberger, "Bootstrapping adaptive cross pol cancelers for satellite communications," in *Proc. International Communications Conference*, Philadelphia, PA, pp. 4F.5.1–4F.5.5, Jun. 1982.

11. Y. Bar-Ness and P. J. B., "Adaptive bootstrap multi-users cdma detector," *Wireless Personal Communications*, vol. 3, no. 1-2, pp. 55–71, 1996. special issue on "Signal Separation and Interference Cancellation for Personal, Indoor and Mobile Radio Communications".

12. Y. Bar-Ness and N. J. M. van Waes, "The complex bootstrap algorithm for blind separation of co-channel qam signals," *Wireless Personal Communications*, forthcoming.

13. X. Li and Y. Bar-Ness, "The bootstrap algorithm: A robust multiuser cdma detector with time delay variation," in *PIMRC'97*, vol. 1, Helsinki, Finland, pp. 68–72, 1997.

14. H. Ge and Y. Bar-Ness, "Comparative study of the linear minimum mean squared error(lmmse) and the adaptive bootstrap multi-user detectors for cdma," in *Proc. of International Conf. on Communications (ICC)*, vol. 1, Dallas, pp. 78–82, Jun. 1996.

15. M. Varanasi and B. Aazhang, "Multistage detection in asynchronous code-division multiple-access communications," *IEEE Trans. Commun.*, vol. 38, no. 4, pp. 509–519, Apr. 1990.

16. Y. C. Yoon, R. Kohno, and H. Imai, "A spread-spectrum multiaccess system with cochannel interference cancellation for multipath fading channels," *IEEE JSAC*, vol. 11, no. 7, pp. 1067–1075, Sept. 1993.

17. A. J. Viterbi, "Very low rate convolutional codes for maximum theoretical performance of spread-spectrum multiple-access channels," *IEEE JSAC*, vol. 8, pp. 641–649, May 1990.

18. A. Duel-Hallen, "Decorrelating decision-feedback multiuser detector for synchronous code-division multiple access channels," *IEEE Trans. Commun.*, vol. COM-41, no. 2, pp. 285–290, Feb. 1993.

19. P. Patel and J. Holtzman, "Performance comparison of a ds/cdma system using a successive interference cancellation (ic) scheme and a parallel ic scheme under fading," in *Proc. IEEE Int. Conf. Commun.*, vol. 1, New Orleans, LA, pp. 510–514, May 1994.

20. L. K. Rasmussen, T. J. Lim, and A. L. Johansson, "A matrix-algebraic approach to successive interference cancellation in cdma," *IEEE Trans. Commun.*, vol. 48, no. 1, pp. 145–151, Jan. 2000.

21. K. Jamal and E. Dahlman, "Multi-stage serial interference cancellation for ds-cdma," in *IEEE VTC '96*, vol. 2, Atlanta, Georgia, pp. 671–675, Apr. 1996.

22. D. Divsalar, M. K. Simon, and D. Raphaeli, "Improved parallel interference cancellation for cdma," *IEEE Trans. Commun.*, vol. 46, no. 2, pp. 258–268, Feb. 1998.

23. J. H. Winters, "Diversity gain of transmit diversity in wireless systems with rayleigh fading," in *Proc. IEEE ICC*, vol. 2, pp. 1121–1125, 1994.

24. C. Bontu and et. al, "Delayed diversity transmission for indoor wireless applications," in *PIMRC'94, 5th IEEE International Symposium on Wireless Network - Catching the Mobile Future*, vol. 1, pp. 75–79, 1994.

25. K. Rohani and L. Jalloul, "Orthogonal transmit diversity for direct spread cdma," in *ETSI SMG2 Wideband CDMA Concept Group*, Sept. 1997.

26. A. Wittneben, "Base station modulation diversity for digital simulcast," in *41st IEEE Vehicular Technology Conference, Gateway to the Future Technology in Motion*, pp. 848–853, 1991.

27. L.M.A.Jalloul and et al., "Performance analysis of cdma transmit diversity methods," in *IEEE VTC'99 Fall*, vol. 3, pp. 1326–1330, 1999.

28. S. M. Alamouti, "A simple transmit diversity technique for wireless communications," *IEEE Journal on Selected Areas in Communications*, vol. 16, no. 8, pp. 1451–1458, Oct. 1998.

29. X.Feng and C.Leung, "Performance sensitivity comparison of diversity schemes," *Electronics Letters*, vol. 36, no. 9, pp. 838–839, Apr. 2000.

30. V.Tarokh and H.Jafarkhani, "A differential detection scheme for transmit diversity," *IEEE JSAC*, vol. 18, no. 7, pp. 1169–1174, Jul. 2000.

31. Y. Bar-Ness and N. J. M. van Waes, "Multistage detector for adaptive separation of qam-modulated multiuser cdma signals," in *IEEE 5th International Symposium on Spread Spectrum Techniques and Applications*, vol. 3, pp. 927–931, 1998.

32. S. Parkvall, B. Ottersten, and E. G. Ström, "Sensitivity analysis of linear ds-cdma detectors to propagation delay estimation errors," in *Proceedings IEEE Global Telecommunications Conference*, pp. 1872–1876, Nov. 1995.

33. E. G. Strom, S. Parkvall, S. L. Miller, and B. E. Ottersten, "Propagation delay estimation in asynchronous direct-sequence code-division multiple access systems," *IEEE Trans. on Comm.*, vol. 44, no. 1, pp. 84–93, Jun. 1996.

34. T. Ostman and S. Parkvall, "An improved music algorithm for estimation of time delays in asynchronous ds-cdma systems," *IEEE Trans. on Comm.*, vol. 47, no. 11, pp. 1628–1631, Nov. 1999.

35. M. Missiroli, Y. Guo, and S. Barton, "Near-far resistant channel estimation for cdma systems using the linear decorrelating detector," *IEEE Trans. on Comm.*, vol. 48, no. 3, pp. 514–524, Mar. 2000.

36. S. E. Bensley and B. Aazhang, "Maximum-likelihood synchronization of a single user for code-division multiple-access communication systems," *IEEE Trans. on Comm.*, vol. 46, no. 3, pp. 392–399, Mar. 1998.

37. N. van Waes and Y. Bar-Ness, "The bootstrap algorithm for one-shot matched filtering multiuser detector in a multipath environment," in *48th IEEE Vehicular Technology Conference (VTC)*, Ottawa, Canada, pp. 184–188, May 1998.

38. Y. Bar-Ness, "Asynchronous multiuser cdma detector made simpler: Novel decorrelator, combiner, canceler, combiner(dc^3) structure," *IEEE trans. on communications*, vol. 47, no. 1, pp. 115–122, Jan. 1999.

39. H. Ge and Y. Bar-Ness, "Multi-shot approach to multiuser separation and interference suppression in asynchronous cdma," *Wireless Personal Communications*, vol. 12, pp. 15–26, 2000.

40. M. K. Varanasi and B. Aazhang, "Near-optimum detector in synchronous code-division multiple-access systems," *IEEE trans. Comm.*, vol. COM-39, no. 5, pp. 725–736, 1991.

41. A. Dinc and Y. Bar-Ness, "Bootstrap: a fast blind adaptive signal separator," in *IEEE 1992 International Conference on Acoustic, Speech and Signal Processing, ICASSP'92*, vol. 2, San Francisco, CA, pp. 325–328, 1992.

42. H. Ge and Y. Bar-Ness, "Multi-shot approaches to multiuser separation and interference suppression in asynchronous cdma," in *The 30th Annual Conference on Information Sciences and Systems*, Princeton, NJ, pp. 590–595, Mar. 1996.

43. N. J. M. van Waes and Y. Bar-Ness, "Joint adaptive channel gain estimator and multiuser decorrelator for asynchronous cdma time-variant multipath channels," in *GlobeCom'99*, Rio de Janeiro, Brazil, pp. 2385–2389, Dec. 1999.

44. D. P. Bertsekas and J. N. Tsitsiklis, *Parallel and Distributed Computation*, Prentice Hall, Englewood Cliffs, NJ.

45. W. Kellermann and W. Granzow, "Analysis of low-par modulation schemes for wideband-cdma," in *IEEE 5th International Symposium on Spread Spectrum Techniques and Applications*, vol. 1, pp. 314–317, 1998.

46. P. W. Baier, P. Jung, and A. Klein, "Taking the challenge of multiple access for third-generation cellular mobile radio systems-a european view," in *IEEE Comm. Magazine*, vol. 34, pp. 82–89, Feb. 1996.

47. I. Oppermann, "Capacity of a ds-cdma system supporting mixed modulation," in *IEEE Globecom*, vol. 6, pp. 3403–3407, 1998.

48. T. Kawahara and T. Matsumoto, "Joint decorrelating multiuser detection and channel estimation in asynchronous cdma mobile communications channels," *IEEE Trans. on Vehicular Tech.*, vol. 44, no. 3, pp. 506–515, Aug. 1995.

49. M. A. Visser and Y. Bar-Ness, "Frequency offset correction for ofdm using a blind adaptive decorrelator in a time-variant selective rayleigh fading channel," in *IEEE 49th Vehicular Technology Conference '99*, vol. 2, pp. 1281–1285, 1999.

50. M. Wax and Y. Anu, "Performance analysis of minimum variance beamformer," *IEEE trans. on Signal Processing*, vol. 44, pp. 928–937, Apr. 1996.

51. S. Roy, "Subspace blind adaptive detection for multiuser cdma," *IEEE Trans. on Comm.*, vol. 48, no. 1, pp. 169–175, Jan. 2000.

52. U. Madhow and M. L. Honing, "Mmse interference suppression for direct sequence spread-spectrum cdma," *IEEE trans. Comm.*, vol. COM-42, no. 12, pp. 3178–3188, Dec. 1994.

53. D.A.Pados and G.N.Karystinos, "An iterative algorithm for the computation of the mvdr filter," *IEEE trans. on Signal Processing*, vol. 49, no. 2, pp. 290–300, Feb. 2001.

54. I. N. Psaromiligkos and S. N. Batalama, "Interference-plus-noise covariance matrix estimation for adaptive space-time processing of ds/cdma signals," in *IEEE VTS Fall VTC 2000*, vol. 5, pp. 2197–2204, 2000.

55. J. L.S.Reed and L.E.Brennan, "Rapid covergence rate in adaptive arrays," *IEEE trans. on Aerosp. Electron. Syst.*, vol. AES-10, pp. 853–863, Nov. 1974.

56. S. M. Kay, *Fundamentals of Statistical Signal Processing-Estimation Theory*, Prentice Hall, Upper Saddle River, N.J., 1993.

57. S. Haykin, Prentice Hall, , 1996.

58. A. Jakobsson and A. L. Swindlehurst, "A blind frequency domain method for ds-cdma synchronization using antenna arrays," in *The Thirty-Second Asilomar Conference on Signals, Systems and Computers*, vol. 2, pp. 1848–1852, 1998.

59. D. Brillinger, *Time Series: Data Analysis and Theory*, Holden-Day Inc., San Francisco, 1981.

60. D. Zheng, J. Li, S. L. Miller, and E. G. Strom, "An efficient code-timing estimator for ds-cdma signals," *IEEE Trans. on Signal Processing*, vol. 45, no. 1, pp. 82–89, Jan. 1997.